

Fall 12-2009

Application of Molecular Modeling in the Noncovalent Dispersion of Carbon Nanomaterials

Praveen Kumar Madasu
University of Southern Mississippi

Follow this and additional works at: <https://aquila.usm.edu/dissertations>

 Part of the [Chemistry Commons](#)

Recommended Citation

Madasu, Praveen Kumar, "Application of Molecular Modeling in the Noncovalent Dispersion of Carbon Nanomaterials" (2009). *Dissertations*. 1088.
<https://aquila.usm.edu/dissertations/1088>

This Dissertation is brought to you for free and open access by The Aquila Digital Community. It has been accepted for inclusion in Dissertations by an authorized administrator of The Aquila Digital Community. For more information, please contact aquilastaff@usm.edu.

The University of Southern Mississippi

APPLICATION OF MOLECULAR MODELING IN THE NONCOVALENT
DISPERSION OF CARBON NANOMATERIALS

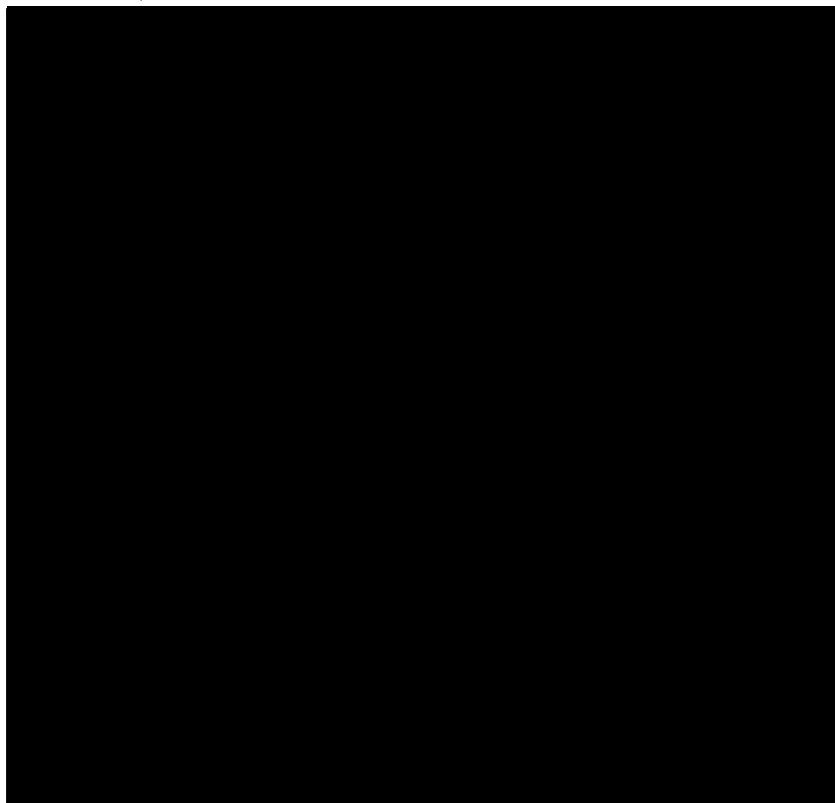
by

Praveen Kumar Madasu

A Dissertation

Submitted to the Graduate School
of The University of Southern Mississippi
in Partial Fulfillment of the Requirements
for the Degree of Doctor of Philosophy

Approved:



December 2009

COPYRIGHT BY
PRAVEEN KUMAR MADASU

2009

The University of Southern Mississippi

APPLICATION OF MOLECULAR MODELING IN THE NONCOVALENT
DISPERSION OF CARBON NANOMATERIALS

by

Praveen Kumar Madasu

Abstract of a Dissertation
Submitted to the Graduate School
of The University of Southern Mississippi
in Partial Fulfillment of the Requirements
for the Degree of Doctor of Philosophy

December 2009

ABSTRACT

APPLICATION OF MOLECULAR MODELING IN THE NONCOVALENT DISPERSION OF CARBON NANOMATERIALS

by Praveen Kumar Madasu

December 2009

Molecular modeling is a powerful tool to better understand the intermolecular interactions of carbon nanostructures. It provides structures and energies not easily obtainable from experiments and predicts properties that can be tested experimentally. Intermolecular interactions play an important role in the aggregation of various carbon nanomaterials. Three molecular modeling studies of carbon nanomaterial dispersions are presented in this dissertation, with an emphasis on illustrating how effective these theoretical techniques are in providing insight on the selection of dispersion additives. To achieve our goals, we employed molecular mechanics based methods, along with semi-empirical methods, and quantum mechanical methods, such as density functional theory. Of these techniques, molecular mechanics based methods were the more frequently applied. Chapter I serves as a brief review of computational methods with an emphasis on molecular mechanics.

The first project (Chapter II) includes theoretical studies on the dispersion of single-walled carbon nanotubes (SWNTs) via non-covalent attachment of dispersing polymers. This effort involved the investigation of the binding affinities between specific polymers and SWNTs. Dispersion of SWNTs has been of great interest for many years due to numerous applications promised by their unique combination of electronic, mechanical, chemical, and thermal properties. SWNTs are incompatible with most

solvents and polymers, which results in poor dispersion of these compounds in the polymer matrix. Van der Waals attraction among tubes over a large surface area leads to significant agglomeration, thus preventing efficient transfer of their superior properties to the matrix. Improving our fundamental understanding of the interactions of polymer-SWNT interactions at the molecular level is needed for the development of new materials based on SWNTs. Structures of SWNT-polymer complexes were optimized using molecular mechanics, employing COMPASS forcefield. The optimized complexes enabled a morphological analysis of the arrangement of polymer strands on the SWNT surface and calculations of the intermolecular interaction energies. Our calculations identified a strong binding affinity between SWNTs and conjugated polymers containing heteroatoms. The inclusion of solvent effects in the theoretical calculations produced results matching experimental observations from laboratory dispersion studies.

The second project (Chapter III) consists of computational studies on the potential dispersion of metallic nitride fullerenes (MNFs), e.g. $\text{Sc}_3\text{N}@C_{80}$, using a solvent-compatible complexing agent. MNFs have a unique hollow-ball shape built from 12 carbon pentagons and 30 hexagons, possessing truncated icosahedra symmetry and encapsulating a trimetallic-nitride cluster at the core of the cage. This unique structure results in its distinctive physical and chemical properties. The ability of MNFs to bring a functional metal to polymeric nano-composite systems opens up the possibility for extraordinary properties, e.g. magnetic, electroactive, and radioactive properties, which hold great promise for medical, optical, and electronic applications. Incorporation of MNF materials in a polymer support material involves the uniform dispersion of MNFs in the matrix. Due to the all-carbon cage, MNFs are very hydrophobic materials and

possess minimal solubility in common organic solvents (mg/mL scale), monomers, and polymers, complicating the dispersion process. The ability to disperse MNFs in polymers is paramount to realizing the potential of these materials in future commercial applications. MNFs are difficult to chemically functionalize without altering the desirable intrinsic properties; therefore, an important aspect of this work is the focus on potential non-covalent dispersion techniques using co-additives, which is a versatile, nondamaging chemistry and preserves all of the intrinsic properties of MNF.

Here we studied the interactions between dispersing additive molecules and MNFs using molecular mechanics and specifically calculating interaction energies between MNFs and a variety of additive molecules. A series of resorcinarene and calixarene compounds were surveyed, and characteristics of suitable candidates were identified. Select resorcinarene and calixarene compounds were used in experimental MNF dispersion studies, analyzing samples by particle size measurements and NMR chemical shifts. These experimental studies supported theoretical results, and the dispersion of MNFs in DMF was achieved.

In a third project (Chapter IV), interactions of naphthenic acids with crude oil asphaltenes were examined; thereby contributing significantly to the volume of knowledge available describing the affinities of these acidic and basic components of crude oil. In this project a molecular mechanical analysis with an accepted structure of asphaltene was performed, and intermolecular interactions between asphaltene and naphthenic acids dispersants were calculated. The geometries of the asphaltene-naphthenic acid complexes were optimized and five resultant regioisomers of the asphaltene-naphthenic acid complex were analyzed. The molecular mechanical

calculations suggest that the intermolecular interactions between asphaltene and naphthenic acids consist of vdW and electrostatic interactions.

DEDICATION

I would like to dedicate this document to my wife, parents, and my brother for their encouragement and support.

ACKNOWLEDGMENTS

This dissertation would not have been possible without the help and support of a number of people. Perhaps the individual to whom I am most indebted is Dr. Paige Phillips. I would like to express tremendous respect and a deep sense of gratitude to her as my advisor, for her guidance, training, support and encouragement during my Ph.D. study at The University of Southern Mississippi. Despite her demanding schedule, she was always available for both scientific and personal consultations. Her guidance and optimism has helped me accomplish my goals and tackle obstacles in academic research. I especially appreciate her encouragement to pursue different research projects that have now developed into this dissertation.

In addition, I would like to thank my Ph.D. committee members, Dr. Steven Stevenson, Dr. John Pojman, Dr. Yong Zhang, and Dr. Anthony Bell, for their various suggestions and insightful advice throughout the years. Especially, I would like to thank Dr. Steven Stevenson for his valuable advice and for the precious MNF samples that he provided. Particularly, I am grateful to Dr. Stevenson for his guidance on personal issues that helped me with my career. I would also like to express my thanks to Dr. John Pojman for his precious time and support. It is an honor to have Dr. Pojman as one of my committee members. I would also like to thank Dr. Yong Zhang for his advice in the modeling work. He was always willing to share his expertise and gave me valuable suggestions. I would like to specially thank my committee member, Dr. Anthony Bell for his precious time and help when I was in need of support. I would also like to thank our department's chair, Dr. Robert Bateman for his help and support during my graduate school experience and for his excellent management.

I also acknowledge the Mississippi Center for Super Computing Research (MCSR) and its personnel, particularly Dr. Jason Hale, Dr. Taner Pirim, and Dr. Brian Hopkins, for providing computer resources and for modeling support for my calculations. I would also thank all my lab mates for their constant support. I would like to thank Mr. Gary Cook for his NMR support, and all the department staff members, Ms. Rosemary Stuart, Ms. Sharon King, and Ms. Carla for their help during my stay. I would also like to thank several people for support and assistance with various aspects of my work, primarily Dr. Charles Hoyle.

Last but not least, I would like to thank my family members, my wife, my parents, and my brother, without their love and support, I would not be able to stand here and finish my Ph.D. study. Especially, I want to thank my wife, Rama Devi, who has been always with me and helped me persevere throughout my Ph.D. study.

TABLE OF CONTENTS

| | |
|--|-----|
| ABSTRACT..... | ii |
| DEDICATION..... | vi |
| ACKNOWLEDGMENTS..... | vii |
| LIST OF TABLES..... | xii |
| LIST OF ILLUSTRATIONS..... | xiv |
| CHAPTER | |
| I. MOLECULAR MODELING..... | 1 |
| 1.1 Introduction..... | 1 |
| 1.1.1 Research Overview..... | 2 |
| 1.2 Introduction to Modeling Methods..... | 3 |
| 1.2.1 Quantum Mechanical Methods..... | 3 |
| 1.2.2 Classical Computational Methods..... | 6 |
| 1.2.3 Monte Carlo Simulations (MC)..... | 8 |
| 1.2.4 Hybrid Quantum Mechanics/Molecular Mechanics (QM/MM) Methods..... | 8 |
| 1.3 Molecular Mechanics..... | 9 |
| 1.4 Tools in Molecular Modeling Software..... | 17 |
| 1.4.1 Molecular Graphics..... | 17 |
| 1.4.2 Script Programming..... | 18 |
| 1.5 Parameter Selection and Method Description..... | 18 |
| 1.5.1 Selection of Minimization Methods for Molecular Mechanics..... | 19 |
| 1.5.2 Setting Convergence Level..... | 20 |
| 1.5.3 Selection of Forcefield..... | 20 |
| 1.5.4 Selection of Non-bond Parameters..... | 21 |
| 1.5.5 Assigning Partial Charges..... | 22 |
| II. DISPERSION OF SWNTs..... | 25 |

| | | |
|-------|--|----|
| 2.1 | Significance..... | 25 |
| 2.1.1 | Potential Applications of SWNT-Polymer Composites..... | 26 |
| 2.1.2 | Structure of Carbon Nanotubes..... | 28 |
| 2.2 | Modeling of SWNT-Polymer Interactions..... | 31 |
| 2.2.1 | Construction of SWNTs and Polymers..... | 31 |
| 2.3 | Interaction Energy 1..... | 32 |
| 2.4 | Interaction Energy 2..... | 37 |
| 2.4.1 | Morphology of Polymers on SWNT Surface..... | 42 |
| 2.4.2 | Normalized Interaction Energies Per Unit Contact Area..... | 49 |
| 2.5 | Required Polymer for Two Unit Long (12,6) SWNT..... | 53 |
| 2.6 | Interactions-Solvent Effects..... | 55 |
| 2.7 | Conclusions..... | 57 |
| 2.8 | Experimental Dispersion of SWNTs | 58 |
| 2.8.1 | Introduction..... | 58 |
| 2.8.2 | Experimental Details..... | 59 |
| 2.8.3 | Results and Discussions..... | 63 |
| 2.9 | Conclusions..... | 64 |
| III. | DISPERSION OF $Sc_3N@C_{80}$ METALLIC NITRIDE FULLERENE..... | 69 |
| 3.1 | Introduction..... | 69 |
| 3.2 | Methods..... | 72 |
| 3.2.1 | Structure Modifications for Molecular Mechanics Approach | 72 |
| 3.2.2 | DFT Minimization of $Sc_3N@C_{80}$ and Similar Compounds.... | 73 |
| 3.2.3 | Verification of Molecular Mechanics Results against DFT Results..... | 75 |
| 3.2.4 | Verification of DFT Results against Experimental Results.... | 76 |
| 3.3 | Calculations with 4-member Ring Resorcinarene Compounds (set 1) | 78 |
| 3.3.1 | Summary of Modeling Results from Set1 | 84 |

| | |
|--|-----|
| 3.4 Calculations with Modified Resorcinarenes (set 2)..... | 85 |
| 3.4.1 Summary of Modeling Results from Set 2 | 88 |
| 3.5 Calculations with Calixarenes (set 3) | 89 |
| 3.6 Experimental Dispersion Studies of Sc ₃ N@C ₈₀ | 92 |
| 3.6.1 Dynamic Light Scattering Studies | 94 |
| 3.7 Conclusions..... | 99 |
| IV. DISPERSION OF ASPHALTENES | 100 |
| 4.1 Introduction..... | 100 |
| 4.2 Method Description and Association of Asphaltene Dimers..... | 103 |
| 4.3 Calculations with Naphthenic Acids..... | 105 |
| 4.4 Summary of Asphaltene-Naphthenic Acid IEs..... | 114 |
| APPENDIX | |
| SUPPLEMENTARY SWNT-POLYMER INTERACTION ENERGY VALUES..... | 118 |
| REFERENCES | 120 |

LIST OF TABLES

Table

| | | |
|----|---|----|
| 1 | Convergence levels for various methods | 20 |
| 2 | SWNT properties and potential applications | 28 |
| 3 | Classification of carbon nanotubes | 30 |
| 4 | Total energies and interaction energies for polymer-wrapped carbon SWNTs... | 34 |
| 5 | List of constructed polymers..... | 38 |
| 6 | Interaction energy values with vdW and electrostatic components..... | 39 |
| 7 | Comparison of interaction energy values from method1 and method2..... | 40 |
| 8 | Interaction energies for 100 atoms of polymer..... | 48 |
| 9 | Interaction energies normalized for contact area..... | 51 |
| 10 | Required number of polymer strands and polymer repeat units..... | 55 |
| 11 | Water interactions with polymer strands with and without ionic groups | 56 |
| 12 | Qualitative results of polymer wrapping experiments..... | 65 |
| 13 | Polymer water interaction energies..... | 66 |
| 14 | Required number of strands for different polymers..... | 67 |
| 15 | Interaction energies for resorcinarene-1 | 78 |
| 16 | Interaction energies for resorcinarene-2 | 80 |
| 17 | Interaction energies for resorcinarene-3 | 82 |
| 18 | Interaction energies for resorcinarene-4, -5, and -6..... | 83 |
| 19 | Structures and interaction energies for resorcinarenes | 86 |
| 20 | Summary of interaction energy values from optimizations and from single point energy calculations for resorcinarenes..... | 88 |
| 21 | Interaction energy values for calixarenes-Sc ₃ N@C ₈₀ complexes..... | 92 |

| | | |
|----|--|-----|
| 22 | Solubilities of host guest materials | 94 |
| 23 | Weights of host and guest materials used in the DLS studies | 95 |
| 24 | Volume average particle size measurements in DMF | 96 |
| 25 | Number average particle size measurements in DMF | 96 |
| 26 | Change in total and interaction energy values with rotation angle for asphaltene dimer | 105 |
| 27 | Structures of naphthenic acids used in calculations..... | 107 |
| 28 | Interaction energy values for 5 β -cholanic acid (isomer-2)..... | 108 |
| 29 | Interaction energy values for naphthalenepentanoic acid..... | 109 |
| 30 | Interaction energy values for naphthalenoic acid | 110 |
| 31 | Interaction energy values for methyl abietate..... | 111 |
| 32 | Interaction energy values for reduced methyl abietate | 112 |
| 33 | Interaction energy values for 5 β -cholanic acid (isomer-1)..... | 113 |
| 34 | Interaction energy values for 5 β -cholanic acid-3-one | 113 |
| 35 | Average interaction energies of naphthenic acids with asphaltenes..... | 115 |
| 36 | Interaction energy values for a specific length of polymer with SWNT | 118 |
| 37 | Interaction energies between polymer strands in polymer wrapped SWNT | 118 |
| 38 | Interaction energies between free polymers strands | 119 |
| 39 | Normalized interaction energies for polymer-SWNT composites..... | 119 |

LIST OF ILLUSTRATIONS

Figure

| | | |
|----|--|----|
| 1 | Graphical representation of functional forms used in molecular mechanics force fields..... | 16 |
| 2 | Formation of carbon nanotubes from graphite..... | 30 |
| 3 | Combinations for conducting and semiconducting carbon nanotubes | 31 |
| 4 | SWNT structures built using nanotube builder..... | 32 |
| 5 | Minimized structures of SWNT-polymer composites | 36 |
| 6 | Stepwise increase of polymer strand on SWNT | 38 |
| 7 | Optimized geometries of polymer-nanotube composite structures | 41 |
| 8 | Arrangement of polymer strands on SWNT surface after energy minimization . | 42 |
| 9 | Schematic representation of dihedral angle measurement..... | 43 |
| 10 | Probability vs dihedral angle plot for poly(sodium styrene sulfonate)..... | 44 |
| 11 | Probability vs dihedral angle plot for poly(thiophene sulfonic acid) | 45 |
| 12 | Probability vs dihedral angle plot for polyaniline..... | 45 |
| 13 | Probability vs dihedral angle plot for emeraldine..... | 46 |
| 14 | Probability vs dihedral angle plot for poly(ethyl-3-thiophene acetate) | 47 |
| 15 | Schematic showing measurement of Connolly or accessible surface area | 50 |
| 16 | Figures showing Connolly surfaces of composite, nanotube, and polymer | 50 |
| 17 | Connolly or accessible surface areas of polymer strands | 51 |
| 18 | Two unit long nanotube with hydrogen termination..... | 53 |
| 19 | Stepwise addition of polymer strands to SWNT..... | 54 |
| 20 | Some optimized geometries of two unit (12,6) SWNT with full polymer coverage | 54 |

| | | |
|----|--|----|
| 21 | Polymer strands with ionic groups and with hydrogen atoms in place of ionic groups..... | 56 |
| 22 | Dispersed SWNTs in polymer solutions..... | 60 |
| 23 | General method used for the large scale dispersion of SWNTs | 61 |
| 24 | TEM images of undispersed and dispersed (polymer-wrapped) SWNTs taken 12000X magnification..... | 63 |
| 25 | Flowchart of the large-scale polymer-wrapping experiment performed..... | 64 |
| 26 | Comparison of fullerenes, metallofullerenes, and MNFs | 70 |
| 27 | Refinement of $\text{Sc}_3\text{N}@C_{80}$ from crystal structure..... | 72 |
| 28 | Molecular mechanics and DFT minimized structures of $\text{Sc}_3\text{N}@C_{80}$ | 75 |
| 29 | Comparison of theoretical (DFT) and experimental results | 76 |
| 30 | Structure of resorcinarene-1 | 78 |
| 31 | Minimized structures of resorcinarene-1 and $\text{Sc}_3\text{N}@C_{80}$ complex | 78 |
| 32 | Conformations of resorcinarene-1 | 79 |
| 33 | Structure of resorcinarene-2..... | 79 |
| 34 | Minimized structures of resorcinarene-2 and $\text{Sc}_3\text{N}@C_{80}$ complex | 80 |
| 35 | Conformations of resorcinarene-2 | 81 |
| 36 | Structure of resorcinarene-3 and it's complex with $\text{Sc}_3\text{N}@C_{80}$ | 81 |
| 37 | Structures of resorcinarene 4, 5 and 6..... | 82 |
| 38 | Otmized structures of $\text{Sc}_3\text{N}@C_{80}$ -resorcinarene complexes..... | 86 |
| 39 | Structures of calix[5]arene, calyx[6]arene, and calyx[8]arene | 90 |
| 40 | Minimized geometries of calix[5]arene-, calix[6]arene-, and calix[8]arene- $\text{Sc}_3\text{N}@C_{80}$ complexes | 90 |
| 41 | Structures of resorcinarenes and calixarenes used in experimental studies..... | 93 |
| 42 | Bowl shape retention of calixarenes due to hydrogen bonding | 97 |

| | | |
|----|--|-----|
| 43 | Color generated from complexation of resorcinarens/calixarenes with Sc ₃ N@C ₈₀ in DMF | 98 |
| 44 | Particle size of Sc ₃ N@C ₈₀ in the presence and absence of resorcinarene in toluene | 98 |
| 45 | Interaction energy vs rotation angle plot for asphaltene dimer..... | 104 |
| 46 | Most stable and second most stable conformations of asphaltene dimer..... | 105 |
| 47 | Schematic showing interaction energy calculations for naphthenic acids..... | 106 |
| 48 | Sites of hydrogen bonding for naphthenic acids on asphaltene molecule | 107 |
| 49 | Most stable conformations of methyl abietate, 5β-cholanic acid, hydrogenated methyl abietate, and 5β-cholanic acid-3-one with asphaltene | 116 |

CHAPTER I

MOLECULAR MODELING

1.1 Introduction

Molecular modeling refers to theoretical methods and computational techniques to mimic the behavior of molecules and molecular systems [1]. Computer models, with the advances in hardware and software, can store and provide precise details of a molecular system, implemented with high level mathematics to describe the complex relations between each component. Thus, computer models allow complex systems to be understood and visualized, and their behavior to be predicted within the scope of the model. The computer modeling used in studying chemistry at the molecular or atomic level gives us a means of observing unusual systems, and measure properties that cannot be done under normal conditions. It also allows for screening virtual compound libraries which leads to saving time, effort, and expense. Besides chemical and biochemical applications, molecular modeling is also currently used in chemical engineering and nanotechnology [2].

There are two different approaches to molecular modeling: quantum mechanics and molecular mechanics (or classical mechanics). Quantum mechanics is a procedure based on the principles of quantum physics. In this approach, nuclei are arranged in space and the corresponding electrons are spread all over the system in a continuous electronic density, which is computed by solving the Schrodinger equation. Quantum mechanics explicitly represents the electrons in a calculation, and so it is possible to derive properties that depend upon the electronic distribution and, in particular, to investigate

chemical reactions in which bonds are broken and formed. When chemical reactions do not need to be simulated, molecular mechanics can describe the geometrical behavior of a molecular system. Molecular mechanics can be used to compute the energy of systems containing a large number of atoms, such as molecules or complex systems of biochemical and biomedical interest. In contrast to quantum mechanics, molecular mechanics ignore electrons and compute the energy of a system only as a function of the nuclear positions.

This dissertation deals with molecular modeling of carbon nanomaterials. For this purpose we primarily employed molecular mechanical methods. To a lesser extent we also employed quantum mechanical methods such as density functional theory (DFT) [3] and semiempirical methods. This chapter gives a brief introduction to some concepts used in molecular modeling, such as quantum mechanics, molecular mechanics, and molecular dynamics and a detailed background on the methods employed in this study.

1.1.1 Research Overview

This dissertation comprises three molecular modeling projects, which focus on the specific interactions between select carbon nanostructures and solution additives to enhance dispersion stability or promote matrix stability. Specifically these projects include nanotube-polymer interactions, metallic nitride fullerene-calixarene interactions, and asphaltene-naphthenic acid interactions.

Chapter I provides a background on molecular modeling methods.

Chapter II describes a molecular modeling study of SWNTs with different polymeric materials mainly using molecular mechanics approach. Modeling results are

validated by the experimental dispersion of SWNTs. The goals of this study are (1) to calculate the binding energy between SWNTs and polymers (2) demonstrate the experimental dispersion of SWNTs (3) and to compare the modeling data with experimental SWNTs dispersions.

Chapter III presents a molecular modeling of $\text{Sc}_3\text{N}@C_{80}$ metallic nitride fullerene with a series of calixarenes. The goals of this study are (1) to determine the relative binding energies between $\text{Sc}_3\text{N}@C_{80}$ and different calixarene compounds (2) and demonstrate the experimental dispersion of $\text{Sc}_3\text{N}@C_{80}$ using select calixarene compounds.

Chapter IV presents a molecular modeling of asphaltenes with a series of naphthenic acids. The goals of this study are (1) to determine the relative binding energies between asphaltenes and different naphthenic acids (2) and demonstrate the experimental dispersion of asphaltenes using select naphthenic acids.

1.2 Introduction to Modeling Methods

1.2.1 Quantum Mechanical Methods

Chemical phenomena are determined by the behaviors of electrons, which are governed by the laws of quantum mechanics. Ab initio methods are based entirely on theory from first principles. Other methods are called empirical or semi-empirical because they employ experimental results, often from acceptable models of atoms or related molecules, to approximate some elements of the underlying theory. Thus ab initio approach would require solving Schrödinger's equation for the chemical system under study. Schrodinger's equation can yield the exact energy of a system if the complete wave

function and Hamiltonian are employed. However, a complete wave function and Hamiltonian are far too computationally expensive to be tractable and are difficult to define for multi-electron systems. A series of approximations have been adopted to simplify the Hamiltonian, thereby limiting the number calculations that must be performed on a system [1, 4].

1.2.1.1 Hartree–Fock (HF) methods

The simplest type of ab initio electronic structure calculation is the Hartree–Fock (HF) scheme, in which the instantaneous Coulombic electron-electron repulsion is not specifically taken into account. Only its average effect (mean field) is included in the calculation. This is a variational procedure; therefore, the obtained approximate energies, expressed in terms of the system's wave function, are always equal to or greater than the exact energy, and tend to a limiting value called the Hartree–Fock limit. The HF method is based on the Born–Oppenheimer and orbital approximations [1]. Under the Born–Oppenheimer approximation the nuclear and electronic degrees of freedom of a molecule are decoupled, and the nuclei are held fixed while the electronic contribution to the energy is calculated. In the orbital approximation, the electrons occupy individual spin-orbitals, and as a consequence the N -electron Schrödinger equation is transformed into N one-electron equations. Both approximations facilitate computation, and the HF method proceeds by selecting a trial wave function (a molecular orbital formed as a linear combination of atomic orbitals, LCAO-MO) [5] containing adjustable parameters, and subsequently solving a set of N coupled integro-differential equations through an iterative (self-consistent field) procedure.

1.2.1.2 Møller–Plesset perturbation methods (post HF methods)

HF calculations for small to intermediate sized molecules generally yield reliable geometries, but fail to various degrees in predicting other important molecular properties. This is due to the electron correlation error introduced by the orbital approximation. Post Hartree-Fock (post-HF) methods introduce electron correlation into the calculation either by Møller–Plesset perturbation methods (MP2 and MP4), or by using wave functions based on many electron configurations (configuration interaction), rather than the single Slater determinant wave functions used in the HF method. These computationally expensive methods yield excellent results.

1.2.1.3 Semiempirical quantum mechanical methods

Within the framework of Hartree-Fock calculations, some pieces of information (such as two-electron integrals) are sometimes approximated or completely omitted. In order to correct for this loss, semi-empirical methods are parametrized, that is their results are fitted by a set of parameters, normally in such a way as to produce results that best agree with experimental data, but sometimes to agree with ab initio results. They are very important in computational chemistry for treating large molecules where the full Hartree-Fock method without the approximations is too expensive. The use of empirical parameters appears to allow some inclusion of electron correlation effects into the methods. The computational effort in ab initio calculations increases as the fourth power of the size of the basis set, and, therefore, its application to large molecules is expensive in terms of time and computer resources. Consequently, semiempirical methods treating only the valence electrons, in which some integrals are ignored or replaced by empirically

based parameters, have been developed. The various semiempirical parameterizations now in use (MNDO, AM1, PM3, etc.) have greatly increased the molecular size that is accessible to quantitative modeling methods and also the accuracy of the results.

1.2.1.4 Density functional theory (DFT) methods

Density functional theory (DFT) is a quantum mechanical method used to investigate the electronic structure of molecules in chemistry. In DFT, the properties of a molecular system are determined using functional of spatially dependent electron density. DFT is based on Hohenberg-Kohn (H-K) theorems. The H-K theorem states that the ground state properties of a many-electron system are uniquely determined by an electron density that depends on only 3 spatial coordinates. The computational savings of DFT comes from the fact that the wave function of an N-electron molecular system depends on 3N spatial coordinates (Hartree-Fock methods and its descendants), where as the electron density depends on 3 spatial coordinates, through the use of functionals of the electron density. Consequently, DFT calculations generally scale as the third power of the size of the basis set, rather than the fourth power of the HF methods. The time-dependent form of this theorem is used to describe excited states of molecular systems. DFT is one of the most frequently used methods for electronic structure calculations in chemistry due to their relatively low expense compared to Hartree-Fock (HF) and post-HF methods and for the array of available functionals which can be employed.

1.2.2 Classical Computational Methods

Large biological systems or material assemblies contain many thousands to millions of atoms. They are computationally extremely expensive or impossible for

quantum mechanical methods due to explicit treatment of electrons in these methods. Such large systems can be modeled using classical computational methods. Classical computational methods do not provide electronic structure information. Each atom is simulated as a single particle and bonded interactions are treated as "springs" with certain force constants.

1.2.2.1 Molecular mechanics (MM)

MM is a nonquantum mechanical method of computing molecular structures, energies, and other properties of molecules. The potential energy of molecular systems in molecular mechanics is calculated using force fields. The molecular potential energy is calculated classically in terms of internal degrees of freedom such as bond lengths, bond angles, dihedral angles, and electrostatic and van der Waals nonbonding interactions from energetic penalty of the molecular system based upon deviations from an idealized geometry. MM relies on an empirical parametrization of the force fields. Because MM treats electrons in an implicit way, it is a much faster method than QM and is able to handle molecules with thousands of atoms. A limitation of MM is that bond-making and bond-breaking processes cannot be modeled.

1.2.2.2 Molecular dynamics (MD)

In molecular dynamics, atomic motions are simulated using Newtonian laws: $F_i(t) = m_i a_i$, where the force F_i exerted on each atom a_i is obtained from an empirical force field. Integrating Newton's equations of motion allows exploring the constant energy surface of a system. Dynamics simulations are usually carried out in two stages, equilibration and data collection. The purpose of equilibration is to bring the system to

the most probable configuration. After equilibrating the system at the target temperature and pressure, production stage is started during which data and statistics are collected. This kind of simulation is frequently used in biochemistry in the study of protein-folding, as well as in materials science.

1.2.3 Monte Carlo Simulations (MC)

Simple energy minimization with QM or MM locates a single, stable structure (the local minimum) on the potential energy surface, which may or may not be the global minimum. MC sampling methods involve a more complete searching of the potential energy surface for low energy states. MC computational methods are used to solve a wide variety of problems in mathematics and the natural sciences, including the evaluation of integrals, the solution of differential equations, and the modeling of physical phenomena. Beginning with a collection of particles, the system's initial energy configuration is computed. One or more particles are randomly moved to generate a second configuration, whose energy is "accepted" for further consideration, or "rejected," using the Boltzmann factor, $e^{-E/kT}$. If this new configuration passes the test, it is included (properly weighted, statistically) in the manifold of ensemble states that are used to calculate the average thermodynamic properties of the system being modeled. Millions of structures on the potential energy surface are sampled randomly. Averaged energies and averaged properties are thus obtained.

1.2.4 Hybrid Quantum Mechanics/Molecular Mechanics (QM/MM) Methods

Every method has its unique features. This method is designed to model a large system with molecular mechanics while only one small region of interest to be modeled

with quantum mechanics. Molecular mechanics can simulate big systems efficiently, but cannot model the bond-breaking and bond-making that occurs within enzyme-substrate complexes at active sites. Quantum mechanics is capable of accurately computing bond-breaking and bond-making for small molecules. The hybrid quantum mechanics/molecular mechanics approach (QM/MM) allows us to accurately model a crucial region of the system with quantum mechanics while the most environment part is treated with molecular mechanics [6-8]. Therefore, the key interactions can be modeled quantum mechanically at a reasonable speed. So using QM/MM hybrid approach, QM is used to model the active site and MM are used for the rest of the enzyme structure. Another approach is to incorporate orbital-based terms in a molecular mechanics method [9].

1.3 Molecular Mechanics

Many of the problems that we would like to tackle in molecular modeling are unfortunately too large to be considered by quantum mechanics. Biomolecules, such as proteins and nucleic acids, may contain hundreds or thousands of atoms. Thus, these molecules and systems are too large to be tackled by quantum mechanics. Molecular mechanics (also known as force field methods) are the primary tools used by computational biochemists. Molecular mechanics is based upon a rather simple model of the bonded and non-bonded interactions within a system. Within the molecular mechanics framework, the *total energy* of a molecular system is described in terms of a sum of four different types of contribution arising from distortions from “ideal” bond distances (“stretch contributions”), bond angles (“bend contributions”), and dihedral

angles (“torsion contributions”), together with contributions due to “nonbonded” (van der Waals and Coulombic) interactions.

Force field methods were formulated by Hoffman (1852) and used to calculate conformations once various classical interactions were parameterized. Classical potential functions describe the motions of the atoms in Cartesian space; the atoms are considered as point masses and electron effects are included through parameters. The potential energy is the sum of atomic interactions, such as bond stretch and angle bending forces, parameterized with theoretical and empirical data to approximate the exact potential. With well-defined parameters, MM calculations give accurate, rapid, and useful classical molecular potential energies, for large molecules. The Born-Oppenheimer approximation, again, is one of the most important assumptions in molecular mechanics. Molecular Mechanics methods treat molecular systems in a manner different from the quantum mechanical methods. Typically, molecules are represented as spheres and bonds as springs in molecular mechanics. Parameterization of constants with experimental data based on Hooke’s Law allows systems to be expressed with classical physics and simple potential energy functions. This approach omits the explicit treatment of electrons in molecular systems, so that larger systems can be simulated. The major drawback is that it is unable to model the excited states, bond making, and bond breaking. And the accuracy of molecular mechanics is heavily dependent on parameterization of the force fields for different atom types.

Benefits

Quantum mechanical methods deal with the electrons in a system so that even if some of the electrons are ignored a large number of particles must still be considered, and the calculations are time-consuming. Molecular mechanical methods ignore the electronic motions and calculate the energy of a system as a function of nuclear positions only. Molecular mechanics is thus invariably used to perform calculations on systems containing significant numbers of atoms. In some cases molecular mechanics can provide answers that are as accurate as even the highest level quantum mechanical calculations, in a fraction of the computer time.

Drawbacks

However, molecular mechanics cannot of course provide properties that depend upon the electronic distribution in a molecule. Molecular mechanics calculates the energy of a system as a function of nuclear position. It ignores electronic motion and behavior of the system; therefore, those properties involved in electronic distributions such as bond breaking or forming, excited state, or transition states cannot be modeled by molecular mechanics. In molecular mechanics, the molecules are modeled as atoms held together by bonds. The atoms may have different sizes, “softness”, and partial charges, and the bonds may be more or less “stiff”, i.e., the molecules are described by a “ball and spring” model [10].

Applications beyond the capability of most forcefield methods include the following:

- Electronic transitions (photon absorption)

- Electron transport phenomena
- Proton transfer (acid/base reactions)

Molecular Mechanics methods are embodied in the form of force fields. All force-fields contain bonded and non-bonded interaction terms, but the exact format of the terms is different. The total potential energy of a molecule in many of the molecular modeling force field methods can be expressed as a sum of all bonded and non-bonded interactions, specifically, bond, angle, and dihedral (bonded), coulombic and van der Waals (non-bonded) terms [11].

$$E_{FF} = E_{str} + E_{bend} + E_{tors} + E_{vdw} + E_{el} + E_{other} \quad \text{Equation 1}$$

The first three summations in Equation 1 represent the bonded interactions in the system. These summations are over all “bonds”, all “bond angles”, and all “dihedral angles”, respectively. E_{str} is the energy function for stretching a bond between two atoms, E_{bend} represents the energy required for bending an angle, E_{tors} is the torsional energy for rotation around a bond, E_{vdw} and E_{el} describe the non-bonded van der Waals and electrostatic interactions, and E_{other} represents some other terms used in a specific force field [6-8]. So the total energy of a system determined in molecular mechanics is the total strain energy of the system. The stretch and bend terms are most simply given in terms of quadratic (Hook’s law) forms, Figure 1. The equations for these various terms are as follows.

Bond stretch energy:

$$E_{\text{str}} = \sum_{\text{bonds}} k_b (b - b_0)^2 \quad \text{Equation 2}$$

where b is the bond distance between two atoms, b_0 is the “ideal” (equilibrium) bond length taken either from experiment or from quantum chemical calculations. And k_b is stretch “force constant”. In the COMPASS force field [12], quartic polynomials are used for bond stretching. Each bond is treated as a spring. Energy penalties are calculated from the deviations of the bonds away from the “equilibrium” bond length.

Bond bending energy:

$$E_{\text{bend}} = \sum_{\text{angles}} k_\theta (\theta - \theta_0)^2 \quad \text{Equation 3}$$

Here θ is the bond angle, θ_0 is the “ideal” (equilibrium) bond angle taken either from experiment or from quantum chemical calculations, and k_θ is bend “force constant” for changing the equilibrium bond angles θ_0 to θ . This term is a harmonic second order expression, and is only accurate close to equilibrium. In the COMPASS force field [12], quartic polynomials are used for angle bending. This term accounts for the deformation energy of valence angles between covalent bonds.

Torsional energy:

$$E_{\text{tors}} = \sum_{\text{torsions}} V_n (1 + \cos(n\phi - \beta)) \quad \text{Equation 4}$$

where ω is the torsion angle, n is periodicity, which gives the number of minimum/maximum points as the bond is rotated through 360° , V_n can be referred to as the “barrier” height (maximum), and γ is the phase factor to determine where the torsion angle passes through its minimum value. This gives description of the torsional potential that models how energy changes as a bond rotates.

The van der Waals energy:

$$E_{\text{vdw}} = \sum_{i < j} \left(\frac{A_{ij}}{r_{ij}^{12}} - \frac{B_{ij}}{r_{ij}^6} \right) \quad \text{Equation 5}$$

The repulsion term A_{ij}/r_{ij}^{12} represents the repulsion between the electrons of atom i and atom j ; the attraction term B_{ij}/r_{ij}^6 represents the dispersion forces. When the distance between two atoms is large, the attraction term (r^{-6}) dominates; when the distance between two atoms is very small, the repulsion term (r^{-12}) dominates. COMPASS [12] uses r^{-9} for repulsive part rather than customary r^{-12} term.

Electrostatic energy:

$$E_{\text{el}} = \sum_{i < j} \frac{q_i q_j}{4\pi\epsilon\epsilon_{ij}} \quad \text{Equation 6}$$

This term uses the Coulomb’s Law to calculate the attraction or repulsion potential between two particles. The q_i and q_j represent the partial charges on atom i and atom j . A dielectric constant ϵ (may be a variable function) is included to model the solvation effects. Electrostatic potential energies between non-bonded atoms are calculated as classical monopole-monopole interactions.

All the above potential functions are employed in almost every early force-field. To be more accurate, more complicated forms are applied to represent the interactions. Other terms may be included in other sophisticated force fields, such as cubic and higher-order forms of the stretch and bend terms, as well as “cross terms” (bend-stretch, stretch-torsion, and so forth) to count for correlations between stretch and bend components may be used, and improper terms to account for the energy penalty in a distorted plane system or maintain a specific configuration at a chiral center. Other nonbonded interactions terms which count for effects such as hydrogen bonding may also be included. All the cross terms up through third order that have been found to be important are also included in COMPASS [12].

The atom type defines the chemical environment of an atom. The basic idea is that atoms of the same elements are distinguished by hybridization, formal charge on the atom, and immediate bonded neighbors. The molecular mechanics interactions are computed between atom types instead of elements. The parameter set is the set of values of the constant parameters involved in the functional forms (values of k_b and k_θ , etc). Taken together, functional form and parameterization (the constant parameters involved) constitute what is termed a force field. A force field is generally designed to predict certain structural properties and is parameterized accordingly. Some of the common force fields are COMPASS, CVFF, MMFF, MM2, MM3, AMBER, SYBYL and OPLS [12-17].

Force fields can be parameterized from experimental observations of vibrational spectroscopy, gas-phase molecular structures, thermodynamic properties and crystal

structures. The quantum mechanical data is also used to generate Quantum Mechanical Force Fields (QMFF) which may account for the natural anharmonic nature of certain molecular system.

The interactions are graphically shown in Figure 1. Bond stretch (a) is the interaction between 2 atoms; AB, angle bend (b) is the interaction between 3 atoms; ABC, angular torsion (c) is the interaction between 4 atoms; ABCD, etc. The illustrations (e) to (k) represent cross terms and (l) the nonbonded interactions: van der Waals, electrostatic and hydrogen bond. Graphical representation of functional forms used in molecular mechanics force fields are shown in (Figure 1), where a) bond stretch AB, b) angle bend ABC, c) torsion ABCD, d) inversion ABCD. Cross terms are described in e to k; e) stretch-stretch, f) angle bend-angle-bend, g) stretch-bend, h) stretch-torsion, i) stretch/torsion, j) bend-torsion and k) bend-torsion- bend, while l) shows the non-bonded interactions A-D, A-E, B-D, B-E, C-D, and C-E [13, 18].

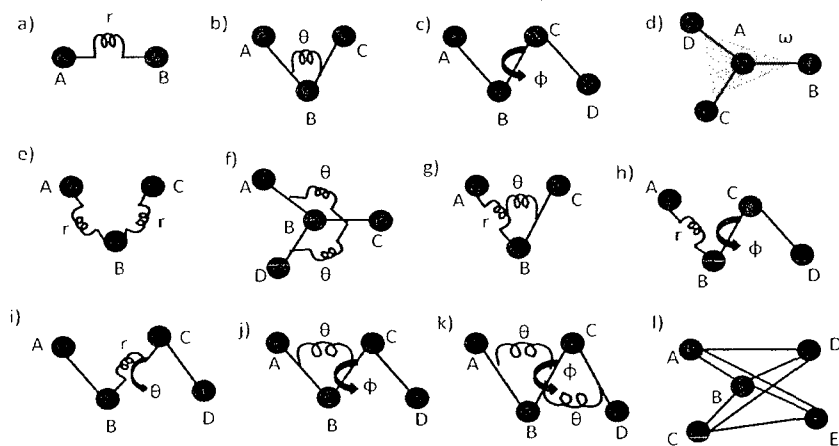


Figure 1 Graphical representation of functional forms used in molecular mechanics force fields [18]

1.4 Tools in Molecular Modeling Software

In general, molecular modeling software should be able to accomplish one or more tasks: (1) create the molecules *in silico*, (2) visualize and manipulate the molecules in three- dimensional space, (3) calculate the properties of the molecules quantum mechanically, molecular mechanically or statistical mechanically, and (4) analyze and interpret the molecular data. There are many computer modeling software packages available. Some are sophisticated commercial packages; some are developed by academic researchers.

1.4.1 Molecular Graphics

Almost every molecular modeling study begins with the construction of a model structure. Materials Visualizer is the core module in MS Modeling, providing modeling, analysis, and visualization tools [19]. Materials Visualizer provides fast, interactive tools for building, visualizing, and editing structures. The sketching tools in the Materials Visualizer allow creation of new nonperiodic molecular structures and modification of existing structures. Crystal building and polymer building features are also available for crystal structures or macromolecules. It allows visualization of 3D models with a variety of display styles, labels, and measurement tools such as bond lengths, angles, etc. It also provides Connolly contact surfaces or solvent accessible surfaces and volumes for a molecular system. 3D structures are presented in a 3D viewer and allow rotation, translation, and zooming for various observations. If a trajectory is generated during a calculation, system evolution can be visualized with motion of atoms.

1.4.2 Script Programming

Although graphic interfaces are widely used in modeling, modeling work can also be done by command-based scripts. Scripts allow modifications that are not available through graphical interface. For example, Discover (Accelrys Inc) performs a simulation after reading a script file written in BTCL (Biosym Tool Command Language) after reading the molecular coordinate file (.cor) and the molecular data file (.mdf). BTCL can be used to write scripts that perform the most trivial of tasks through to ones that implement a new simulation algorithm using a standard editor. The script file contains commands and control structures to instruct Discover how to carry out the simulation. Additional commands can be added to the input file to calculate properties such as vibrational modes [20].

1.5 Parameter Selection and Method Description

The following tasks were involved in performing molecular mechanics minimizations:

1. Selection of a forcefield
2. Set up the required non-bond parameters
3. Selection of minimization method or methods
4. Selection of an algorithm for the methods
5. Set up convergence level for all selected methods
6. Specify the maximum number of iterations for the minimization
7. Minimize the structure

1.5.1 Selection of Minimization Methods for Molecular Mechanics

There are several different minimization methods available in the Discover module of Materials Studio [20]. For the present calculations the following methods were used in a cascade. Energy minimizations were started with the steepest descent method, followed by the conjugate gradient method and finally Newton method.

Steepest descent method has to be used first in a minimization as it is most likely to converge, even if the structure is very crude. Within a few iterations the total potential energy of the structure is reduced. Usually structures are built graphically before a calculation for which the gradients are very large and the configurations are far from the energy minimum. It also has to be used in converging poor crystal structures.

Conjugate gradient method stores information from the previous iteration, which is computationally less expensive compared to Newton methods. With respect to computer resources, this method falls between steepest descent and Newton methods. Newton method is too expensive for large systems and conjugate gradient method can be used in such situations. In the Discover package Fletcher-Reeves and Polak-Ribiere algorithms are available for this method.

Newton methods calculate and store second derivatives and are thus computationally very expensive. For example, the Newton-Raphson method in Discover is only recommended for systems with a maximum of 200 atoms. Newton method's convergence is very efficient during final stages of a minimization and thus it is used last in a minimization after achieving reasonable convergence by using other methods. Discover package provides three other variants of the Newton method. The BFGS and

DFP quasi-Newton algorithms use an updated formula to simulate a second-derivative matrix. Truncated Newton method has the strengths of the conjugate gradient and Newton-Raphson methods. Conjugate gradient and Newton minimization method, support different algorithms. Fletcher-Reeves algorithm for conjugate gradient method and BFGS algorithm for Newton method were used for the present calculations.

1.5.2 Setting Convergence Level

Convergence levels used for different methods are shown in Table 1.

Table 1 Convergence levels for various methods

| Used methods | Applied convergence |
|--------------------|----------------------------------|
| Steepest descent | 1000 kcal/mol/A° |
| Conjugate gradient | 10 kcal/mol/A° |
| Newton | 1.0×10^{-6} kcal/mol/A° |

1.5.3 Selection of Forcefield

Discover is equipped with several forcefields such as CVFF, PCFF, COMPASS, and AMBER [20]. The results of any molecular mechanics calculation depend on the forcefield. Each atom in the molecular system has to be assigned a forcefield type before starting an energy calculation or a minimization. These forcefields cannot be just based on element type alone, but properties such as hybridization and atom connectivity are to be considered.

COMPASS was parameterized against a wide range of experimental observables for organic compounds containing H, C, N, O, S, P, halogen atoms and ions, alkali metal cations, and several biochemically important divalent metal cations. COMPASS is a new version of PCFF. PCFF is based on CFF91, extended so as to have a broad coverage of

organic polymers, (inorganic) metals, and zeolites. COMPASS stands for ‘Condensed-phase Optimized Molecular Potentials for Atomistic Simulation Studies’. In contrast to earlier CFF91 and PCFF forcefields, COMPASS is the first ab initio-based forcefield to have been parameterized using extensive data for molecules in the condensed phase [12]. Thus, COMPASS can predict properties of a broad range of compounds both in isolation and in condensed phases [20]. Extensive validations have been performed and presented in the literature for COMPASS. The properties studied using COMPASS are molecular structures and conformations [21], IR frequencies, PVT behavior of liquids [22], heats of vaporization and solubility parameters for polymers [23], cell structures and lattice energies of crystal structures.

1.5.4 Selection of Non-bond Parameters

Van der Waals energy does not converge until approximately 20\AA for periodic system [24]. For a non-periodic system such as present study, 15 \AA would be a very good choice. Same or different non-bond cutoff values can be used for van der Waals and Coulomb interactions in a calculation depending on the requirement. A summation method is used to determine non-bond energies. Discover provides different summation methods and related values for non-bonded interactions, depending on whether the system is periodic or nonperiodic and depending on the total number of atoms in the system [20]. For a nonperiodic system an atom based cutoff method is based on all atoms within the sum of the cutoff and buffer-width distances of an atom. For high precision results the atom based method with a cut-off of 15.5 \AA , spline width of 5.0 \AA , buffer width of 2.0 \AA , and a relative dielectric of 1 was used for both Coulomb and van der

Waals interactions in the present study. In a calculation, cutoff distance specifies the distance at which the non-bond interactions are neglected from the list of interactions for energy calculation. Similarly spline width specifies the width of the region in which the non-bond interactions smoothly decrease from their full value to zero, for atom based method. This smoothing function is used to prevent discontinuity in energy values due to numerical nature of cutoff values. Buffer width is the width of the region beyond cutoff distance where non-bond interactions are zero, but the atoms in this region are considered in the atom based method. Relative dielectric value is the dielectric constant relative to the permittivity of free space [20].

1.5.5 Assigning Partial Charges

MS Modeling provides two charge equilibration methods [19]. Molecular mechanics calculations require information of partial charge on each atom in the structure for the calculation of electrostatic energy. In Discover, charges are assigned to each atom when forcefield types are assigned, as each forcefield contains information of charge. However, manual assignment of a charge is needed in some situations, such as sodium ion of sulfonate group in the present study. Sometimes charging may fail if the forcefield has not been parameterized for the structure or a functional group in the system under consideration. In such situations it may be possible to use *ab initio* methods to calculate charges for small systems. However, for large systems, it is computationally very expensive or impossible to obtain point charges by using *ab initio* approaches and an alternative quick method is needed. MS Modeling provides two methods for quick calculation of atomic point charges, QEq and Gasteiger. The QEq method [25] calculates

atomic charges using information on arrangement and electronegativities of atoms in the molecular system [25]. QEq method does not make use of the bonding pattern of the molecular system contrary to the Gasteiger method. It uses an iterative procedure for calculating atomic charges if the molecular system contains hydrogen atoms. MS Modeling provided a revised version of QEq method for better treatment of charges. The Gasteiger [26], method calculates atomic charges of a molecular system using orbital electronegativities. In this method, atoms are identified by their orbital electronegativities, which are calculated using an iterative procedure. In Gasteiger method, only the connectivities of the atoms are important in the calculation of partial charges. An augmented version of the original Gasteiger method provided by MS Modeling was used for the present calculations [20].

1.5.6 Energy Minimizations

The majority of our calculations involve energy minimizations. An important method of studying a molecule is to find its (most) stable conformation, which means locating the minima points on the usually complicated potential energy surface. Energy minimization techniques are designed to find a minimum, though it may not be global minimum, by adjusting the atomic coordinates.

At a minimum point, the first derivatives of the energy function with respect to each coordinate are zero and the second derivatives are all positive. Steepest descent (SD) and conjugate gradients (CG) are two minimization algorithms based on the first derivatives (gradient) of the potential energy. The direction of the gradient indicates where the minimum lies, and the magnitude of the gradient indicates the steepness of the

local slope. The energy of the system can be lowered by moving each atom in response to the force acting on it. The steepest descent method moves atoms in the direction parallel to the net force. After finding a minimum in this direction, the next step is made perpendicular (orthogonal) to the previous direction. The conjugate gradient method moves the atoms in a direction computed from the gradient of the current point and the previous direction. The Newton-Raphson method uses both first and second derivatives of the energy function to locate a minimum. A Hessian matrix of $3N \times 3N$ (N is the number of atoms) second derivatives is calculated and inverted in each iteration. Thus, only small molecules are suitable for this minimization method. The steepest descent method can be superior to conjugate gradients method when the starting structure is far from the minimum. However, conjugate gradients method has much better convergence characteristics once the function is already near to a minimum [1].

CHAPTER II

DISPERSION OF SWNTs

2.1 Significance

Carbon nanotubes (NTs), an allotropic form of carbon discovered by Iijima in the early 1990s, exist as single-walled, multi-walled and more complex carbon micro-structures [27]. Single-wall nanotubes (SWNTs) consist of single layers of graphite sheet rolled into perfect cylinders with a diameter ranging from 0.7-2 nm, and multi-wall nanotubes (MWNTs) consist of sets of concentric cylindrical shells of graphite sheet generally with larger diameters. Due to their nanoscale dimensions, electron transport in carbon nanotubes takes place through quantum effects and propagates along the long axis of the tube. Because of this anisotropic transport property, carbon nanotubes are frequently referred to as “one- dimensional” in scientific articles [28, 29].

As-produced SWNTs are held together in bundles of 50 to a few hundred individual SWNTs by very strong van der Waals interactions [30]. Baughman et al. [31] has suggested that bundling results in diminished mechanical and electrical properties as compared to theoretical predictions related to individual SWNTs. The successful dispersion of SWNTs into individual tubes or thin bundles of tubes is a significant technical challenge to their successful incorporation into films and coatings. Two major methods have been explored by researchers for the dispersion of individual SWNTs in a polymer matrix. These methods include the (1) modification of the walls of the SWNTs by functionalization and (2) polymer wrapping. However, both methods of dispersion have challenges. Many researchers have tried to solubilize NTs through various

functionalization routes [32-36]. NT dispersion into a polymer matrix via functionalization to improve the electrical properties of the resulting materials has not proven successful. The grafting on NT walls significantly disturbs the π electron system of the NT, and thus negatively affects the electrical properties [37]. As a result of direct functionalization, conversion of the sp^2 -hybridized carbons forming the conductive NT walls to sp^3 -hybridized occurs. Polymer wrapping method would yield better dispersions while minimizing the unwanted effects. The effective utilization of nanotubes (NT) as a filler to obtain NT-polymer composites with enhanced mechanical, electrical, thermal, electrochemical, and optical properties depends on the ability to disperse the NTs throughout the polymer matrix without damaging the NTs.

The goal of the project is to improve the properties of polymer-SWNT composites by studying the individual molecular interactions of the constituent elements. Theoretical calculations combined with experimentation will aid in the identification of critical parameters affecting wrapping polymers and improve solvent and polymer dispersions of SWNTs. Our approach included a combination of theoretical and experimental investigations of the polymer-wrapping technique to disperse carbon nanotubes. Dispersions of carbon nanotubes were prepared using a combination of modeling and experimentation. Parameters controlling the interactions between carbon nanotubes, wrapping polymers, and solvent were defined.

2.1.1 Potential Applications of SWNT-Polymer Composites

The physical properties of nanotube/polymer composites arise from the nanotube and polymer characteristics as well as from the microstructures produced while fabricating

and processing these nanocomposites, **Table 2** [38]. The first polymer nanocomposites using carbon nanotubes as a filler were reported in 1994 by Ajayan et al.[39] Carbon nanotubes possess high flexibility,[40] low mass density (1.3 g/cm^3),[41] and large aspect ratio (typically ca. 300-1000). They have also been found to have specific surface areas as high as $1350 \text{ m}^2/\text{g}$ [38]. CNT have a unique combination of mechanical, electrical, and thermal properties that make nanotubes excellent candidates to substitute or complement the conventional nanofillers in the fabrication of multifunctional polymer nanocomposites. Some nanotubes are stronger than steel, lighter than aluminum, and more conductive than copper. For example, theoretical and experimental results on individual single-wall carbon nanotubes (SWNT) show extremely high tensile modulus [42] (640 GPa to 1 TPa) and tensile strength [43] (150-180 GPa). Depending on their structural parameters, SWNT can be metallic or semiconducting, which further expands their range of applications. Because of the nearly one-dimensional electronic structures, metallic nanotubes can transport electrons over long tube lengths without significant scattering (electronic mean free path for metallic SWNT is on the order of several microns[44]). Similarly, SWNT exhibit large phonon mean free path lengths that result in high thermal conductivity (theoretically $>6000 \text{ W/(mK)}$) [45]. The enhancements obtained often surpass the performances of traditional additives.

Table 2 SWNT properties and potential applications

| Materials | Property Attributes | Potential Applications |
|--|---|--------------------------------------|
| Polymer/SWNT Composite film and fibers | Strength (37 GPa) | Structural Composites |
| Bi-Component Fibers | Stiffness (640 GPa) | Functional Textiles |
| Hollow Fibers | Light Weight (density 1.30 g/cm ³) | Energy storage-superapacitors |
| Bulk Composites | Electrical Conductivity (10 ⁶ S/m) | Fuel Cell Electrodes |
| SWNT Films and Fibers | Thermal Conductivity (2000 W/m/K) | Electrically Conducting Coatings |
| SWNT Coatings | Specific Surfaced Area (1350 m ² /g) | Actuators, artificial tissue |
| Carbon/SWNT Composites | Anisotropic Optical Properties | Heat dissipation/ thermal management |
| | Bio-compatibility | |

Due to their high intrinsic conductivity and large aspect ratio, single walled carbon nanotubes are expected to produce highly conductive coatings at low weight percent loadings of tubes in polymer. Low loadings of additives preserve the desired mechanical properties of coatings, which are frequently compromised when large volumes of fillers (conductive or other) are employed. The first realized major commercial application of carbon nanotubes is expected to be their use as electrically conducting components in polymer composites [31, 46, 47]. Several orders of magnitude enhancement in electrical conductivity has been achieved with very small loadings [48] of nanotubes in the polymer matrices, while maintaining the other performance aspects of the polymers such as optical clarity, mechanical properties, low melt flow viscosities, etc.

2.1.2 Structure of Carbon Nanotubes

Single walled carbon nanotubes (SWNTs) consist of single layer graphite sheet rolled into a hollow cylindrical shape with a diameter ranging from 0.7-2 nm, and multi-

wall nanotubes (MWNTs) consist of sets of concentric cylindrical shells of graphite sheet generally with larger diameters. The so-called chiral vector of the nanotube, C_h , is defined by $C_h = n\hat{a}_1 + m\hat{a}_2$, where \hat{a}_1 and \hat{a}_2 are unit vectors in the two-dimensional hexagonal lattice, and n and m are integers that satisfy the condition $0 \leq |m| \leq n$ [49].

Another important parameter is the chiral angle, which is the angle between chiral vector, C_h and \hat{a}_1 . When the theoretical graphene sheet is rolled up to form the cylindrical part of the nanotube, the ends of the chiral vector meet each other. The chiral vector thus forms the circumference of the nanotube's circular cross-section, and different values of n and m lead to the different nanotube structures. Armchair nanotubes are formed when $n = m$ and the chiral angle is 30° . Zigzag nanotubes are formed when either n or m is zero and the chiral angle is 0° . All other nanotubes, with chiral angles intermediate between 0° and 30° , are known as chiral nanotubes (Table 3). The properties of nanotubes are determined by their diameter and chiral angle, both of which depend on n and m . SWNT can be conducting or semiconducting depending on the values of n and m [50]. If $(n-m)$ is either 0 or a multiple of 3, the nanotube would be conducting and for other values nanotube would be semiconducting (Figure 3).

Figure 2 plots the relevant vectors on graphene that define carbon nanotubes with indices (6,6) (armchair), (6,1) (chiral), and (6,0) zig-zag. These integers signify the number of unit vectors in two directions across the graphene sheet. For example, the (6,6) SWNT is formed when the point A_1 meets C_1 and B_1 meets D_1 . Similarly other two nanotubes are formed as shown in Figure 2.

Table 3 Classification of carbon nanotubes

| Type | Chiral angle (θ) | C_h | Shape of cross section |
|----------|---------------------------------|----------|--------------------------|
| Armchair | 30° | (n, n) | Cis-type |
| zigzag | 0° | $(n, 0)$ | Trans-type |
| Chiral | $0^\circ < \theta < 30^\circ$ | (n, m) | Mixture of cis and trans |

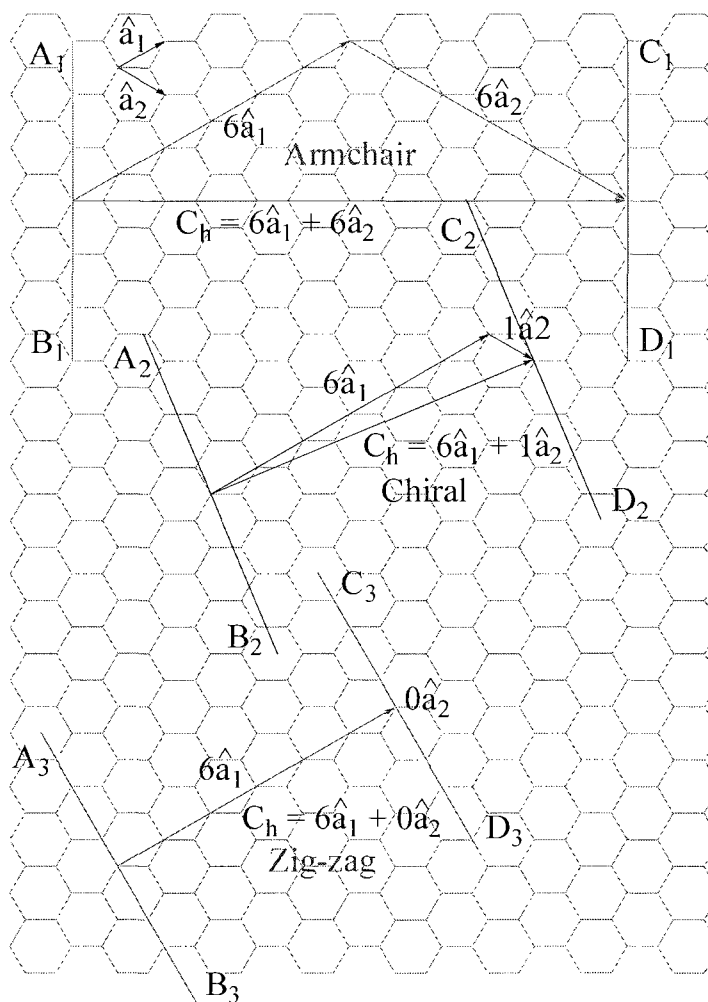


Figure 2 Formation of carbon nanotubes from graphite

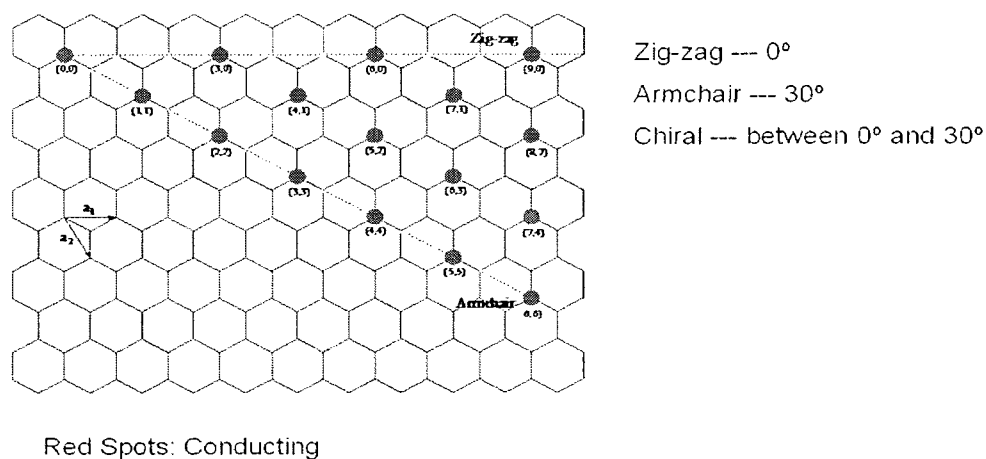


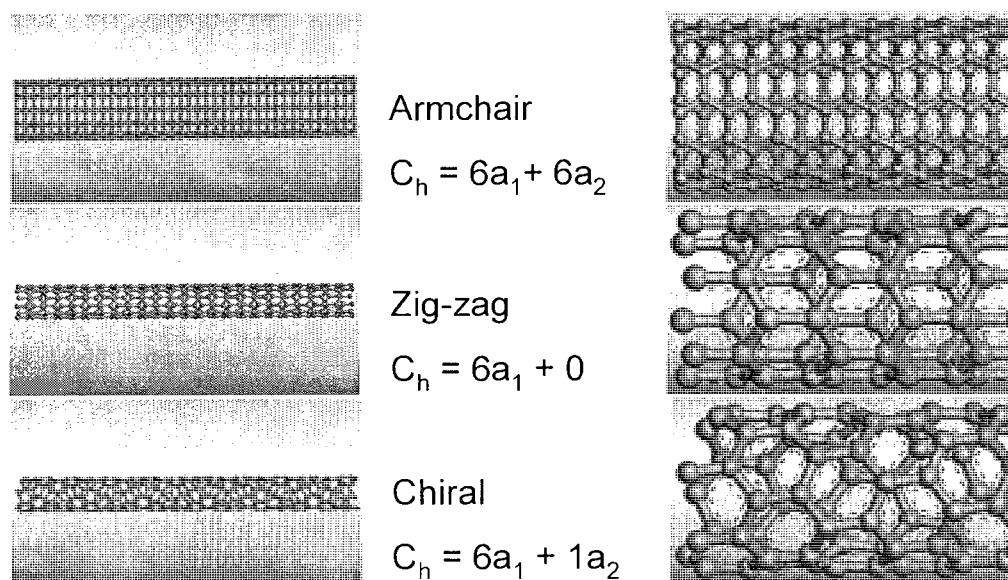
Figure 3 Combinations for conducting and semiconducting carbon nanotubes

2.2 Modeling of SWNT-Polymer Interactions

Present molecular modeling study focus on physisorption of polymers on SWNTs. Hence there is no change in intramolecular bonding, and therefore classical molecular mechanics simulations can be used effectively.

2.2.1 Construction of SWNTs and Polymers

Different (12,6) conducting carbon nanotube were constructed using Materials Studio's nanotube builder (Figure 4), with a diameter 12.43 Å and with 'H' termination at both ends. Other longer and shorter nanotubes were constructed in a similar fashion as required for the calculations. (12,6) carbon nanotube is one of the experimentally observed nanotubes in a typical electric arc synthesis, and is selected for use in our modeling studies. Select polymers were constructed, each with upto 30 repeat units or as required for calculations using a polymer builder available in Materials Studio.



C_h = chiral vector, a_1 & a_2 are lattice vectors of graphene sheet

Figure 4 SWNT structures built using nanotube builder

2.3 Interaction Energy 1

A (12,6) conducting carbon nanotube was constructed using Materials Studio's nanotube builder, with a diameter 12.43 Å and length of 56.35 Å with 'H' termination at both ends. The following polymers were constructed, each with 30 repeat units.

Polymers were constructed using the polymer builder, and the calculation was initiated at a polymer-nanotube distance of approximately 10 Å.

Polymers: poly(ethyl thiophene-3-acetate)

polyaniline

polyallylamine

polyvinyl alcohol

polyethyleneglycol

dextran

The molecular systems were subject to minimization using the Discover molecular module employing the COMPASS force field within Materials Studio software (Accelrys, Inc., San Diego CA). An atom based summation method was utilized with the non-bonded interactions cutoff set to a distance of 15.5 Å, accompanied by a spline width of 5.0 Å and a buffer width of 2.0 Å. The models were first minimized (potential energy) using the steepest descent convergence method until the convergence is reached 1000 kcal/mol/Å, followed by conjugate gradient convergence method until the convergence is reached 10 kcal/mol/Å, followed by a Newton convergence method until the final convergence reached 1.0×10^{-6} kcal/mol/Å. Fletcher-Reeves algorithm was used for conjugate gradient method and BFGS algorithm was used for Newton method. Whenever necessary atomic charges were calculated using Gasteiger and or QEq methods within Materials Studio.

The polymer chain was initially placed at a distance of about 10 Å, such that part of the polymer was within the cutoff distance of the van der Waals interactions with SWNT atoms, and subsequently during minimization the polymer adsorbed on to the SWNT due to attractive forces. For SWNT-polymer pair, different initial orientations were tested-confirmed that the initial orientation does not significantly alter the final adsorption energy if not the final orientation.

Interfacial interaction energy

The interaction between a nanotube and a polymer comes from the electrostatic and van der Waals forces in the molecular system. Generally, the interaction energy is

estimated from the energy difference, ΔE , between the total energy of the composite and the sum of the energies of individual molecules as follows:

$$E_{\text{interaction}} = \Delta E = E_{\text{(total)}} - E_{\text{(nanotube)}} - E_{\text{(polymer)}} \quad \text{Equation 7}$$

where $E_{\text{(total)}}$ is the total energy of the composite, $E_{\text{(nanotube)}}$ is the energy of the nanotube without the polymer, and $E_{\text{(polymer)}}$ is the energy of the polymer without the nanotube. In other words the interaction energy can be calculated as the difference between the minimum energy and the energy at the infinite separation of the nanotube and polymer. The results of the calculated total energies are shown in Table 4.

Results of interaction energy 1

Interaction energies were calculated according to Equation 7 and are listed in Table 4.

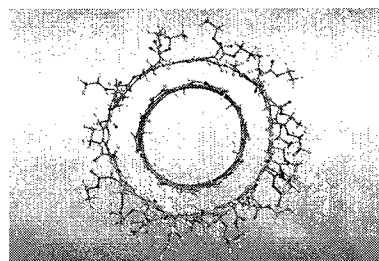
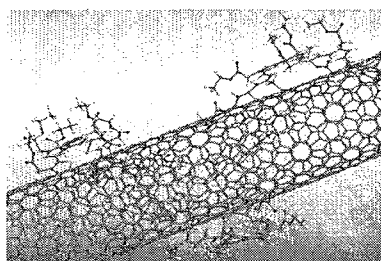
Table 4 Total energies and interaction energies for polymer-wrapped carbon SWNTs

| Polymer | Nanotube | E_{total} Kcal/mol | E_{nanotube} Kcal/mol | E_{polymer} Kcal/mol | $E_{\text{interaction}}$ Kcal/mol |
|---------------------------------|----------|--------------------------------|-----------------------------------|----------------------------------|--------------------------------------|
| poly(ethyl thiophene-3-acetate) | (12,6) | 42461.4 | 40749.9 | 1934.7 | -223.2 |
| Polyaniline | (12,6) | 39968.6 | 40749.9 | -570.1 | -211.2 |
| Polyallylamine | (12,6) | 40479.7 | 40749.9 | -259.8 | -10.4 |
| Polyvinyl alcohol | (12,6) | 39991.9 | 40749.9 | -685.0 | -73.0 |
| Polyethyleneglycol | (12,6) | 40676.1 | 40749.9 | 27.9 | -101.7 |
| Dextran | (12,6) | 41758.4 | 40749.9 | 1197.5 | -189.0 |

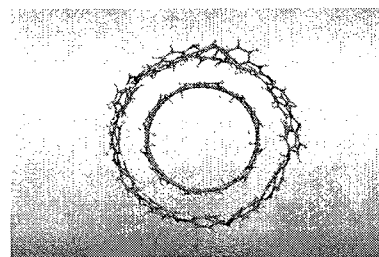
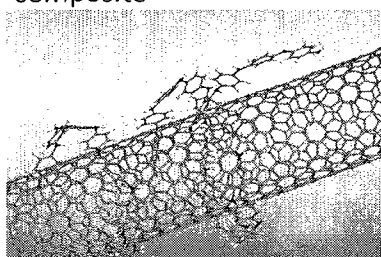
(E_{total} is the energy of the nanotube and the polymer, E_{nanotube} is the energy of the nanotube without the polymer and E_{polymer} is the energy of the polymer without the nanotube.)

Table 4 shows that all the polymers have an obvious attractive interaction with the nanotube, the specific monomer structure plays a very important role in determining adhesion to the SWNT. It is seen that poly(ethyl thiophene-3-acetate) exhibits the

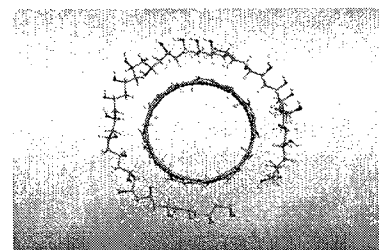
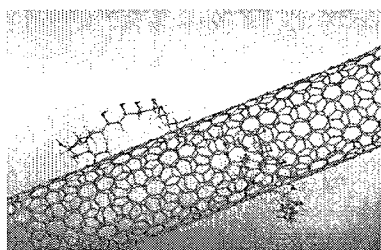
strongest interaction with the SWNT, then polyaniline, dextran, PEG and PVA. The polymers with aromatic rings in the backbone (conjugated polymers) (PT and PANI) have stronger interactions with the SWNTs than those without conjugation in the backbone. This is possibly due to π - π interaction similar to the interactions between graphite layers and nanotube bundles. The conjugated polymers (poly(ethyl thiophene-3-acetate) and polyaniline) have a flat backbone, where more atoms can come closer to SWNT surface giving a higher interaction energy. It is noted that the interaction energies for nanotube-polyallylamine and nanotube-polyvinyl alcohol are -10.4 kcal/mol and -73.0 kcal/mol, respectively, which are smaller comparatively. This is attributed to several factors: 1) lack of conjugation in the backbone lacks π - π interactions, and 2) bulky allylic side chains twist the backbone into a non-planar conformation. In the minimized geometry majority of the atoms are far from van der Waals interaction range from SWNT surface (Figure 5d).



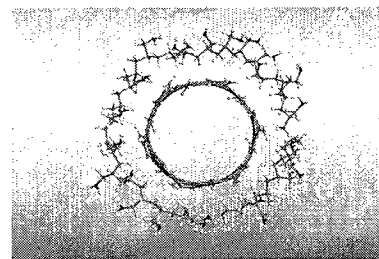
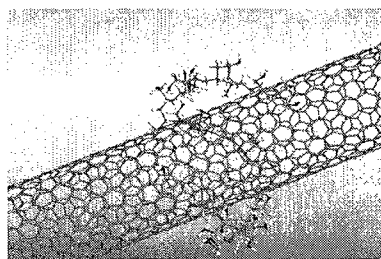
a) Minimised structure of SWNT-poly(ethyl thiophene-3-acetate) composite



b) Minimised structure of SWNT-polyaniline composite



c) Minimised structure of SWNT-polyvinyl alcohol composite



d) Minimised structure of SWNT-polyallylamine composite

Figure 5 Minimized structures of SWNT-polymer composites

Select minimized polymer-wrapped structures are provided in Figure 5. The orientation of the backbones of poly(ethyl thiophene-3-acetate) and polyaniline indicates clear association between the π -system of nanotube and π -system (and lone pairs of hetero atom) of the polymers.

Polymer was submitted to SWNT in a single job with full length for these calculations. Analysis of optimized SWNT-polymer composite structures revealed conformation locking in non-global minima. So, in the next section, a better approach is presented where length of the polymer was gradually increased after each minimization. This approach increases the chances for reaching a global minimum for the SWNT-polymer composite. More diverse polymer types were considered in the new calculations to order to obtain a greater understanding of the interactions. As expected improved interaction energy values were obtained with the new approach.

2.4 Interaction Energy 2

The following modifications were made to improve the polymer-nanotube interaction energies and final conformations of the polymer on SWNT surface.

- Increased the length of the SWNT to avoid edge effects on interaction energies
- Length of the polymer was gradually increased starting with 5 repeat units to 25 repeat units with an increment of 5 repeat units each time, with the structures minimized before each increment.

Gradual increase in length of polymer after a minimization increases the chances for reaching a global minimum for the SWNT-polymer composite. More polymer types were considered in these calculations.

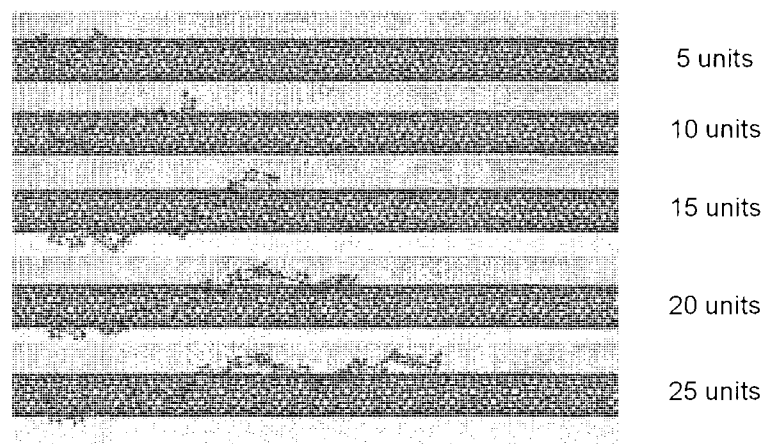


Figure 6 Stepwise increase of polymer strand on SWNT

We constructed different polymers having up to 25 repeat units from corresponding monomers using polymer builder and nanotube was constructed using nanotube builder of the Materials Studio program package (Accelrys, Inc., San Diego CA). A chiral carbon nanotube (12,6) that corresponds to tube diameter of 12.43 Å was used. The length of the nanotube was set to 202.88 Å with outer carbon atoms saturated with hydrogen, and it is composed of 3060 carbon atoms. List of constructed polymers are shown in table Table 5. Structures are minimized using previously used settings, but minimized each time after 5 repeat unit increment of the polymer. Total potential energy of the final structure was used for IE calculations.

Table 5 List of constructed polymers

| Constructed polymers |
|---------------------------------|
| poly(ethyl thiophene-3-acetate) |
| poly(allylaminehydrochloride) |

| |
|-------------------------------|
| polyaniline |
| emeraldine base |
| poly(allylamine) |
| poly(thiophenesulfonic acid) |
| poly(vinyl alcohol) |
| poly(sodiumstyrene sulfonate) |
| poly(ethylene glycol) |
| dextran |

Interaction energies were calculated using Equation 7 and obtained IEs are shown in Table 6. Interaction energy values from method1 and method2 are compared in Table 7. (In method1 polymer was presented to nanotube as a long chain and in method2, polymer was grown in 5 unit increments following each minimization.)

Table 6 Interaction energy values with vdW and electrostatic components

| Polymer | Interaction Energy (25 units) | vdW | Electrostatic |
|--------------------------------|--------------------------------------|------------|----------------------|
| Poly(ethyl-3-thiopheneacetate) | -307.84 | -329.35 | 1.81 |
| Polyaniline | -193.94 | -203.75 | 11.14 |
| Polyvinyl alcohol | -91.41 | -88.22 | -2.78 |
| Polyallylamine | -64.70 | -73.44 | 3.22 |
| Polyethyleneglycol | -107.03 | -107.94 | 0.034 |
| Dextran | -141.34 | -175.58 | 28.05 |
| Poly(sodiumstyrenesulfonate) | -220.87 | -138.73 | -95.57 |
| Emeraldine base | -225.86 | -228.14 | -0.01 |
| Poly(thiophenesulfonicacid) | -630.45 | -365.84 | -273.98 |
| Poly(allylaminehydrochloride) | -65.42 | -70.00 | -0.51 |

Carbon atoms on the nanotube are covalent in nature. So the electrostatic interactions are much smaller than the van der Waals interactions for polymers not having ionic components (Table 6). But there is a significant attractive electrostatic interaction with SWNT for poly(thiophenesulfonicacid) and poly(sodiumstyrenesulfonate) due to the presence of H^+ and Na^+ ions respectively. Na^+ ions are known to interact well with SWNTs [51]. There is a repulsive electrostatic interaction for dextran possibly due to internal repulsions between charged groups in the structure.

Table 7 Comparison of interaction energy values from method1 and method2.

| Polymer | Interaction energy (kcal/mol) (25 units) | |
|---------------------------------|---|----------|
| | Method 1 | Method 2 |
| Poly(ethyl-3-thiophene acetate) | -186.00 | -307.83 |
| Polyaniline (neutral) | -176.00 | -193.93 |
| Poly(ethyleneglycol) | -84.75 | -107.02 |
| Poly(vinyl alcohol) | -60.83 | -91.4 |
| Poly(allylamine) | -8.67 | -64.69 |
| Poly(sodiumstyrenesulfonate) | - | -220.87 |
| Dextran | -157.50 | -141.34 |
| PTsulfonic acid | - | -630.45 |
| Emeraldine | - | -225.85 |
| Poly(allylamine)(HCl) | - | -65.42 |

Minimized structures of SWNT-polymer composites are shown in Figure 7, where a) PTsulfonic acid, b) emeraldine, c) poly(ethyl-3-thiophene acetate), d)

polyaniline, e) poly(sodiumstyrenesulfonate) f) dextran g) poly(ethyleneglycol) h) poly(vinyl alcohol) i) poly(allylamine) and j) poly(allylamine)(HCl). There is an obvious improvement in the interaction energy values from method 1 to method 2 (Table 7) and also there is an improvement in the conformation of polymers around SWNT (Figure 7).

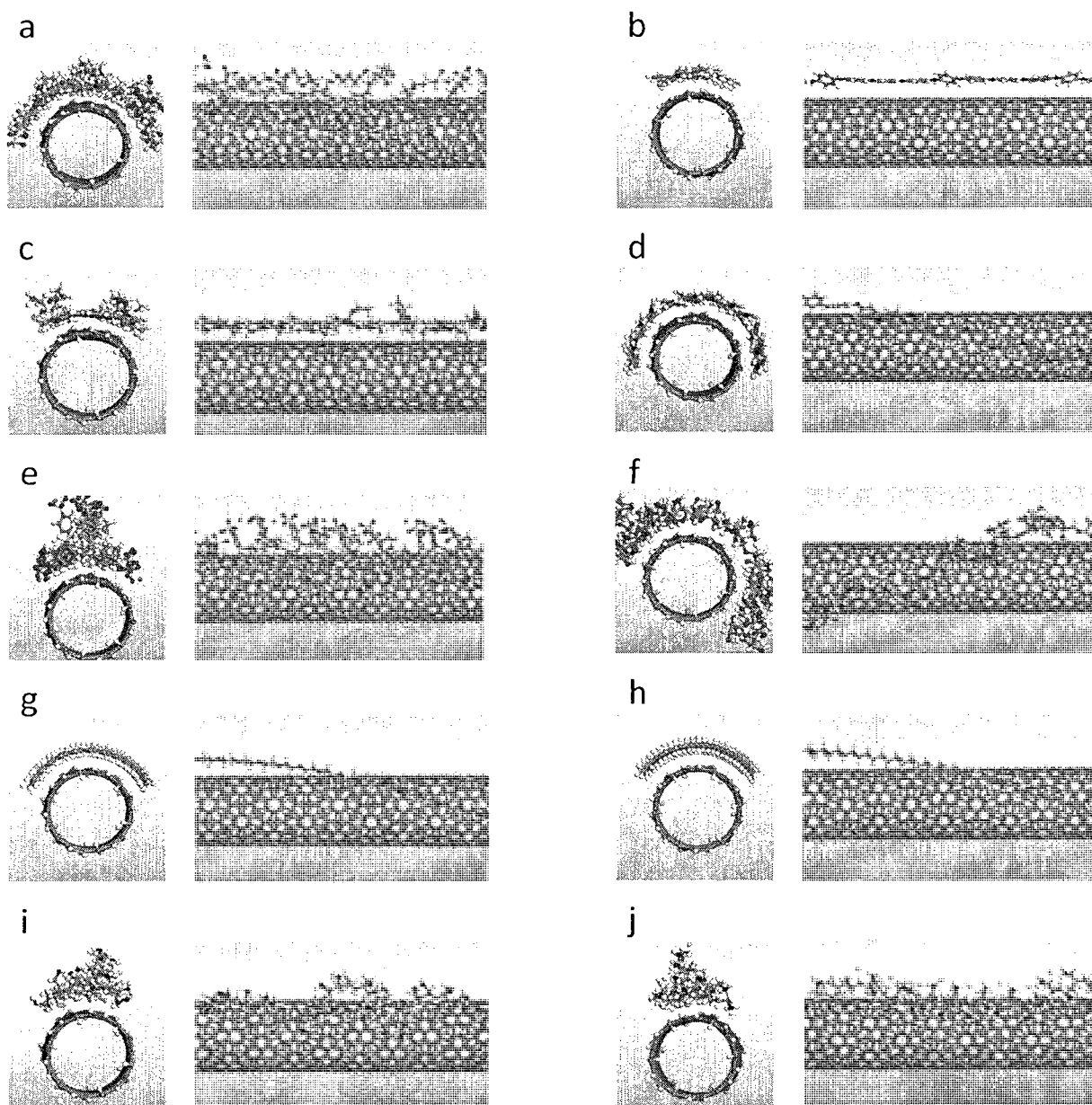


Figure 7 Optimized geometries of polymer-nanotube composite structures

This is because when the polymer is submitted as one big single strand (method 1), there is a possibility for getting trapped in a high energy local minima. But when the polymer is added in incremental fashion the chances of reaching low energy global minima is considerably increased. Only a small improvement of IE is there for polyaniline. This is because of the rigid flat conformation of the polymer, which is always close to global minima. Big improvements of IEs are observed for polymers having flexible backbones or for polymers having flexible side chains. These polymers have a tendency to be locked in a local conformation when submitted at full length.

2.4.1 Morphology of Polymers on SWNT Surface

We investigate the morphological aspects of polymer-SWNT interactions on the local level, where the focus was on the arrangement of the backbone of the polymer with

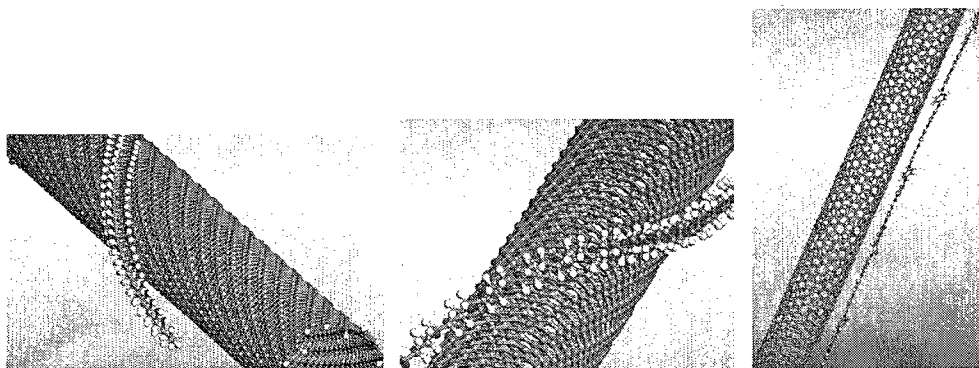


Figure 8 Arrangement of polymer strands on SWNT surface after energy minimizations

respect to the hexagons that constitute nanotube surface. The atomic arrangement of carbon atoms in the backbone of conjugated polymers is isomorphic to their hexagonal arrangement in graphite sheets. Aromatic rings are therefore expected to possess a strong attractive interaction with the surface of the SWNTs and may play an important role in

providing effective adhesion. The same kind of isomorphism is responsible for the strong tendency of SWNTs to stick together. To calculate the relative arrangement of polymer aromatic rings with respect to the SWNT surface, the dihedral angles between the SWNT surface and the plane of the aromatic rings were calculated, Figure 9.

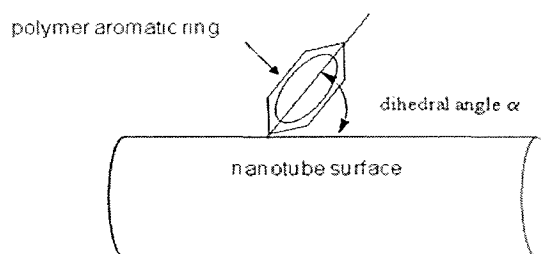


Figure 9 Schematic representation of dihedral angle measurement

The equilibrium separation between the aromatic polymer chain and the wall of SWNT is slightly above 3 Å. Dihedral angle, α is defined as the angle between hexagons of SWNT and aromatic rings of polymers directly above the hexagons. Angles were calculated using plane equations. The equations of the planes passing through the hexagons of SWNT were obtained from three points on each hexagon. The equations of the planes passing through the aromatic rings of polymers were obtained in a similar fashion from three points on each aromatic ring. The dihedral angle between the two planes, α is expressed as shown in Equation 8.

$$\cos\alpha = \hat{n}_1 \cdot \hat{n}_2 = \frac{a_1a_2 + b_1b_2 + c_1c_2}{\sqrt{a_1^2 + b_1^2 + c_1^2} \sqrt{a_2^2 + b_2^2 + c_2^2}} \quad \text{Equation 8}$$

After obtaining dihedral angles, plots were made for angle probability vs dihedral angle. Aromatic rings of the polymer are said defined as perfectly parallel to SWNT if the dihedral angle is 0° or 180° . A dihedral angle of 90° indicates perpendicular alignment of

aromatic rings of polymer. For example, a dihedral angle of 5° is same as the dihedral angle of 175° . Each of the polymers containing an aromatic ring is analyzed in this fashion, and the results are presented in the following section.

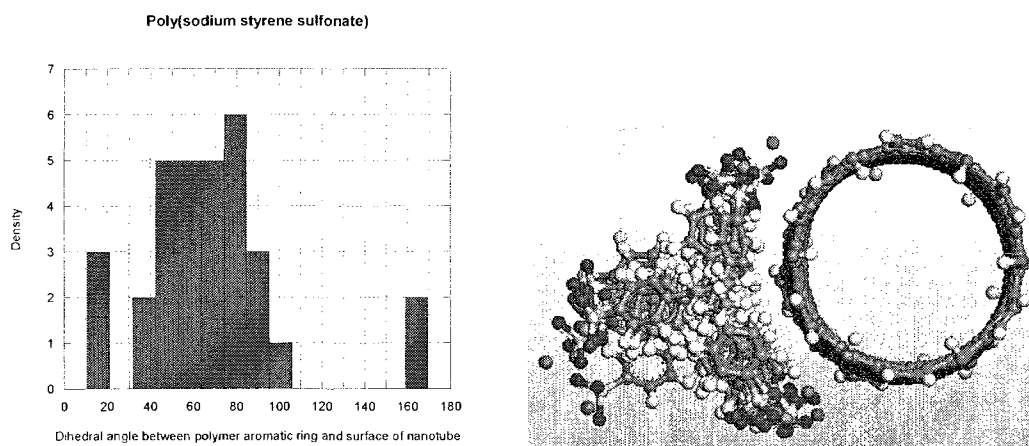


Figure 10 Probability vs dihedral angle plot for poly(sodium styrene sulfonate)

The aromatic rings of PSS are not present in the polymer's backbone, so they do not orient parallel to the surface of SWNT for better interaction. Instead they align parallel to each other thereby minimizing the total energy of the system. Due to steric repulsions, the aromatic rings of PSS formed into three sets, and there is an interaction between the rings of each set. Aromatic rings closer to the surface of SWNT are not parallel and interact sideways with SWNT. As a result, only a few aromatic rings align approximately parallel to SWNT, which is indicated by the peaks between $10\text{-}20^\circ$ and $160\text{-}170^\circ$ in the Figure 10.

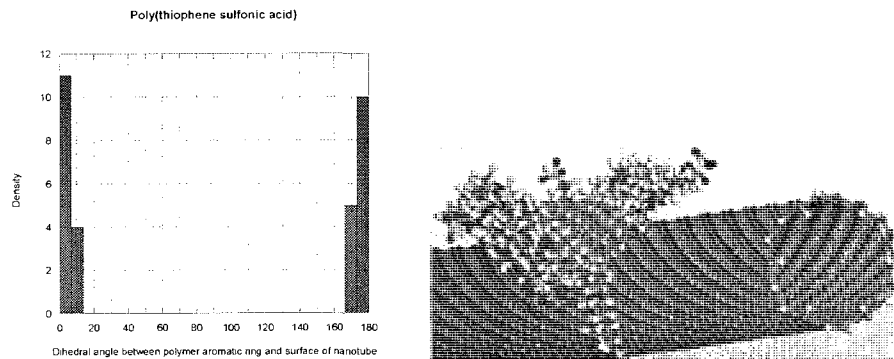


Figure 11 Probability vs dihedral angle plot for poly(thiophene sulfonic acid)

Poly(thiophene sulfonic acid) has a flexible thiophene backbone, and it aligns parallel to the surface of SWNT. Contrary to PSS, aromatic rings of poly(thiophene sulfonic acid) are located in the backbone of polymer, which can orient parallel to SWNT. The thiophene rings in the backbone have a permanent dipole due to the presence of the sulfur atom, and it generates attractive interaction between adjacent thiophene rings. Due to this reason poly(thiophene sulfonic acid) tends to follow the spiral arrangement of carbon atoms on the surface of SWNT. Perfect parallel alignment of thiophene rings is indicated by the presence of major peaks between $0-5^\circ$ and $175-180^\circ$ (Figure 11).

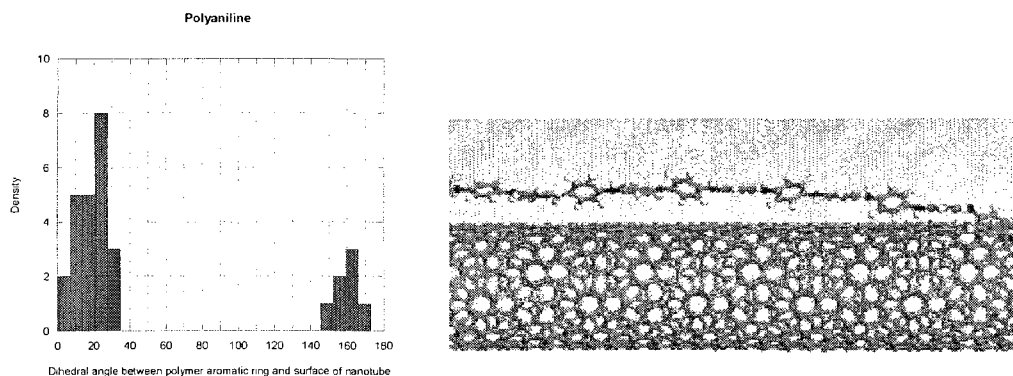


Figure 12 Probability vs dihedral angle plot for polyaniline

Polyaniline (fully reduced form) has aromatic rings connected by sp^3 hybridized nitrogen atoms. Many of the aromatic rings of the backbone cannot come parallel to the surface of SWNT due to angle strain at the nitrogen atom (Figure 12). Some of the Ph rings align parallel, the remaining interact sideways with SWNT. This misalignment is indicated by broad peaks between $0-35^\circ$ and $145-180^\circ$ (Figure 12).

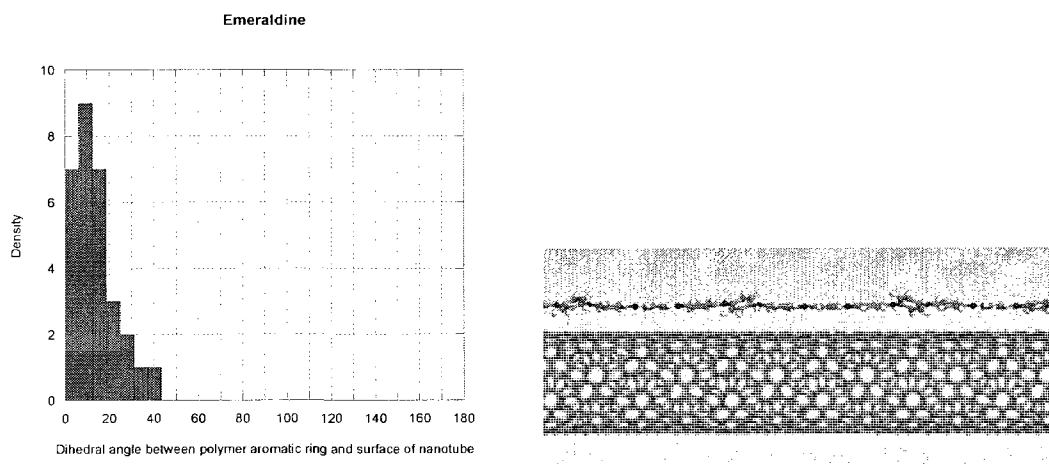


Figure 13 Probability vs dihedral angle plot for emeraldine

Emeraldine (50% oxidized form polyaniline) has two types of nitrogen atoms in the backbone. Half of the nitrogen atoms are sp^2 hybridized and remaining half are sp^3 hybridized. Sp^2 hybridized nitrogen atoms in the backbone connect to nearby phenyl ring by a double bond and bring planarity to the backbone (Compare Figure 12 and Figure 13). In the case of emeraldine more of phenyl rings come parallel to the surface of SWNT when compared to polyaniline. This better alignment is indicated by major peak between $5-10^\circ$ (Figure 13).

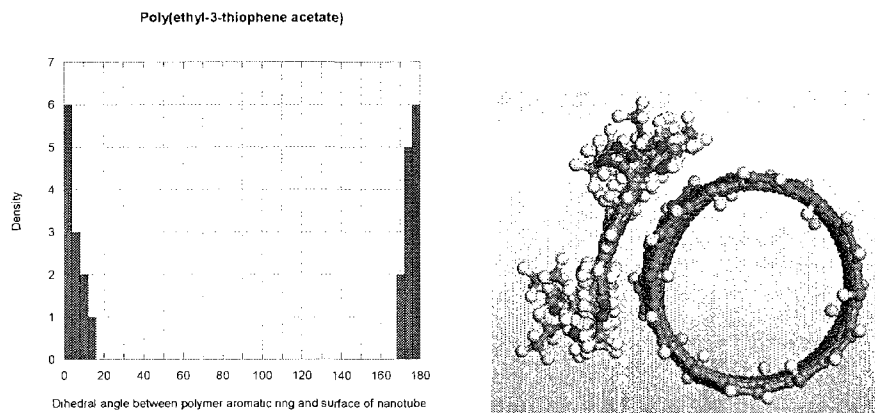


Figure 14 Probability vs dihedral angle plot for poly(ethyl-3-thiophene acetate)

Similar to poly(thiophene sulfonic acid), poly(ethyl-3-thiophene acetate) has a flexible backbone. Thiophene rings of poly(ethyl-3-thiophene acetate) align parallel to the surface of SWNT due to strong π - π interactions. As mentioned previously, a permanent dipole in the thiophene rings provides for a strong interaction between adjacent thiophene rings and alignment with SWNT. When compared to poly(thiophene sulfonic acid), poly(ethyl-3-thiophene acetate) has smaller side chains, which enables better flexibility and alignment. This is indicated by major peaks between 0-5° and 175-180°.

Interaction energy per 100 atoms of polymer

Interaction energy per 100 atoms of each polymer was calculated to obtain a better understanding of the nature of interactions. If the simulated polymers have a comparable number of atoms, the magnitude of the interaction energy gives a direct measure of the strength of their binding to the SWNT. Table 8 shows that the specific monomer structure plays a very important role in determining adhesion to the SWNT. All the polymers with aromatic rings in the backbone (conjugated polymers) have stronger

interactions with the SWNTs than those either with side group aromatic rings (PS) or non-conjugated polymers.

Table 8 Interaction energies for 100 atoms of polymer

| polymer | # atoms/25 units | IE/25 units | IE/100 atoms |
|----------|------------------|-------------|--------------|
| PTester | 477 | -307.83 | -64.53 |
| PANI | 302 | -193.93 | -64.22 |
| PVA | 177 | -91.40 | -51.64 |
| PAA | 277 | -64.69 | -23.35 |
| PEG | 178 | -107.02 | -60.12 |
| Dextran | 528 | -141.34 | -26.77 |
| PSS | 502 | -220.87 | -44.00 |
| PTacid | 752 | -630.45 | -83.84 |
| PAA(HCl) | 327 | -65.42 | -20.01 |
| EMER | 290 | -225.85 | -77.88 |

Polythiophene sulfonic acid (PTsulfonic acid) has highest interaction energy (-83.84 kcal/mol) due to the presence of a flat conjugated backbone. A flat conjugated backbone provides π - π interactions and draws more atoms closer to the surface of SWNT (Van der Waals interactions are short range and decrease at a rate of $1/r^6$). PTsulfonic acid also has side chains that can align parallel to the surface of SWNT. Similarly emeraldine (50% oxidized form of polyaniline) has a very high interaction energy (-77.88 kcal/mol) due to its flat conjugated backbone. Polyaniline in the reduced form has a slightly lower interaction energy of -64.22 kcal/mol due to strain in pyramidal 'N' atoms (reduced form has 50% more pyramidal 'N' atoms, which prevent perfect planarity). Non-conjugated PAA and PAA(HCl) have very low interaction energy values (-23.35 and -20.01 kcal/mol respectively) due to irregular conformation around SWNT, causing atoms to reside farther from the surface of SWNT. Similarly dextran and PSS

have several of their atoms far from the surface of SWNT and have low interaction energies (-26.77 and -44.00 kcal/mol respectively).

2.4.2 Normalized Interaction Energies Per Unit Contact Area

Interaction energies between SWNT and polymers were calculated per unit contact area of the polymer. Interaction energy per unit contact area of polymer is a direct measure of binding energies of polymers with SWNT. Small polymers are expected to give low interaction energy values, whereas big polymers give high interaction energy values.

Accessible surface area for (12,6) SWNT on each polymer were calculated assigning a Connolly diameter equal to the diameter of SWNT. This gives the surface area that would be accessible for SWNT used in the calculations. This feature is generally used to calculate surface areas and volumes accessible to a solvent or other molecule (spherical).

The accessible surface is traced out by a probe sphere center as it rolls over the molecule. It is analogous to an expanded van der Waals surface. The union of the expanded atoms is what is called the solvent-excluded volume, and it is the region enclosed by the accessible surface. The diameter of the probe is important in this case, because it affects the measured area, Figure 15.

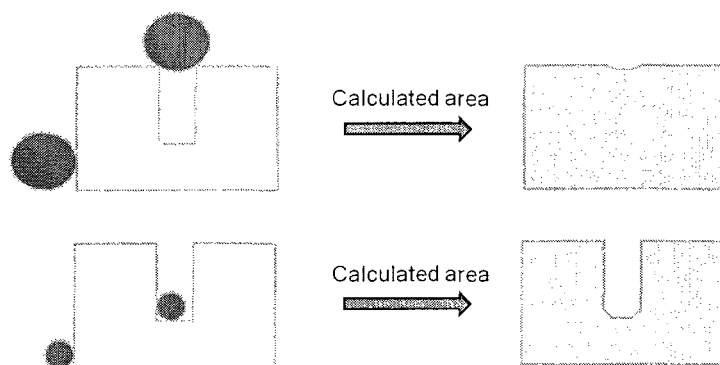


Figure 15 Schematic showing measurement of Connolly or accessible surface area

The contact surface area between SWNT and polymer strands was measured as described below. Surface areas were measured for (SWNT + polymer) composite, for polymer strand alone, and for SWNT alone (Figure 16). Contact surface area was determined using Equation 9.

$$\text{Contact surface area} = \frac{(\text{Area}_{\text{SWNT}} - \text{Area}_{\text{Polymer}}) - \text{Area}_{\text{Composite}}}{2} \quad \text{Equation 9}$$

$\text{Area}_{\text{SWNT}}$ is the surface area of SWNT alone, $\text{Area}_{\text{Polymer}}$ is the surface area of polymer alone, and $\text{Area}_{\text{Composite}}$ is the surface area of (SWNT + polymer) composite. Select Connolly surface areas of polymer strands are shown in Figure 17.

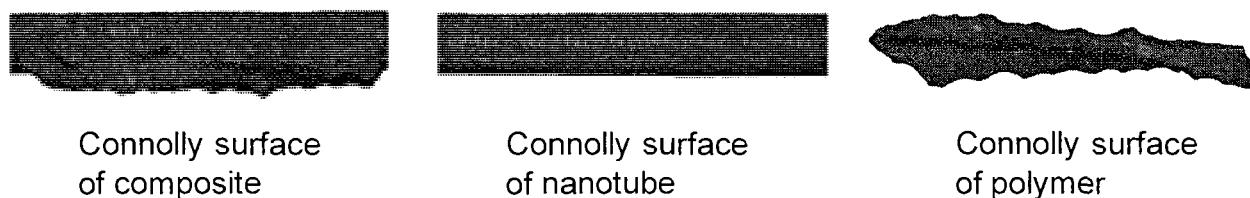


Figure 16 Figures showing Connolly surfaces of composite, nanotube, and polymer

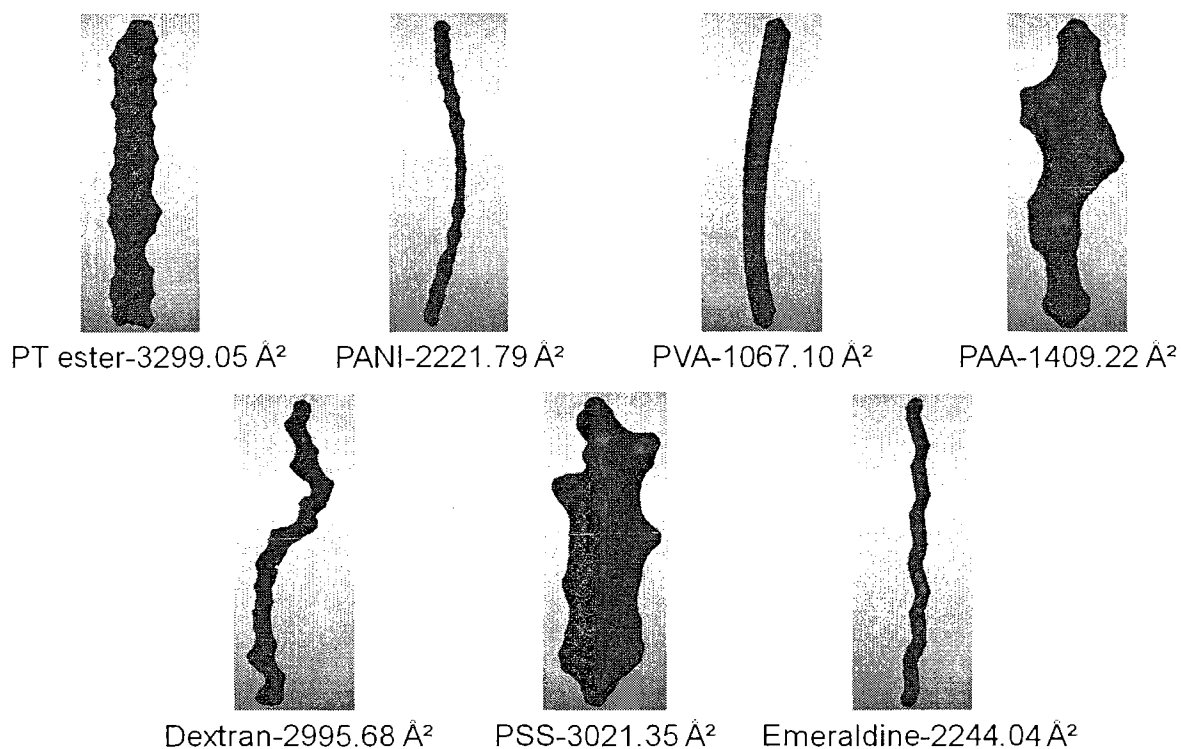


Figure 17 Connolly or accessible surface areas of polymer strands

Table 9 Interaction energies normalized for contact area

| Polymer | SWNT Surface Area | Polymer Surface Area | Total Surface Area | Contact Surface Area | I.E./100 sq A° Contact Area |
|-----------------|-------------------|----------------------|--------------------|----------------------|-----------------------------|
| PTester | 7563.41 | 3299.05 | 8704.79 | 1078.84 | -28.53 |
| PANI | 9727.06 | 2221.79 | 10528.48 | 710.19 | -27.31 |
| PEG | 7103.60 | 1332.69 | 7636.05 | 400.12 | -26.75 |
| PVA | 5280.45 | 1067.10 | 5706.97 | 320.29 | -28.54 |
| PAA | 4084.88 | 1409.22 | 4789.83 | 352.14 | -18.37 |
| PSS | 4916.52 | 3021.35 | 6445.87 | 746.00 | -29.61 |
| Dextran | 8284.46 | 2995.68 | 9766.63 | 756.76 | -18.68 |
| PTsulfonic acid | 7217.35 | 4435.35 | 8767.69 | 1442.51 | -43.71 |
| Emeraldine | 10058.41 | 2244.04 | 10812.63 | 744.91 | -30.32 |
| PAA(HCl) | 4616.76 | 1694.88 | 5469.85 | 420.90 | -15.54 |

Surface areas of SWNT, polymer strands and contact surface areas are shown in Table 9 along with interaction energy for 100 sq A° of contact area. Similar to previous

results, conjugated polymers have high calculated interaction energy values due to π - π interactions. PTester has a backbone with thiophene rings, which have a permanent dipole generating strong interaction between adjacent thiophene rings and the polymer aligns parallel to SWNT surface. Its thiophene backbone interacts strongly with SWNT surface, but its side chains do not, leading to an interaction energy of -28.53 kcal/mol per 100 Å^2 of contact area. PTsulfonic acid has the highest interaction energy per 100 Å^2 of contact area. Similar to PTester, its thiophene backbone has a very strong interaction with the SWNT surface. PANI has π - π interactions with SWNT due to its conjugated backbone, as expected it has a reasonably high calculated interaction energy. All nitrogen atoms in PANI are sp^3 hybridized, but 50% of emeraldine nitrogen atoms are sp^2 hybridized. The sp^2 hybridized nitrogen atoms in emeraldine reduce angle strain and let the polymer align parallel to the surface of SWNT. Emeraldine has a higher interaction energy compared to analogous polyaniline. Even unconjugated polymers (PVA, PEG) have considerable interaction energies due to the presence of permanent dipoles in the structures. Polyallylamine and polyallylamine hydrochloride have low interaction energy values. These polymers have bulky allyl side chains, which make the polymer twist in an irregular fashion. Due to this reason, atoms reside at a distance from the surface of SWNT in the most stable conformation. Van der Waals interactions are sensitive to distance and decrease at a rate of $1/r^6$. These polymers therefore have very low interaction energy values.

2.5 Required Polymer for Two Unit Long (12,6) SWNT

Required number of polymer repeat units (RPU) for two unit long SWNT, is the number of repeat units of polymer that is required to cover the surface of a two unit long (12,6) SWNT. RRU is different for different polymers due to the differences in the size of repeat units. In order to calculate RPU and number of strands for different polymers, a stepwise docking process was used which involved addition of polymer strands to (12,6) SWNT and minimizations. For these optimizations a short SWNT (2 repeat unit long with hydrogen termination at both ends) was considered to be able to run the jobs in reasonable amount of time.

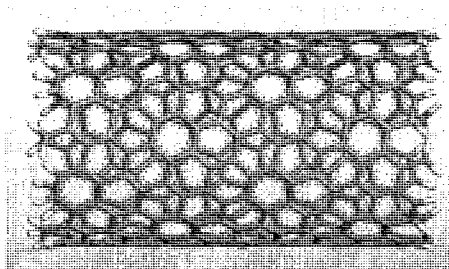


Figure 18 Two unit long nanotube with hydrogen termination

Details of structures: Two repeat units long (12,6) SWNT with 'H' termination at both ends was constructed using nanotube builder. The resulting tube has a length of 22.54 Å, and a diameter of 12.43 Å (Figure 18). Polymer strands were constructed using polymer builder with a length needed to cover the SWNT (lengths vary depending on orientation of polymer on SWNT surface).

Polymer strands were added to SWNT after each minimization until the surface was covered with a monolayer of polymer. Figure 19 shows insufficient number of strands in (a) and (b) and excessive number of strands in (c). When a polymer strand was

added in excess to SWNT (which is confirmed after optimization), one strand was removed and the structure was reoptimized.

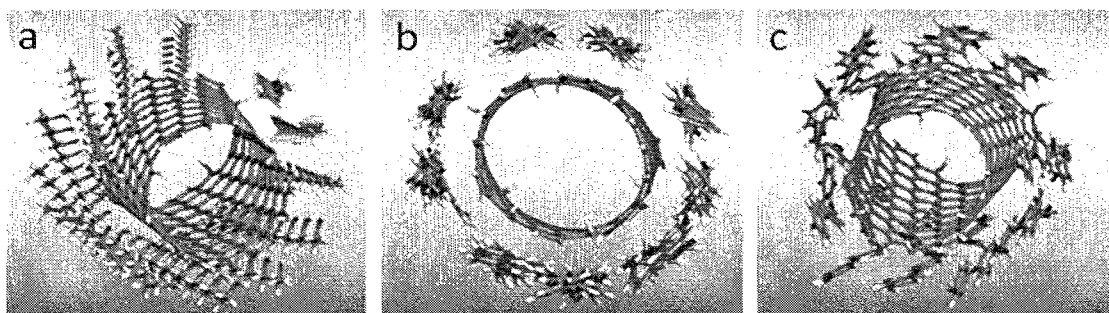


Figure 19 Stepwise addition of polymer strands to SWNT

COMPASS forcefield was used for these optimizations with the non-bonded interactions cutoff set to a distance of 15.5 Å, accompanied by a spline width of 5.0 Å and a buffer width of 2.0 Å.

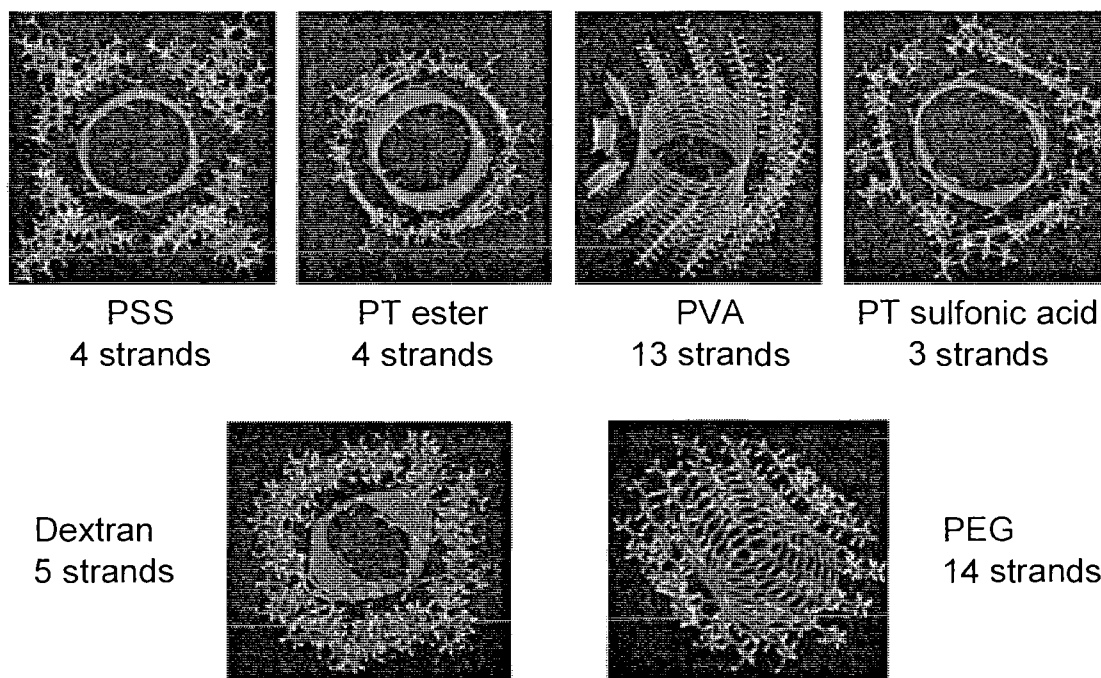


Figure 20 Some optimized geometries of two unit (12,6) SWNT with full polymer coverage

Table 10 Required number of polymer strands and polymer repeat units

| Polymer | Required polymer units for 2 units long SWNT | Number of strands |
|------------------|--|-------------------|
| PTester | 28 | 4 |
| PANI | 36 | 9 |
| PEG | 84 | 14 |
| PVA | 117 | 13 |
| PAA | 66 | 6 |
| PSS | 44 | 4 |
| Dextran | 55 | 5 |
| EMER | 36 | 9 |
| PT sulfonic acid | 21 | 3 |

Only three strands of polymer is required in case of poly(thiophene sulfonic acid), and four strands for PSS and PTester due to big size repeat units (Table 10). 14 strands of polymer is required for PEG and 13 strands of polymer is required for PVA. This information is used for the explanation of experimental dispersion abilities of polymers in the later sections.

2.6 Interactions-Solvent Effects

Solvent interactions are calculated using VAMP from heats of formation of polymer strands in vacuum and in solvent (water). Four water soluble polymers, PEG, PVA, PSS, dextran, and poly(thiophene sulfonic acid) were used in the calculations. When the ionic groups of the polymers were replaced with hydrogen, there is a considerable change in interaction energy with solvent.

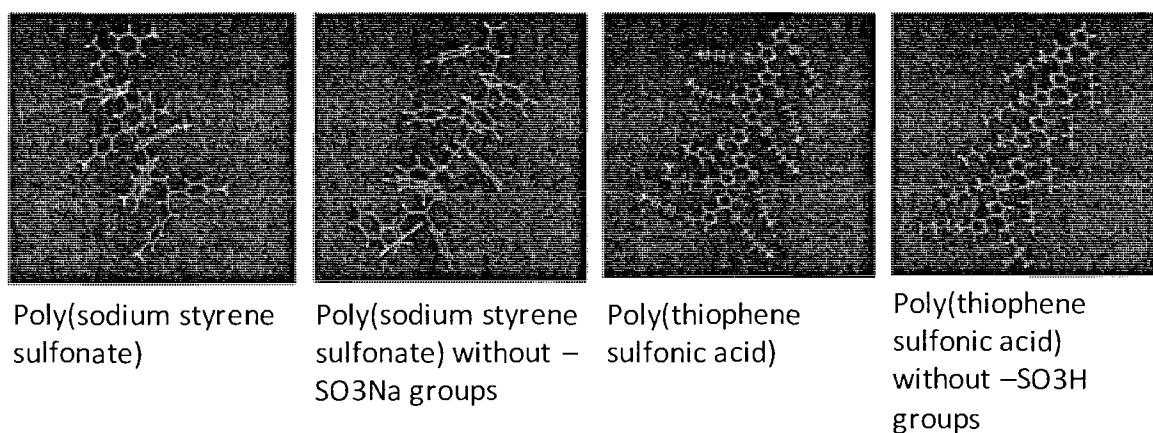


Figure 21 Polymer strands with ionic groups and with hydrogen atoms in place of ionic groups

Interaction of polymer strands with water gave additional information about dispersing polymers. This information was used for the explanation of poor dispersion ability of PVA and PEG, despite the prediction of modest interaction energies.

Table 11 Water interactions with polymer strands with and without ionic groups

| polymer | Required repeat units (RRU) | I.E. with water for (RRU) (Kcal/mol) | I.E. with water without ionic functionality (Kcal/mol) |
|------------------|-----------------------------|--------------------------------------|--|
| PEG | 84 | -336.25 | NA |
| PVA | 117 | -457.42 | NA |
| PSS | 44 | -2106.50 | -112.04 |
| Dextran | 55 | -785.64 | NA |
| PT sulfonic acid | 21 | -1004.41 | -87.94 |

Water interactions were calculated for each polymer for required number of repeat units (RPU). RRU is the number of repeat units that is required to cover the surface of a two unit long (12,6) SWNT. RRU is different for different polymers due to the differences in the size of repeat units. Polymer water interactions indicate that polyvinyl alcohol and polyethyleneglycol have stronger interaction with water than with

the SWNT. Previous calculations indicated that PVA and PEG have strong interaction with SWNT and their interaction energies are comparable with that of polythiophenes and polyanilines. But their interaction with water is much higher than their interaction with SWNT. So, in a solution, PVA and PEG prefer to stay in water than on the surface of SWNT.

Interaction energies of PSS and PTsulfonic acid with water (with and without ionic functionality) indicate that their interaction is dominated by the ionic groups. These results indicate that a polymer with hydrophobic backbone and ionic functional groups would be a better dispersing polymer, when two polymers with similar interaction energies are compared (for water solutions).

2.7 Conclusions

In conclusion polymer nanotube interaction energy calculations provided valuable information about wrapping polymers. Polymers having conjugation or aromatic rings in the backbone are best candidates for SWNT dispersion. Among the conjugated polymers, polymers having hetero atoms in the backbone have stronger interactions with SWNT surface. Conjugated polymers with hetero atom (thiophene unit) have permanent dipole due to electronegativity difference between hetero atom and the carbon atoms. Permanent dipoles of the polymer, conjugation, and the side chains generate a rod like structure and enhance the attraction between tube and polymer. A majority of the interaction is van der Waals with little electrostatic contribution. The flat backbone of these polymers provides for a closer association to SWNT surface and gives high vdW interaction.

Van der Waals interactions are relatively short range, decreasing at a rate of $1/r^6$. This effect results in low interaction energy values for polymers such as polyallylamine and polyallylamine hydrochloride. Bulky allyl substituents on alternate carbons of these polymers give an irregular shape. In the minimum energy conformation, the majority of the atoms are distant from SWNT surface. This gives low vdW interaction and thus low total interaction with SWNT. Other relevant calculations on various IE values are listed in the appendix in Table 36 to Table 39.

Polymers such as PEG and PVA have high calculated interaction energy values and are predicted to pack very efficiently around SWNT due to the absence of side chains and flexible backbones. Solvent interaction energy calculations reveal that they have much higher interaction with water than with SWNT. These details are discussed in next section after experimental SWNT dispersions.

2.8 Experimental Dispersion of SWNTs

2.8.1 Introduction

Incorporation of SWNTs into a polymer matrix is a significant challenge, because as-produced single wall nanotubes (SWNT) are held together in bundles of 50 to a few hundred individual SWNTs by very strong van der Waals interactions. Researchers have demonstrated that bundling results in diminished mechanical and electrical properties when compared to theoretical predictions related to individual SWNTs.

Several methods involving the polymer-wrapping technique are commonly used, such as dispersing the SWNT directly in a polymer solution via sonication and direct mixing [52, 53] and dispersion of the SWNTs in a surfactant solution to which the

polymer is added [54]. These methods have their advantages: they do not disrupt the primary structure of the tube, improve both solubility and processibility, facilitate characterization, and allow the final polymer-tube nanocomposite to be coupled to other materials [55]. The only disadvantage is that to achieve successful polymer wrapping, high ratios of polymer to SWNT have to be used [55].

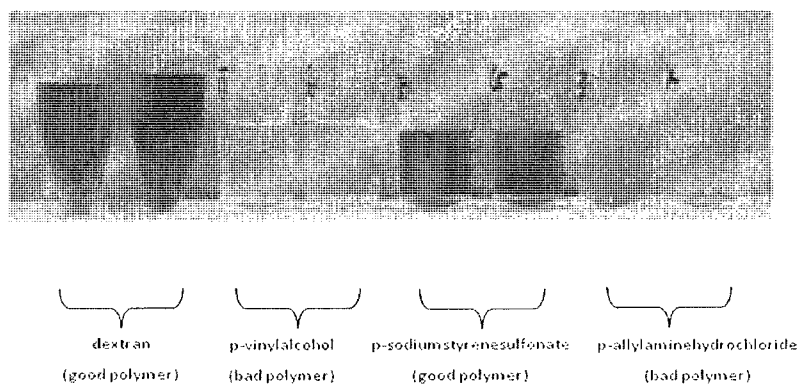
Several studies have been published on polymer wrapping with the use of conjugated polymers [55], biological molecules [56], and starches [57]. However, all of the previously published studies have been performed using a trial-and-error approach. A priority of this project is to replace this trial-and-error method with an “intelligent design” by using molecular modeling to calculate the specific interactions between wrapping polymers and SWNTs. Results of theoretical studies are subsequently used to aid in experimental design. Therefore, providing experimental support to theoretical investigations of polymer-nanotube interactions is the goal of the work in this section.

2.8.2 Experimental Details

2.8.2.1 Dispersion and polymer wrapping utilizing direct mixing and sonication

Using a modified literature procedure [52, 53], six 0.5% (w/w) polymer solutions were prepared from dextran ($M_w \sim 1,500$, Fluka, 31394), poly(vinyl alcohol) (87-89% hydrolyzed, $M_w \sim 13,000-23,000$, Sigma-Aldrich, 363170), poly(sodium 4-styrene-sulfonate) ($M_w \sim 70,000$, Aldrich, 243051), poly(allylamine hydrochloride) ($M_w \sim 15,000$, Aldrich, 283215), polythiophene acid ($M_w \sim 100k-1000k$, American Dye Source, Inc., ADS2000P), and polyethylene glycol (~50% in H_2O , $M_w \sim 20,000$, Fluka, 87006). Between 1.10 mg and 1.14 mg of short, single-walled carbon nanotubes (Aldrich,

652512, 90% purity) were measured into 1.5 mL centrifuge tubes (Fisherbrand, Cat No. 05-408-129) and dispersed with 1 mL of the 0.5% (w/w) polymer solutions. The dispersions were sonicated for 50 min. in an ultrasonic cleaner (Fisher Scientific, FS30). After sonication, the solutions were spun at 2400 x g for 50 min. in a Mikro 22 centrifuge (Hettich Zentrifugen, 1105-01). The supernatants were then separated from the precipitated unwrapped SWNTs and transferred into new centrifuge tubes. This process was repeated three more times to precipitate out any unwrapped or wrapped bundles of SWNTs that still remained in solution. The final supernatants were then drawn off and put into clean centrifuge tubes, then centrifuged at 22000 x g for 3 hrs. to precipitate the polymer-wrapped SWNTs. The supernatants were removed from the centrifuge tubes, and the precipitated polymer-wrapped SWNTs were studied using Transmission Electron Microscopy (TEM) analysis.



Experimental polymer capacity study: dark coloration represents dispersed SWNTs. Above samples were photographed after removing unwrapped SWNTs using centrifugation.

Figure 22 Dispersed SWNTs in polymer solutions

2.8.2.2 Dispersion and polymer wrapping with the aid of surfactants

Using a modified literature procedure [54], approximately 25 mg of short, single-walled carbon nanotubes were measured into 4 oz glass jars and dispersed with 50 mL of a 1% (w/w) sodium oleate (~95% capillary GC, Sigma, O3880) solution. The solutions were sonicated for 50 min in an ultrasonic cleaner (Fisher Scientific: FS30). The resulting dispersions were high-shear mixed at 1200 rpm for 50 min. using a Eurostar power-control visc overhead mixer/stirrer (IKA[®]Werke: 2600000) fitted with an R 1303 dissolver stirrer (IKA[®]Werke: 2746700). Approximately 500 mg of a polymer, poly(sodium 4-styrene-sulfonate), poly(vinyl alcohol), polythiophene acid, or polyethylene glycol, was then added to the solutions along with a stir bar. The solutions were then sonicated for 50 min, held in a 50°C oil bath for 50 min, sonicated for 50 more min, and finally held in the temperature-controlled oil bath to rest for 12 hrs.

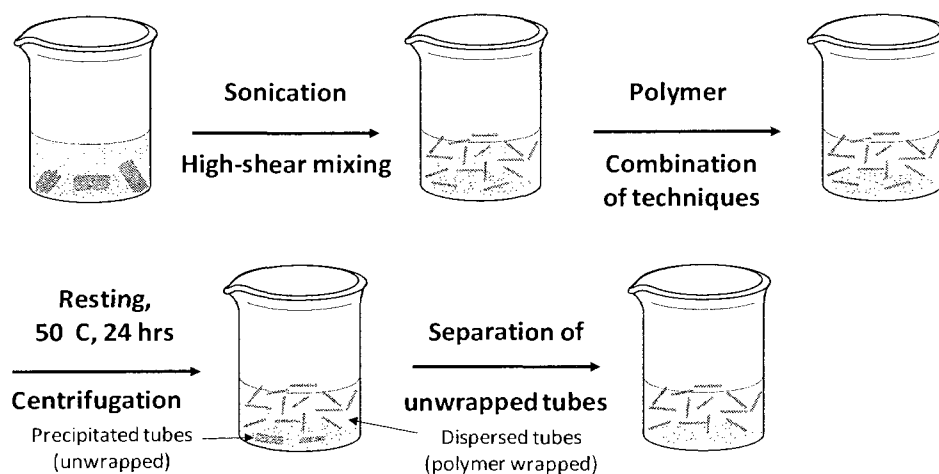


Figure 23 General method used for the large scale dispersion of SWNTs

Once the resting period was completed, the suspensions were allowed to cool to room temperature; after which they were separated into 2 mL natural flat top

microcentrifuge tubes (Fisherbrand: Cat No. 05-408-138). The samples were centrifuged at 2400 x g for 10 min. in a Mikro 22 centrifuge (Hettich Zentrifugen: 1105-01). The supernatants were separated from the precipitated unwrapped SWNTs and transferred into clean centrifuge tubes, after which they were centrifuged at 2400 x g for an additional 10 min. The supernatants were decanted off from the precipitate into clean tubes, and the resulting solutions were then centrifuged at 22000 x g for 3 hrs to precipitate the polymer wrapped SWNTs.

The supernatant was pipetted off and saved, then the remaining solutions of wrapped SWNTs were poured into 50 mL round-bottomed polyallomer centrifuge tubes (Beckman Coulter: 357003). 2-propanol (Fisher Scientific: A416-4) was then used to wash any remaining precipitate from the 2 mL centrifuge tubes. Enough 2-propanol was added to fill the 50 mL tubes, which were then centrifuged at 40000 x g in an Avanti high performance centrifuge (Beckman Coulter: J-26 XP). The 2-propanol was decanted off, and the precipitated polymer/polymer-wrapped SWNTs were washed with water to remove excess polymer. After washing, the polymer-wrapped SWNTs were filtered through 5.0 μm hydrophilic Durapore discs (Millipore: SVLP02500). After drying, the mass of wrapped SWNTs recovered was found to be 0.69 mg for the PSS, 0.11 mg for the PVA, 4.02 mg for the PT and 0.06 mg for the PEG.

2.8.2.3 Transmission electron microscopy (TEM) analysis

TEM images in Figure 24 were taken with a Zeiss High-Resolution Electron Microscope (Carl Zeiss, Oberkochen, Germany) operated at 50 kV and at a magnification of 12k. SWNT/PSS solution was placed on a 300 mesh copper grid with a carbon type-b

support film (Ted Pella, Inc.: 01813). The grid was dried for an hour before TEM observation.

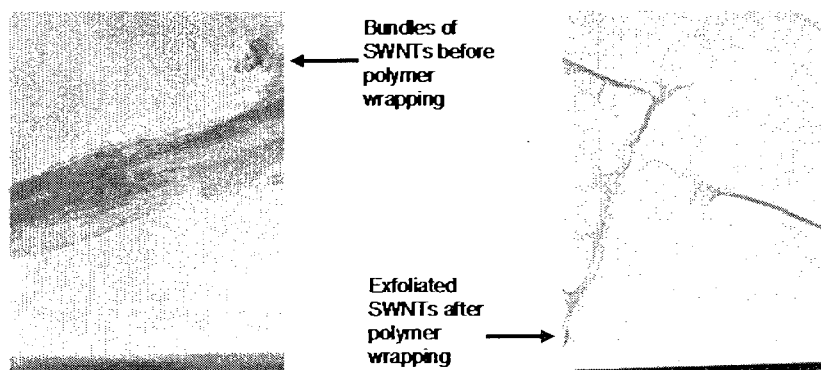


Figure 24 TEM images of undispersed and dispersed (polymer-wrapped) SWNTs taken at 12000x magnification

2.8.3 Results and Discussions

Figure 24 shows the results of the TEM analysis of the polymer-wrapped SWNTs produced by a combination of direct mixing, sonication, and polymer wrapping; individual polymer-wrapped nanotubes could not be visualized because of the magnification limitations of the microscope used, but the images show dispersed rather than bundled nanotubes and their orientation throughout the grid closely resembles a percolation pathway necessary for a conductive coating. Initial attempts to quantify recovered mass from polymer-wrapping experiments yielded large errors due to small sample masses. However, the appearance of the dispersions produced by the polymers showed clear differences (Figure 22). A large-scale procedure was adapted where mass balances could be obtained for the solutions tested. This technique, shown in Figure 23, used a combination of dispersion and polymer wrapping with the aid of surfactants. Interaction energies of specific polymer and nanotube are consistent with results of solubilizing capacity of these polymers from literature [54]. The resulting relative masses

of 67 for the poly(thiophene-sulfonic acid) (PT), 11.5 for the Poly(sodium-styrene sulfonate) (PSS), 1.8 for the Poly(vinyl alcohol) (PVA), and 1 for the Poly(ethylene glycol) (PEG) were isolated (Figure 25).

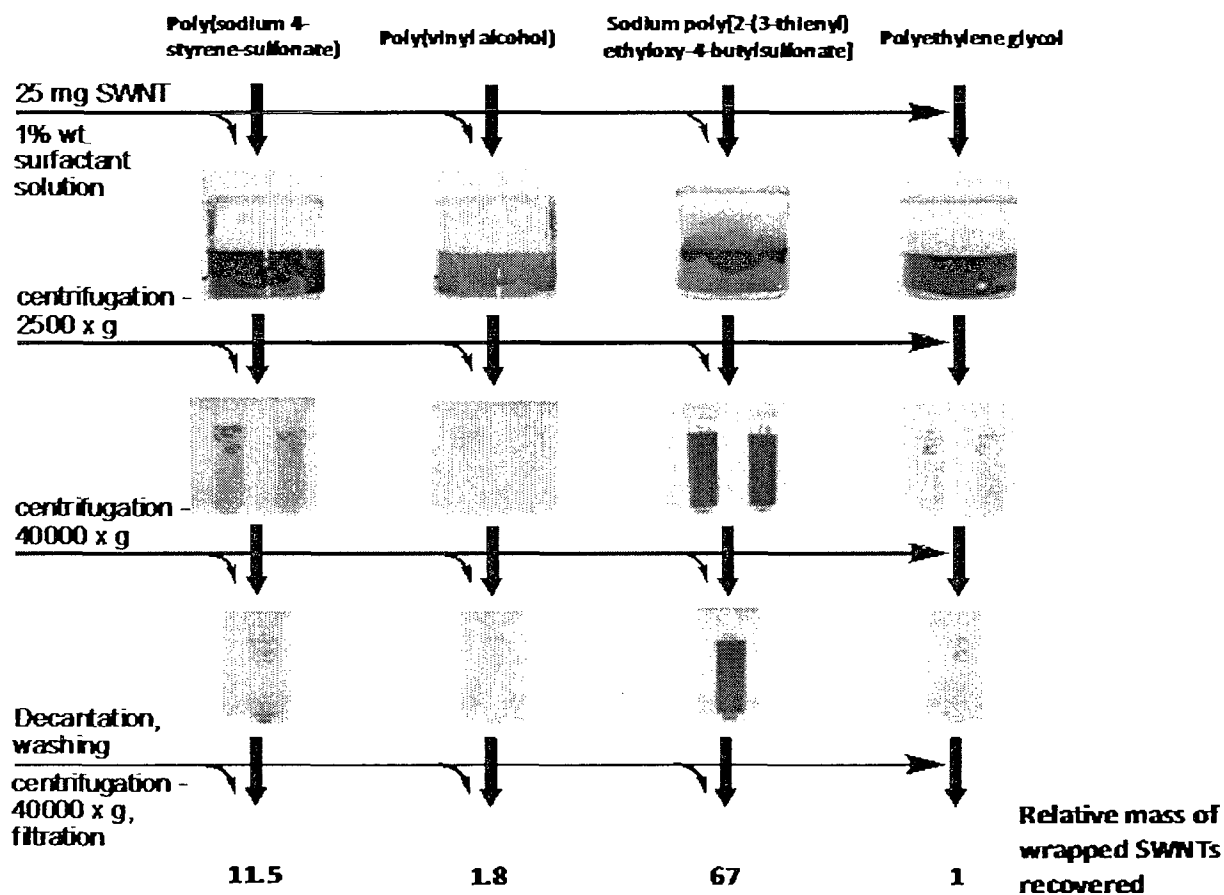


Figure 25 Flowchart of the large-scale polymer-wrapping experiment performed

2.9 Conclusions

Six water soluble polymers were used in the experimental dispersion of SWNTs by polymer wrapping. Initial small scale dispersions gave qualitative information but failed to give quantitative information due to the difficulties involved with sub-milligram

weighings. However these initial experiments established qualitative definitions for good and bad polymers for wrapping. Good polymers are defined as the polymers that disperse SWNTs and bad polymers as that cannot disperse SWNTs. Four polymers were used in large scale dispersions of SWNTs. The dispersion of the bundled SWNTs was confirmed through TEM analysis. The results of the experimental SWNT dispersions are qualitatively shown in Table 12.

Table 12 Qualitative results of polymer wrapping experiments

| Polymer | Dispersion ability (experimental) | Dispersion ability (molecular modeling) |
|-----------------|-----------------------------------|---|
| PEG | Not good | Excellent |
| PVA | Not good | Excellent |
| PSS | Good | Good |
| Dextran | Good | Good |
| PTsulfonic acid | Excellent | Excellent |
| PAA(HCl) | Not good | Not good |

Poly(thiophene sulfonic acid) performed best (with relative mass of 67) in the dispersion of SWNTs. This enhanced dispersing ability is supported by molecular modeling results. It has a conjugated backbone with permanent dipoles due to the presence of sulfur atoms. Molecular mechanics calculations showed that polymers with conjugated backbone and permanent dipole interact strongly with SWNTs. Calculations of water interaction with polymer revealed that its backbone has higher interaction with SWNT than with water, supporting original assumptions.

Poly vinyl alcohol and polyethylene glycol performed poorly (with relative masses of 1.8 and 1.0, respectively). According to molecular mechanics calculations they

have reasonably good interaction with SWNT. Interactions of these polymers with solvent (water) are shown in Table 13.

Table 13 Polymer water interaction energies

| polymer | Required units (RU) | I.E. with water for (RU) (Kcal/mol) | I.E. with water without ionic functionality (Kcal/mol) |
|------------------|---------------------|-------------------------------------|--|
| PEG | 84 | -336.25 | NA |
| PVA | 117 | -457.42 | NA |
| PSS | 44 | -2106.50 | -112.04 |
| Dextran | 55 | -785.64 | NA |
| PT sulfonic acid | 21 | -1004.41 | -87.94 |

Polyvinyl alcohol and polyethylene glycol have a stronger interaction with solvent molecules (water) (-457.42 kcal/mol and -336.25 kcal/mol, respectively) than with SWNT surface. They prefer to stay in solvent rather than to adsorb on SWNT surface. These polymers are not efficient for the dispersion of SWNTs. On the other hand poly(sodium styrene sulfonate) and PT sulfonic acid have hydrophobic core or backbone which prefer to adsorb on to SWNT surface. The apparent water interactions (-2106.50 kcal/mol and -1004.41 kcal/mol) are attributed solely to ionic groups present in the side chains.

From the molecular modeling the number of strands required to cover the surface of SWNT for different polymers is as follows, Table 14.

Table 14 Required number of strands for different polymers

| Polymer | Number of strands for (12,6) SWNT | Required polymer repeat units for two unit long (12,6) SWNT |
|-----------------|-----------------------------------|---|
| PT | 4 | 28 |
| PANI | 9 | 36 |
| PEG | 14 | 84 |
| PVA | 13 | 117 |
| PAA | 6 | 66 |
| PSS | 4 | 44 |
| Dextran | 5 | 55 |
| PTsulfonic acid | 3 | 21 |
| EMER | 9 | 36 |
| PAA(HCl) | 6 | 66 |

The number of strands required to cover the surface of SWNT is very high for polyvinyl alcohol and polyethyleneglycol, i.e., there would be a large entropy penalty when these polymers adhere to the SWNTs. On the other hand, a very small number of strands are required in the case of polythiophenes, poly(sodium styrene sulfonate), and dextran. Polythiophenes and polyanilines have a rod like conformation even before polymer wrapping, i.e., the entropy penalty for these polymers after polymer wrapping would be relatively low. Dextran's ability to disperse SWNT can be attributed to the combination of a low entropy penalty (fewer strands required), strong interaction between polymer strands (see Table 37 in Appendix) on the surface of SWNT, and reasonable interaction with SWNT.

In summary, the ability of polymers to disperse SWNTs depends on four major parameters: 1) magnitude of interaction with SWNTs, 2) magnitude of polymer backbone or core interaction with solvent, 3) entropy effects, 4) macroscopic arrangement of polymer strands and SWNTs in solution. We quantitatively addressed the parameters 1

and 2, and qualitatively addressed parameter 3 from the number of strands required to completely cover a (12,6) SWNT. It was not possible to address parameter 4 using the available software packages, but observed results were well justified using parameters 1, 2, and 3. High resolution TEM analysis showed spiral conformation for polymers around SWNT in literature [58-60], supporting the nanotube-polymer associations described herein.

From molecular modeling and experimentation, the qualities of “preferred” dispersing polymers were identified. Best dispersing polymer have a conjugated backbone with a hetero atom, potential for strong π - π interactions, permanent dipoles, hydrophobic backbone, and a low entropy penalty afforded by a rigid rod like backbone. Solvent compatible functional groups are ideally placed in the side chains of polymer.

CHAPTER III

DISPERSION OF $\text{Sc}_3\text{N}@C_{80}$ METALLIC NITRIDE FULLERENE

3.1 Introduction

Fullerenes are spherical, closed, cage-like structures of carbon that have polygon shaped interatomic arrangements of carbon atoms that are similar to those of graphite [61]. The family of fullerenes ranges from thirty carbon atom C_{30} to structures to those that contain up to an estimated thousand atoms [62]. The buckyball, or C_{60} , is the most common fullerene. It was discovered by Kroto, Smalley, Curl and coworkers [63] and was initially produced in microscopic amounts by laser vaporization techniques.

Krätchmer and co-workers [64] were able to make gram quantities of fullerenes using the arc-discharge method, which produces an arc between two graphite electrodes thereby consuming the electrodes in the production of fullerene containing soot. Arc discharge [65-67] laser ablation [68, 69], and oxidative combustion of benzene or acetylene [70] have all been used to produce mixtures of different sized fullerenes.

Fullerenes,[71-73] classical metallofullerenes,[74-88] and metallic nitride fullerenes [85, 89-115] (Figure 26) have offered the possibility of many exciting applications [116-120]. The metallic nitride fullerenes (MNFs) have a unique shape with 12 pentagons and 30 hexagons. They have a trimetallic nitride cluster at the center of the C_{80} cage. This hollow structure results in its distinctive physical, chemical, and biological characteristics. Modifications of MNFs through organic chemistry and synthesis routes allowed attachment of atoms and molecules to the C_{80} cage without disrupting it's spherical hollow shape.

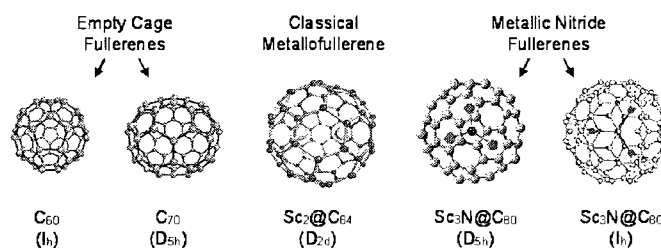


Figure 26 Comparison of fullerenes, metallofullerenes, and MNFs

Classical fullerenes have been incorporated into polymer matrices to form composite films. There is much excitement surrounding fullerene-containing polymers, with the simplest of these being pure photopolymerized C_{60} . Films of photopolymerized C_{60} have shown interesting electronic, magnetic, photochemical, surface, and bulk properties [121-128]. It has been found that the presence of C_{60} lowers the thermal degradation of polystyrene which gives the material as a whole improved thermal stability [ref 88, 89]. In addition, C_{60} in polyethylene has increased composite hardness compared to pristine polyethylene [129, 130]. The most attractive application of C_{60} in composites results from the high photoconductivity of the fullerene polymer mixture. Wang measured a photo-induced discharge in C_{60}/C_{70} doped polyvinylcarbazole (PVK) at the fullerene-polymer interface [131]. Furthermore, Sariciftci et al. observed the same behavior in C_{60} doped poly[2-methoxy,5-(2'-ethyl-hexyloxy)- p-phenylene vinylene] (MEH-PPV) [132]. They showed that photoinduced electrons transfer occurs from the polymer to C_{60} effectively, since C_{60} has extraordinary electron accepting properties. This photoinduced electron transfer produces anions and mobile holes in the polymer, resulting in the generation of photo current. Similar charge transfer is found in other

composites of fullerenes and conjugated polymers, and the effect has potential use for photovoltaic devices [133-135].

Until very recently, the pursuit of realistic research projects using metallofullerenes has been severely limited by sample availability. For the first time, there are sufficient quantities of metallic nitride fullerenes (MNFs, e.g. $\text{Gd}_3\text{N}@C_{80}$, $\text{Gd}_2\text{ScN}@C_{80}$) to pursue film-forming and other device applications, where MNFs are realistic constituents of polymer nanocomposites. The breakthrough in sample availability is due to recent production processes [136-140] discovered by Profs. Stevenson (University of Southern Mississippi, USM) and Dorn (Virginia Tech) and a new purification protocol developed by Stevenson [137, 138].

The added ability of MNFs to bring a functional metal to the film opens up the possibility for more extraordinary properties. The MNF cluster template allows the incorporation of metals having magnetic, electroactive, and radioactive properties, which hold great promise for medical, optical, and electronic applications. Incorporation of MNF materials in a polymer support matrix provide mechanical strength, toughness, adhesion, cohesion for the sample.

Preparation and characterization of thin films from MNF-polymer nanocomposites involves the dispersion of MNFs in a carrier matrix. An important aspect of recent work is the focus on preserving the desired MNF chemical, photochemical, magnetic, or electrical property after incorporation into the film or formulation. Due to the all carbon cage, MNFs are very hydrophobic materials and possess minimal solubility in common organic solvents (mg/mL scale), monomers, and polymers. The ability to

disperse MNFs in polymers is paramount to realizing the potential of these materials in future commercial applications. MNFs, as well as classical fullerenes, have limited solubility in common solvents and polymers. MNF-polymer composite materials are only possible either by (1) primary functionalization to produce solvent and polymer compatible MNFs or (2) non-covalent dispersion of MNFs using suitable complexing agents and subsequent incorporation of the MNFs into the polymer matrix.

In this respect, molecular mechanics calculations were performed to identify suitable dispersing agents for MNFs. A series of resorcinarene and calixarene compounds were surveyed and characteristics of suitable candidates were identified. Select resorcinarene and calixarene compounds were used in experimental MNF dispersion studies to support modeling results.

3.2 Methods

3.2.1 Structure Modifications for Molecular Mechanics Approach

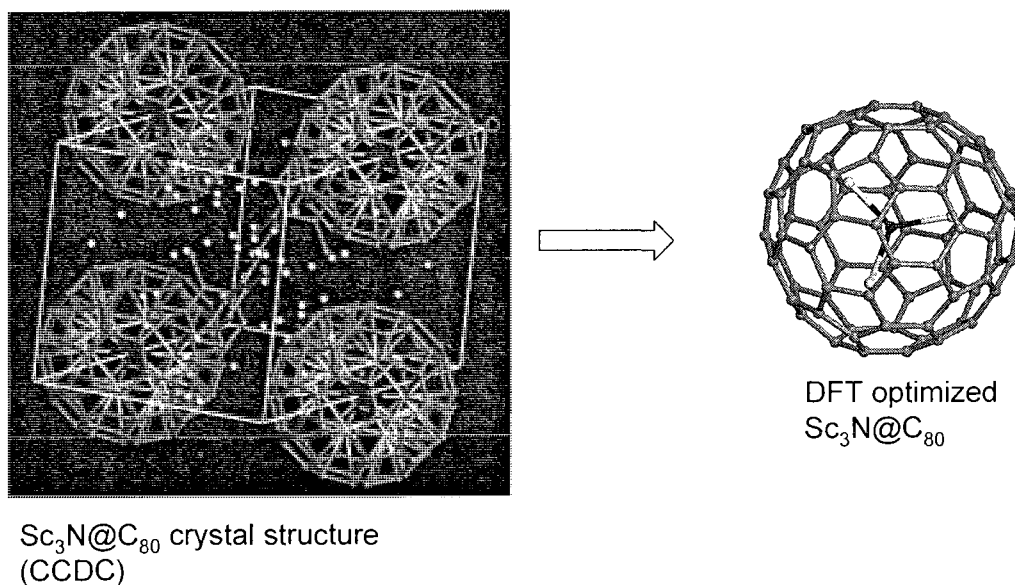


Figure 27 Refinement of Sc₃N@C₈₀ from crystal structure

The structure of $\text{Sc}_3\text{N}@C_{80}$ was obtained from Cambridge Crystallographic Data Center (CCDC) [141]. Unnecessary molecular fragments and excess atoms were removed from crystal structure and optimized using DFT calculations, Figure 27. As previously discussed, $\text{Sc}_3\text{N}@C_{80}$ contains a Sc_3N trimetallic nitride cluster at the center of the C_{80} cage. Sc_3N cluster does not have any covalent bonding with any of the carbon atoms on the cage. There is a transfer of -6 charge from the Sc_3N cluster to the C_{80} cage and so it is represented formally as $[\text{Sc}_3\text{N}]^{+6}[\text{C}_{80}]^{-6}$. Due to this special bonding, a forcefield is not available to describe the Sc-N bonds and their charges. The structure of $\text{Sc}_3\text{N}@C_{80}$ is therefore approximated by an empty C_{80} cage having -0.075e to each carbon, thereby compensating for charge transfer.

3.2.2 Minimization of $\text{Sc}_3\text{N}@C_{80}$ and Similar Compounds

Verification of the modified $\text{Sc}_3\text{N}@C_{80}$ structure and the molecular mechanics approach involved the following steps:

- 1) Verification of molecular mechanics results with DFT results. Modified $\text{Sc}_3\text{N}@C_{80}$ was minimized using molecular mechanics, and unmodified $\text{Sc}_3\text{N}@C_{80}$ was minimized using DFT. Bond lengths and angles were compared in the resulting minimized structures.
- 2) Verification of DFT results with experimental results. Bond lengths and bond angles from DFT results were compared to available experimental results from the literature.

3.2.2.1 *Molecular mechanics minimization of modified $\text{Sc}_3\text{N}@C_{80}$*

For molecular mechanics minimization of modified $\text{Sc}_3\text{N}@C_{80}$ Discover module (Accelrys, Inc., San Diego CA) was used employing the COMPASS force field. An atom

based summation method was utilized with the non-bonded interactions cutoff set to a distance of 15.5 Å, accompanied by a spline width of 5.0 Å and a buffer width of 2.0 Å. Modified Sc₃N@C₈₀ was first minimized (potential energy) using the steepest descent convergence method until the convergence is reached to 1000 kcal/mol/Å, followed by conjugate gradient convergence method until the convergence is reached to 10 kcal/mol/Å, followed by a Newton convergence method until the final convergence is reached to 1.0 X 10⁻⁶ kcal/mol/Å. Fletcher-Reeves algorithm was used for conjugate gradient method and BFGS algorithm was used for Newton method. Charges assignment for carbon atoms (0.075e) was done by using QEq method.

3.2.2.2 DFT minimization of Sc₃N@C₈₀

The energy computed by DFT calculations for a particular molecule depends upon a number of computational parameters. When comparing energies, it is necessary to use the same parameters for each system. The following steps are involved in setting up a DFT calculation.

- 1) Set up of the charge and spin state of the system.
- 2) Set up of the exchange-correlation functional. This specifies the DFT functional that will be used in the calculation. In general, LDA functionals provide quicker calculations, but GGA functional provide more reliable results. For any calculations involving comparison of energies, GGA functionals are recommended.
- 3) Set up of a basis set. This controls the number of atomic orbitals used to describe each molecular orbital.
- 4) Set up of the electronic parameters for the calculation.

The DMol³ module of Materials Studio was used for the density functional theory (DFT) calculations. All electrons were explicitly included in core treatment and also included some relativistic effects. The DNP basis set was used which has one atomic orbital for each occupied atomic orbital, a second set of valence atomic orbitals, a polarization d-function on all non-hydrogen atoms and a polarization p-function on all hydrogen atoms. For exchange-correlation PW91 gradient-corrected (GGA) potential was used. SCF convergence tolerance was set to 10^{-6} . The convergence threshold used for energy is 10^{-5} Hartree, 0.002 Hartree/Å for force, and 0.005 Å for displacement. The maximum number of geometry optimization cycles was set to 150.

3.2.3 Verification of Molecular Mechanics Results against DFT Results

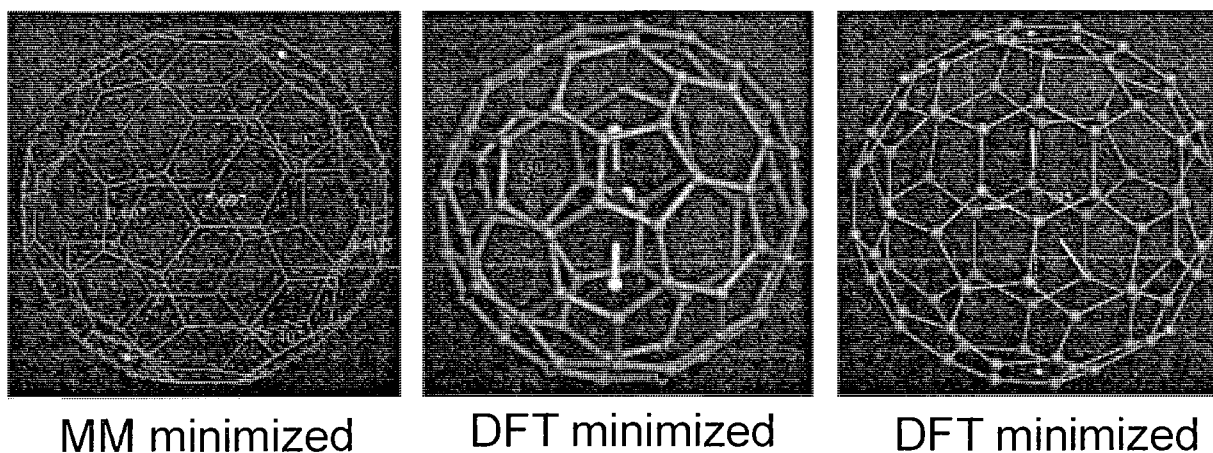


Figure 28 Molecular mechanics and DFT minimized structures of Sc₃N@C₈₀

The results of molecular mechanics minimization of modified Sc₃N@C₈₀ and DFT minimization of unmodified Sc₃N@C₈₀ are provided. Bond lengths and diameters of modified Sc₃N@C₈₀ and unmodified Sc₃N@C₈₀ are very closely matched, Figure 28.

Average C-C distance (Molecular Mechanics) = 1.41 Å

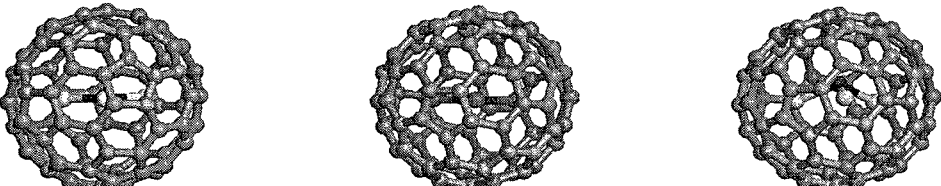
Average C-C distance (DFT) = 1.42 Å

Diameter of the cage (MM) = 7.697 Å

Diameter of the cage (DFT) = 7.795 Å

3.2.4 Verification of DFT Results against Experimental Results

DFT calculations were performed on $\text{Sc}_3\text{N}@C_{80}$ and also on two other similar materials, $\text{Lu}_3\text{N}@C_{80}$ and $\text{Gd}_3\text{N}@C_{80}$. The results of the calculations are compared with experimental results from literature (Figure 29). Results from molecular mechanics calculations with modified $\text{Sc}_3\text{N}@C_{80}$ closely matched with DFT results and DFT results compared favorably with experimental results. The similarity among MM, DFT and experimental results provided confidence in our approach and the modified $\text{Sc}_3\text{N}@C_{80}$ structure. Additional modeling experiments were pursued.



$\text{Sc}_3\text{N}@C_{80}$
 $\text{Lu}_3\text{N}@C_{80}$
 $\text{Gd}_3\text{N}@C_{80}$

| | Experimental | Theoretical | Experimental | Theoretical | Experimental | Theoretical |
|-----------------|--------------|-------------|--------------|-------------|--------------|-------------|
| Bond Length (Å) | 2.0526(14) | 2.034 | 2.001(3) | 2.040 | 2.038(8) | 2.101 |
| | 2.0323(16) | 2.034 | 2.0819(8) | 2.041 | 2.085(4) | 2.108 |
| | 1.9931(14) | 2.033 | 2.0592(10) | 2.042 | 2.117(5) | 2.109 |
| Bond Angle (°) | 120.70(7) | 120.909 | 123.53 | 121.057 | 111.6(2) | 108.488 |
| | 119.21(6) | 120.177 | 121.51 | 120.170 | 110.3(3) | 107.579 |
| | 118.47(7) | 118.906 | 121.00 | 118.760 | | |

Figure 29 Comparison of theoretical (DFT) and experimental results

Resorcinarenes and calixarenes are macrocyclic compounds composed of phenolic units connected by bridging groups such as methylene groups. They generally form a hydrophobic cavity that is capable of forming inclusion complexes with a variety of molecules. Resorcinarenes and calixarenes have been synthesized in a number of sizes. These compounds possess a well-defined cavity with simultaneous polar and nonpolar properties. Also, they can be derivatized in terms of cavity size and functional groups to yield guest compatible compounds capable of forming inclusion complexes [142]. The wider side of the cavity is defined as the upper rim, and the narrower hydroxyl side is the lower rim [143]. Because they are easily derivatized, numerous reaction schemes have been reported that produce these compounds with a variety of functionalities and chemical properties. Control of bowl conformation can be achieved by bulkier substituents on phenyl rings which inhibit rotation. There is a considerable interest in these compounds due to their ability to form complexes with other molecules. The first 1:1 calixarene inclusion complex with aromatic molecules was first reported in 1979 [144]. As expected, larger calixarenes were able to include larger aromatic hydrocarbons. The complexation of calixarenes with fullerenes has also been reported with C_{60} and C_{70} [145-151]. A series of resorcinarenes and calixarenes were used in our calculations to identify the characteristics for strong binding with $Sc_3N@C_{80}$, specifically by calculating interaction energy values. High negative value for interaction energy is an indication of strong binding and dispersion ability.

3.3 Calculations with 4-member Ring Resorcinarene Compounds (set 1)

Resorcinarenes containing four phenyl rings were considered for the first set of calculations. Series ‘a’ has phenyl substituents as side chains and series ‘b’ has n-hexyl substituents as side chains. The structures of the compounds are given along with results and discussions. The bowl shape of these compounds is retained due to the bulky side chains at the bottom and inversion of the phenyl rings is not possible.

Calculations with resorcinarenes 1a & 1b

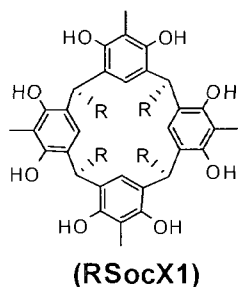


Figure 30 Structure of resorcinarene-1

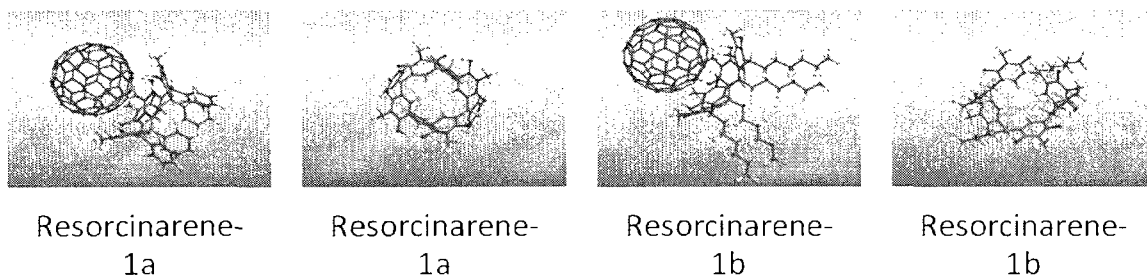


Figure 31 Minimized structures of resorcinarene-1 and $\text{Sc}_3\text{N}@\text{C}_{80}$ complex

Table 15 Interaction energies for resorcinarene-1

| Resorcinarene | Single point | minimization |
|---------------------------------------|------------------|-----------------|
| 1a(R=Ph) | -117.70 kcal/mol | -84.25 kcal/mol |
| 1b(R=C ₆ H ₁₃) | -130.58 kcal/mol | -89.24 kcal/mol |

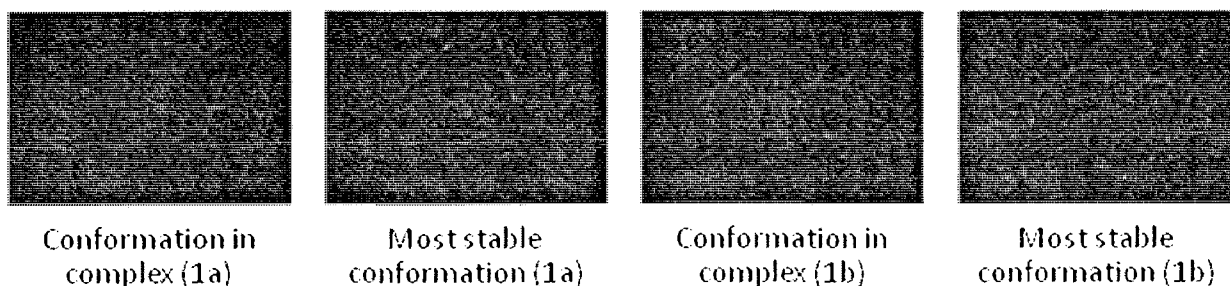


Figure 32 Conformations of resorcinarene-1

N-hexyl substituents are preferred over phenyl substituents. The bowl shape is achieved easily with n-hexyl side chains, which is revealed in larger interaction energy values. Steric repulsion between phenyls substituents causes slight deformation of the bowl shape which decreases the probability of complex formation. Positively charged hydrogen atoms of –OH group interact strongly with the negatively charged C_{80} cage. A bowl is formed with one covalent bond between phenyl rings. This gives flexibility to the bowl to accommodate the large C_{80} cage.

Figure 32 illustrates the most stable conformation of resorcinarene in complex followed by the resorcinarene alone. The ability of the hexyl derivative to retain a conformation suitable for complexation contributes to the larger calculated IE.

Calculations with resorcinarenes 2a & 2b

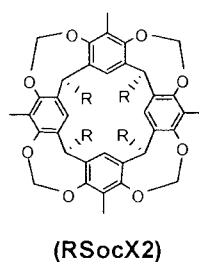


Figure 33 Structure of resorcinarene-2

The general structures of resorcinarenes 2a and 2b are shown in Figure 33. energy minimized structures of the MNF-complex are provided in Figure 34, with the corresponding IE values reported in Table 16. calculated IEs support a stronger association between MNF and resorcinarene-2b, where R = C₆H₁₃. However, values for 2b are significantly less than those calculated for 1a and ab. In structures 2a and 2b, phenyl rings are connected through two points of attachment (covalent bonds), which reduces the flexibility of the bowl toward complexation. In case of resorcinarene 2a, interaction between the phenyl substituents (bottom) deform the bowl and make the bowl entrance smaller. In this conformation, methyl substituents on phenyl rings sterically hinder C₈₀ cage from interaction, leading to a lower IE for resorcinarene-2a. Similar to that observed for structures 1a and 1b, the hexyl derivative adapts a more perfect bowl shape in the complex and alone, Figure 35.

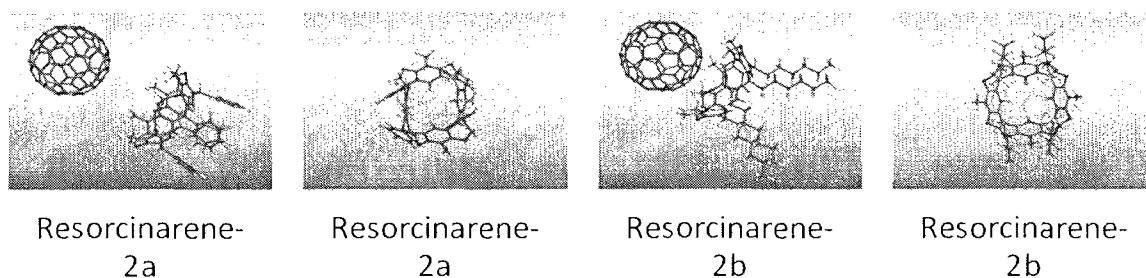


Figure 34 Minimized structures of resorcinarene-2 and Sc₃N@C₈₀ complex

Table 16 Interaction energies for resorcinarene-2

| Resorcinarene | Single point | minimization |
|---------------------------------------|-----------------|-----------------|
| 2a(R=Ph) | -23.04 kcal/mol | -17.67 kcal/mol |
| 2b(R=C ₆ H ₁₃) | -56.72 kcal/mol | -53.82 kcal/mol |

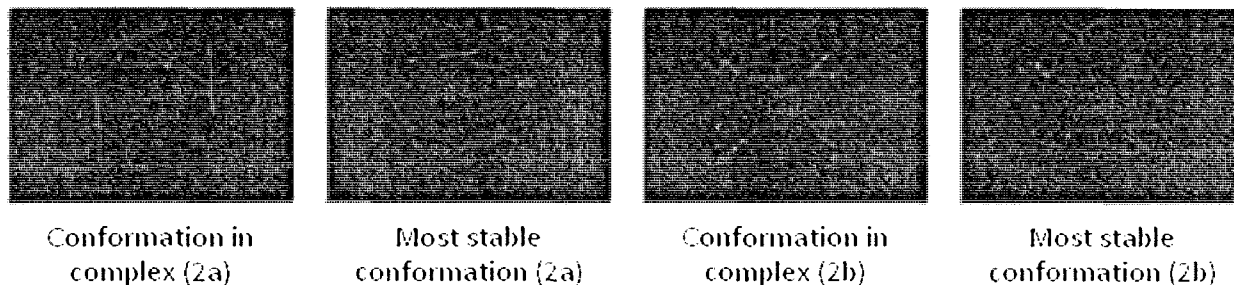
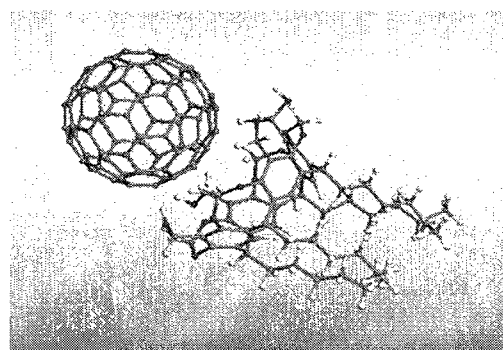
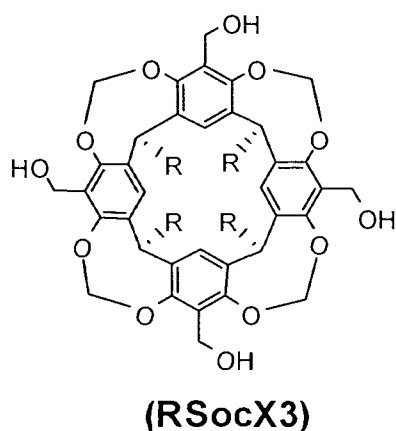


Figure 35 Conformations of resorcinarene-2

Calculations with resorcinarenes 3a & 3b



Resorcinarene-3b

Figure 36 Structure of resorcinarene-3 and its complex with $SC_3N@C_{80}$

The general structures of resorcinarenes 3a and 3b and energy minimized structures of the MNF-complex are provided in Figure 36, with the corresponding IE values reported in Table 17. Resorcinarene-3 has same two point attachment (covalent bonds) for phenyl rings as 2a & 2b (which reduces the flexibility of the bowl toward complexation), but polar component of 1a and 1b (which increases IE and complexation ability). A first approximation based on results from earlier calculations would place IE in between 1a/1b and 2a/2b. A negative effect from covalent bonds between phenyl rings and a positive effect from 'H' of -OH groups lead to lower IE values for resorcinarenes

3a and 3b when compared to resorcinarenes 1a and 1b. For resorcinarene 3a, deformed bowl shape is observed in complex and in the most stable conformation due to steric repulsion between phenyl substituents. For resorcinarene 3b slight deformation of bowl shape is observed in complex, but bowl shape is retained in its most stable conformation.

Table 17 Interaction energies for resorcinarene-3

| Resorcinarene | Single point | minimization |
|---------------------------------------|-----------------|-----------------|
| 3a(R=Ph) | -69.14 kcal/mol | -80.02 kcal/mol |
| 3b(R=C ₆ H ₁₃) | -59.77 kcal/mol | -80.66 kcal/mol |

Calculations with resorcinarenes 4a, 4b, 5a, 5b, 6a, and 6b

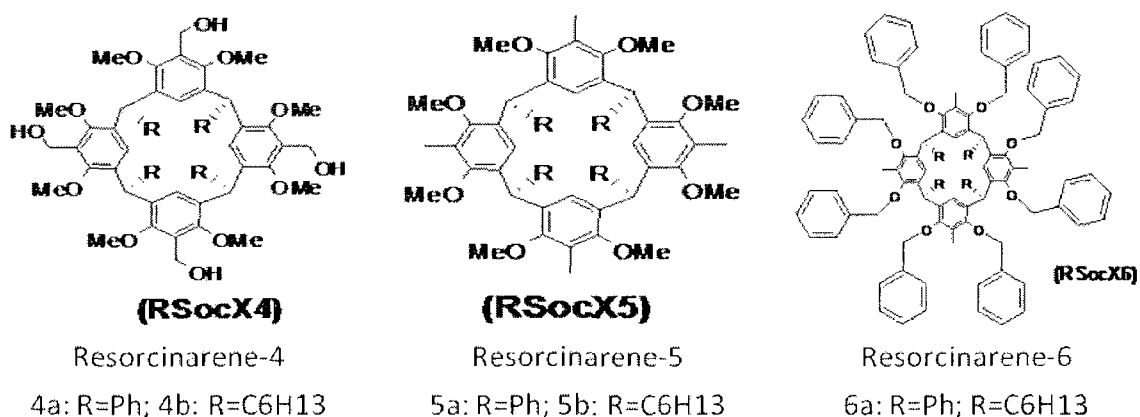


Figure 37 Structures of resorcinarene 4, 5 and 6

The general structures of resorcinarenes 4, 5 and 6 are shown in Figure 37 and the corresponding IE values reported in Table 18. The bowl shape for resorcinarenes 4 and 5 is formed by one covalent bond (one point of attachment) between phenyl rings, similar to bonding in 1a/1b. In the bowl conformation, bulky -OCH₃ groups from adjacent phenyl rings cannot be accommodated in the available space. They sterically repel each other and bring two of the phenyl rings parallel to each other. This effect is more pronounced when there are phenyl substituents (resorcinarenes 6a and 6b). Steric

hindrance from -OCH₃ groups has a negative steric impact on the approaching C₈₀ preventing association. This results in low interaction energy values.

Table 18 Interaction energies for resorcinarene-4, -5, and -6

| Resorcinarene | Single point | minimization |
|---------------------------------------|-----------------|-----------------|
| 4a(R=Ph) | -86.25 kcal/mol | -68.11 kcal/mol |
| 4b(R=C ₆ H ₁₃) | -72.35 kcal/mol | -32.95 kcal/mol |
| 5a(R=Ph) | -36.66 kcal/mol | -29.98 kcal/mol |
| 5b(R=C ₆ H ₁₃) | -42.60 kcal/mol | -35.45 kcal/mol |
| 6a(R=Ph) | -55.20 kcal/mol | -41.17 kcal/mol |
| 6b(R=C ₆ H ₁₃) | -52.59 kcal/mol | -40.80 kcal/mol |

Resorcinarene 6 is also connected by one single bond affording a flexible structure. The presence of huge benzyl and methyl substituents completely deform the bowl shape. Due to this deviation, the effect of substituents (phenyl vs n-hexyl) is negligible. C₈₀ cage interacts with available phenyl rings only in a sideways orientation, so the obtained interaction energy values are low.

Comparision of molecular mechanics and DFT interaction energies

Interaction energies for resorcinarene-1b and resorcinarene-2b with modified Sc₃N@C₈₀ are -89.24 kcal/mol and -53.82 kcal/mol (molecular mechanics).

Interaction energies for resorcinarene-1b and resorcinarene-2b with Sc₃N@C₈₀ are -96.64 kcal/mol and -58.36 kcal/mol (DFT). These results confirmed the accuracy of the molecular mechanics calculations.

3.3.1 Summary of Modeling Results from Set1

| Name | IE1 (optimization) | IE2 (single point) |
|----------|--------------------|--------------------|
| Resor-1a | -84.25 | -117.70 |
| Resor-1b | -89.24 | -130.58 |
| Resor-2a | -17.67 | -23.04 |
| Resor-2b | -53.82 | -56.72 |
| Resor-3a | -69.14 | -80.02 |
| Resor-3b | -59.77 | -80.66 |
| Resor-4a | -68.11 | -86.25 |
| Resor-4b | -32.95 | -72.35 |
| Resor-5a | -29.98 | -36.66 |
| Resor-5b | -35.45 | -42.60 |
| Resor-6a | -41.17 | -55.20 |
| Resor-6b | -40.80 | -52.59 |

Resorcinarenes with 4 member bowls are predicted to be suitable dispersing agents for $\text{Sc}_3\text{N}@C_{80}$ when the phenyl rings are connected by one single bond (one point of attachment) affording a flexible structure which readily attains an optimal bowl geometry. This connectivity gives flexibility to the bowl to open widely. Wide opened bowls can accommodate large C_{80} cages. Resorcinarenes with 4 member bowls are not suitable to disperse $\text{Sc}_3\text{N}@C_{80}$ when the phenyl rings are connected by two single bonds (two points of attachment) to form the bowl shape and simultaneously contain sterically bulky substituents. Resorcinarenes with 4 member bowls and with phenyl rings connected by two single bonds (two points of attachment) are suitable for $\text{Sc}_3\text{N}@C_{80}$ dispersion when they contain small (sterically less hindering) substituents. The size of the bowl is not sufficient for C_{80} cage when the bowl is formed with two single bond connections (two points of attachment) between phenyl rings. But there is a reasonable interaction when the substituents are small. The partial positive charge on hydrogen of the hydroxyl group interacts strongly with negatively charged C_{80} cage and so they are

favorable. Substituents such as OCH_3 , OCH_2Ph are too bulky and $\text{Sc}_3\text{N}@C_{80}$ is unable to gain proximity to the bowl for stronger interaction. Bowl conformation is relatively hard to achieve when phenyls are present as substituents ('a' structures). Side chain phenyl rings sterically repel with each other causing deformation of the bowl shape (prominent when the bowl is formed by two single bonds between phenyl rings). For this reason structures 'a' (phenyl substituents) compounds generally have low interaction energy values compared to structure 'b' (n-hexyl substituents) compounds.

3.4 Calculations with Modified Resorcinarenes (set 2)

In this section some hypothetical structures were used for the calculations to get better understanding of the interactions. These hypothetical structures are obtained by replacing some atoms or fragments in resorcinarene 2b with other atoms or fragments. The minimized structures of the complexes are shown in Figure 38 and interaction energy values are provided in Table 19.

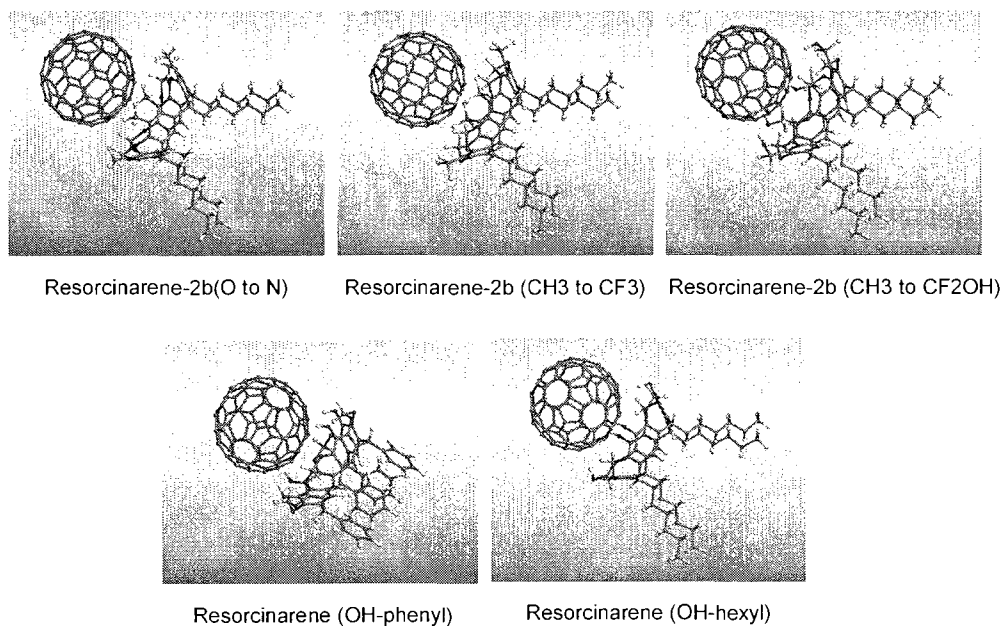
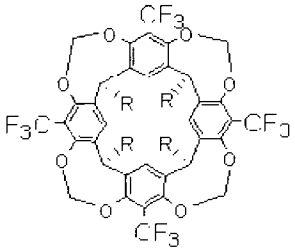
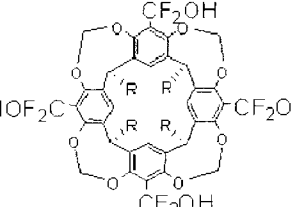


Figure 38 Optimized structures of $\text{Sc}_3\text{N}@C_{80}$ -resorcinarene complexes

Table 19 Structures and interaction energies for resorcinarenes

| Name | Structure | IE1 (optimization) (kcal/mol) | IE2 (single point) (kcal/mol) |
|---------------------------|-----------|-------------------------------------|-------------------------------------|
| Resorcinarene (OH-phenyl) | | -60.53 | -83.95 |
| Resorcinarene (OH-hexyl) | | -66.68 | -90.39 |
| Resorcinarene-2b(O to N) | | -81.71 | -101.80 |

| | | | |
|--------------------------------|---|---------|---------|
| Resorcinarene-2b(CH3 to CF3) |  | -60.26 | -77.84 |
| Resorcinarene-2b(CH3 to CF2OH) |  | -116.85 | -155.12 |

For all the compounds bowl shapes are formed by two single bonds between phenyl rings. When compared resorcinarene-2b(O to N) with resorcinarene-2b, it has less electronegative 'N', so the partial negative charge present on 'N' is relatively small compared to 'O' analog. Since the electronegative atom is directly facing C₈₀ cage, there is some repulsion present in both oxygen and nitrogen analogs. But this repulsion is lessened in case of nitrogen analog due to the presence of positively charged hydrogen atom on nitrogen. This gives a relatively high interaction energy value for this nitrogen analog compared to oxygen analog. In the case of resorcinarene-2b (CH3 to CF3), CF₃ group induces positive charge on phenyl ring and increases partial positive charge on hydrogens of 'OCH₂O'. These partial positive charges interact strongly with negatively charged C₈₀ cage. But negatively charged 'F' atoms repel the cage, indicated by the orientation of 'F' atoms in the minimized structure. So it has a medium IE values. For resorcinarene-2b (CH3 to CF₂OH), the partial positive charge on 'H's of CF₂OH is extremely high and it give strong electrostatic interaction between negatively charged C₈₀

cage and the 'H's of CF₂OH. At the same time 'F' and 'O' atoms give partial positive charge to the neighboring atoms and groups. So the interaction energy is very high. For resorcinarene (OH-phenyl), partial positive charges on hydrogens of 'OH' interact strongly with negatively charged C₈₀ cage. And 'O' atoms in 'OCH₂O' induce partial positive charge on 'CH₂', and on the phenyl rings. This gives strong interaction with C₈₀ cage. Similarly in the case of resorcinarene (OH-hexyl), partial positive charges on hydrogens of 'OH' interact strongly with negatively charged C₈₀ cage. And 'O' atoms in 'OCH₂O' induce partial positive charges on 'CH₂', and on the phenyl rings. This gives stronger interaction with C₈₀ cage and high interaction energy values. And also less steric n-hexyl side chains further increase the interaction energy by giving flexibility to the bowl.

3.4.1 Summary of Modeling Results from Set 2

Table 20 Summary of interaction energy values from optimizations and from single point energy calculations for resorcinarenes

| Name | IE1 (optimization) (kcal/mol) | IE2 (single point) (kcal/mol) |
|---|-------------------------------|-------------------------------|
| Resorcinarene (OH-phenyl) | -60.53 | -83.95 |
| Resorcinarene(CH ₂ OH to OH) | -71.62 | -83.22 |
| Resorcinarene (OH-hexyl) | -66.68 | -90.39 |
| Resorcinarene-2b(O to N) | -81.71 | -101.80 |
| Resorcinarene-2b(CH ₃ to CF ₃) | -60.26 | -77.84 |
| Resor-2b(CH ₃ to CF ₂ OH) | -116.85 | -155.12 |

Summary of interaction energy values from optimizations and from single point energy calculations for resorcinarenes with Sc₃N@C₈₀ are shown in Table 20. In general the following structure property relationships can be defined from modeling results. The electronegative atoms or groups on the bowl rim improve interaction of resorcinarenes

with C_{80} cage, when the electronegative atoms are not directly facing the cage. However, the negative charge on electronegative atoms repels the C_{80} cage, when they are directly facing the cage. Electronegative atoms increase positive charge on nearby connected atoms, and these positive charges give strong interaction with C_{80} cage. Electronegative atoms or groups located farther from the bowl opening (i.e., farther from C_{80} cage) increase interaction energies. Less electronegative atoms give low positive charges on nearby atoms and so they give low interaction energy values when they are not directly facing the C_{80} cage.

3.5 Calculations with Calixarenes (set 3)

Three calixarene compounds were considered for interaction energy calculations. They are calix[5]arene, calix[6]arene, and calix[8]arene. The structures are shown in Figure 39. IEs are calculated as previously described, and results are summarized as follows.

Calculations with 4 member ring resorcinarenes revealed that they are barely big enough to accommodate the C_{80} cage. Four member ring resorcinarenes are suitable when the bowl is formed by one single bond connection (one point attachment) between phenyl rings, and simultaneously if they have less sterically bulky substituents. As a result, additional calculations with bigger calixarene compounds were performed.

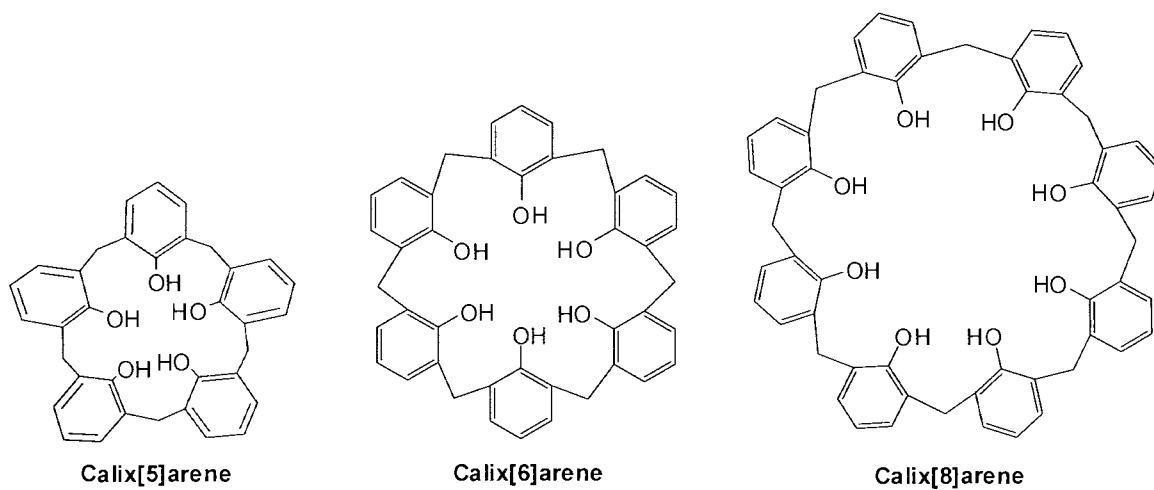


Figure 39 Structures of calix[5]arene, calyx[6]arene, and calyx[8]arene

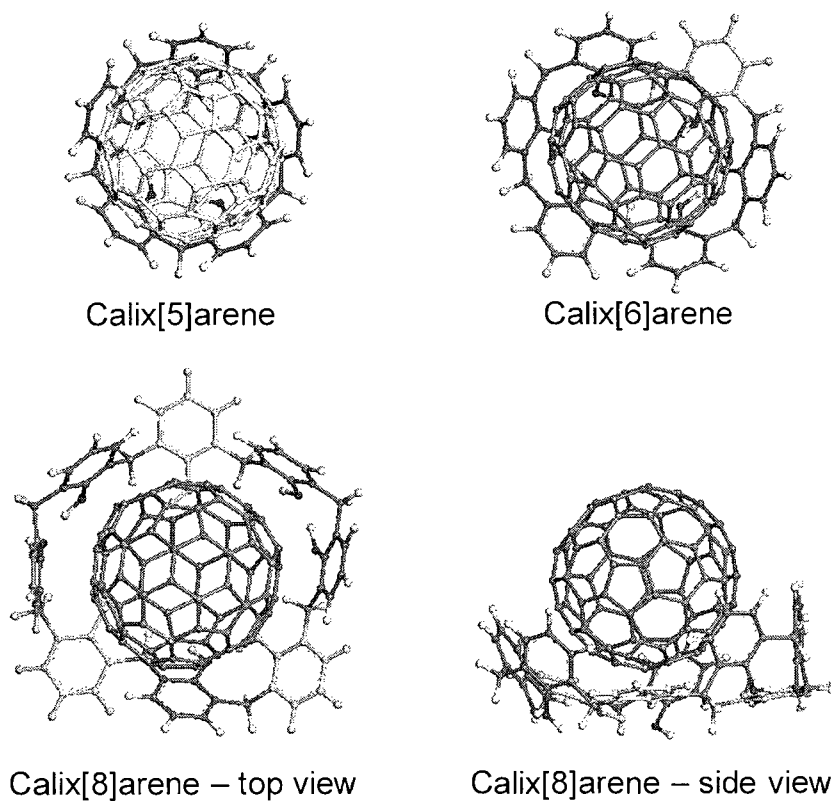


Figure 40 Minimized geometries of calix[5]arene-, calix[6]arene-, and calix[8]arene- $\text{Sc}_3\text{N}@C_{80}$ complexes

The calculated IE between calix[5]arene and $\text{Sc}_3\text{N}@C_{80}$ is -111.43 kcal/mol from structure minimizations. Calix[5]arene visually appears to fit well in complexation with $\text{Sc}_3\text{N}@C_{80}$, Figure 40. The size of the bowl is large enough to accommodate the C_{80} cage. In the complex C_{80} resides close to the phenyls and has strong π - π interactions. The phenyl rings in calix[5]arene do not have bulky substituents at the bottom of the bowl, so i.e., the phenyl rings are free to rotate through the single bonds to yield other conformations. However in the case of this compound, strong hydrogen bonding locks the phenyls in the preferred bowl conformation.

Calix[6]arene is big enough to accommodate the C_{80} cage, as illustrated in Figure 40. The IE between calix[6]arene and $\text{Sc}_3\text{N}@C_{80}$ is -125.21 kcal/mol from structure minimizations. This is very high due to improved π - π interactions. The larger size of the bowl allows C_{80} to move closer to the phenyl rings. Five of the six phenyl rings of calix[6]arene align with the C_{80} cage for π - π interactions. The remaining phenyl ring orients perpendicular to the others to relieve strain. This is contributed to the larger cavity formed from six phenyl rings.

IE between calix[8]arene and $\text{Sc}_3\text{N}@C_{80}$ is calculated to be -165.92 kcal/mol. The size of the bowl is considerably bigger, to accommodate C_{80} cage. Five phenyl rings orient pseudo-parallel to the cage surface for strong π - π interactions. The remaining three rings are forced to adopt a conformation normal to the cage rings. Despite the unfavorable orientation of 3 of the 8 aromatic rings, a higher IE is predicted. This suggests that the existing π - π intermolecular attractions and larger bowl size are overall predicted to be more favorable to complexation.

In summary, the IE values for calixarenes-Sc₃N@C₈₀ complexes are shown in Table 21. IEs between calixarenes and Sc₃N@C₈₀ are found to increase with bowl size. This is due to the gradual improvement in alignment of phenyl rings parallel to hexagons/pentagons on the C₈₀ cage. Parallel alignment gives stronger vdW interactions (π - π) between aromatic rings of calixarenes and Sc₃N@C₈₀. Moreover, the bowl shape is retained for calix[5]arene and calix[6]arene due to hydrogen bonding between –OH groups on phenyl rings. Bowl shape retention is difficult for calix[8]arene due to its large size.

Table 21 Interaction energy values for calixarenes-Sc₃N@C₈₀ complexes

| Calixarene | Interaction energy |
|---------------|--------------------|
| Calix[5]arene | -111.43 kcal/mol |
| Calix[6]arene | -125.21 kcal/mol |
| Calix[8]arene | -165.92 kcal/mol |

3.6 Experimental Dispersion Studies of Sc₃N@C₈₀

An experimental study was conducted to test the complexing ability of select resorcinarenes and calixarenes to Sc₃N@C₈₀. Dynamic light scattering (DLS) was identified as suitable techniques for the analysis of samples. Dynamic light scattering (DLS) gives particle size measurements. Any change in particle size due to dispersion (or complexation) of Sc₃N@C₈₀ with resorcinarenes or calixarenes can be observed by DLS.

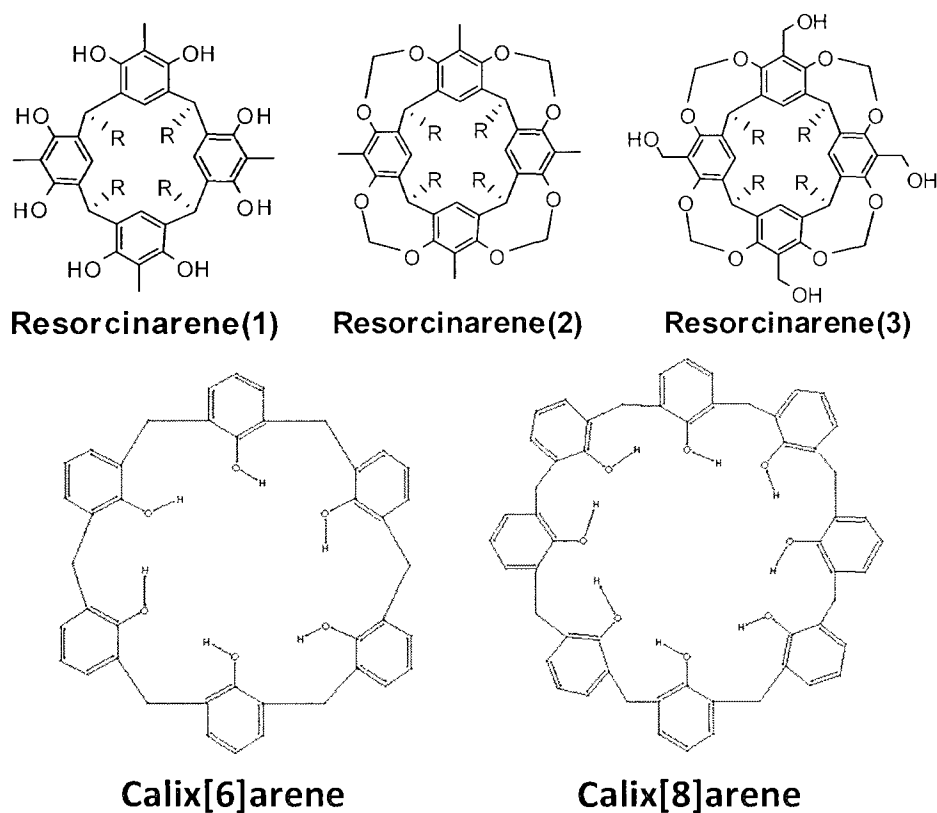


Figure 41 Structures of resorcinarenes and calixarenes used in experimental studies

Five compounds were selected for use in experimental studies and their structures are provided in Figure . Finding a suitable solvent for experimental studies was the first task, due to diverse solubility of the compounds. Crude solubilities were measured in common solvents and tabulated in Table 22. To estimate the solubilities approximately 2 mg of solid was added to 0.5 mL of solvent and qualitative assignments of poor, fair, good, or excellent were made based on a visual inspection of the solid fraction that dissolves.

Table 22 Solubilities of host guest materials

| Compound | Solvent | Solubility |
|-----------------------------------|-------------------------------|------------|
| Sc ₃ N@C ₈₀ | CS ₂ | Fair |
| | Xylenes | Poor |
| | Toluene | Poor |
| | ODCB | Poor |
| | C ₆ H ₆ | Poor |
| | CHCl ₃ | poor |
| Resorcinarene(1) | Toluene | Poor |
| | CHCl ₃ | Poor |
| | THF | Fair |
| | Acetone | Fair |
| | DMF | Excellent |
| Resorcinarene(2) | Toluene | Good |
| | THF | Good |
| | CHCl ₃ | Good |
| | Acetone | Good |
| | DMF | Excellent |
| Resorcinarene(3) | Toluene | Good |
| | THF | Good |
| | Chloroform | Good |
| | Acetone | Fair |
| | DMF | Excellent |
| Calixarene(6) | Toluene | Poor |
| | THF | Poor |
| | Chloroform | Poor |
| | Acetone | Poor |
| | H ₂ O | Poor |
| | Methanol | Poor |
| | Ethanol | Poor |
| | DMF | Good |
| | DMSO | Excellent |
| Calixarene(8) | Toluene | Poor |
| | THF | Poor |
| | Chloroform | Poor |
| | Acetone | Poor |
| | H ₂ O | Poor |
| | Methanol | Poor |
| | Ethanol | Poor |
| | DMF | Good |
| | DMSO | Excellent |

3.6.1 Dynamic Light Scattering Studies

The aim of dynamic light scattering studies was to observe the complexation between resorcinarenes/calixarenes and SC₃N@C₈₀, as evidenced by a change in particle

size in complex solutions versus $\text{Sc}_3\text{N}@\text{C}_{80}$ alone. Changes in particle size are dependent on the extent of aggregation of resorcinarene/calixarene- $\text{Sc}_3\text{N}@\text{C}_{80}$ complexes in solution. A similar complexation of C_{60} with calixarenes was reported recently, where colored solutions of C_{60} became colorless after complexation with calixarenes due to precipitation of the complex [149].

DMF is a common polymer solvent and a bad solvent for fullerenes. In the hope of eventually enabling the fine dispersion of fullerenes in a polymer compatible solvent, DMF was selected as a test solvent. $\text{Sc}_3\text{N}@\text{C}_{80}$ is not significantly soluble in DMF, so a demonstration of a soluble complex formation in this solvent would be a significant discovery and have great utility in the preparation of polymer-fullerene composites. One resorcinarene was found to be soluble in toluene, which is a good solvent for fullerenes. An additional light-scattering study was performed in this solvent for comparison. For the particle size measurements, Nanotrak NPA 151 (Microtrac Inc) DLS instrument was used which is optimized for low concentration measurements and for smaller particle sizes. Measurement range was set to 0.8 to 6500 nm. Data was collected with a 780 nm laser at room temperature. Two data collections were averaged for each measurement.

Table 23 Weights of host and guest materials used in the DLS studies

| Host molecule | Weight of resorcinarene/calixarene | Weight of $\text{Sc}_3\text{N}@\text{C}_{80}$ | Solvent |
|-----------------|------------------------------------|---|---------|
| Resorcinarene-1 | 7.9 mg | 2 mg | DMF |
| Resorcinarene-2 | 8.4 mg | 2 mg | DMF |
| Calix[6]arene | 5.7 mg | 2 mg | DMF |
| Calix[8]arene | 7.7 mg | 2 mg | DMF |

A general experimental procedure for the preparation of complex solutions is as follows. A 2 mg sample of $\text{Sc}_3\text{N}@C_{80}$ is dissolved in 5 ml of selected solvent and a 5 molar excess of resorcinarene/calixarene is dissolved in 1 ml of the same solvent. The solution of $\text{Sc}_3\text{N}@C_{80}$ is sonicated for 10 minutes followed by 60 minutes stirring followed by 10 minutes resting. This cycle was repeated until all of the resorcinarene is added. DLS measurements are taken periodically to monitor changes in particle size, and results are reported in Table 24 and Table 25. Volume and number average particle size values are provided along with standard deviations and calculated IEs. Volume average particle size measurements are prejudiced toward the larger aggregates which may be present and contribute most to the light scattering. Volume average particle size measurements reflect the most probable size and may minimize the contribution from larger species. Both provide critical information about the sample. Each light scattering is the average of multiple scans.

Table 24 Volume average particle size measurements in DMF

| Resorcinarene or calixarene | Average particle size (nm) | Standard deviation (%) | Interaction energy (kcal/mol) |
|-----------------------------|----------------------------|------------------------|-------------------------------|
| Resorcinarene-1 | 168 | 39 | -89.24 |
| Resorcinarene-2 | 171 | 53 | -53.82 |
| Calix[6]arene | 391 | 15 | -125.21 |
| Calix[8]arene | 189 | 49 | -165.92 |

Table 25 Number average particle size measurements in DMF

| Resorcinarene or calixarene | Average particle size (nm) | Standard deviation (%) | Interaction energy (kcal/mol) |
|-----------------------------|----------------------------|------------------------|-------------------------------|
| Resorcinarene-1 | 106 | 37 | -89.24 |
| Resorcinarene-2 | 97 | 31 | -53.82 |
| Calix[6]arene | 370 | 15 | -125.21 |
| Calix[8]arene | 101 | 35 | -165.92 |

3.6.1.1 Results of light scattering

Dispersions of $\text{Sc}_3\text{N}@C_{80}$ were successfully produced in DMF, as shown in the colored solutions of Figure 43. DLS average particle size measurements were similar for resorcinarene-1, resorcinarene-2, and calix[8]arene suggesting that the interactions among fullerene and resorcinarene do not change significantly with the structure variations among these compounds. However, a very unique interaction was observed between $\text{Sc}_3\text{N}@C_{80}$ and calix[6]arene, leading to a larger particle size but more narrow size distribution. This narrow size distribution is suggestive of a more homogeneous sample. A similar observation was made of toluene containing solutions, where the addition of resorcinarene-2 lead to a highly uniform sample distribution, although at a slightly higher average particle size. The volume average particle size distributions are provided in Figure 44 (a and b) for toluene solutions of $\text{Sc}_3\text{N}@C_{80}$ alone (a) and in the presence of resorcinarene-2. Although larger IEs were calculated for the complex produced from $\text{Sc}_3\text{N}@C_{80}$ and calyx[8]arene, this was not supported by the fact that larger ring size calixarenes cannot retain their bowl conformation due to inversion of phenyl rings, Figure 42.

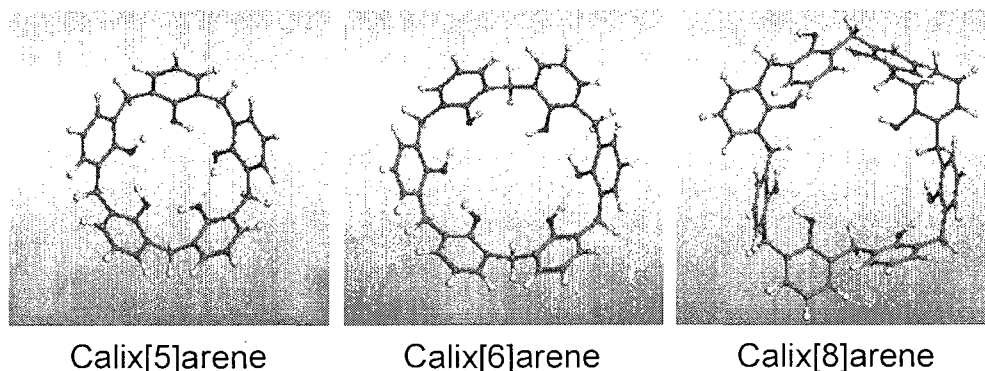
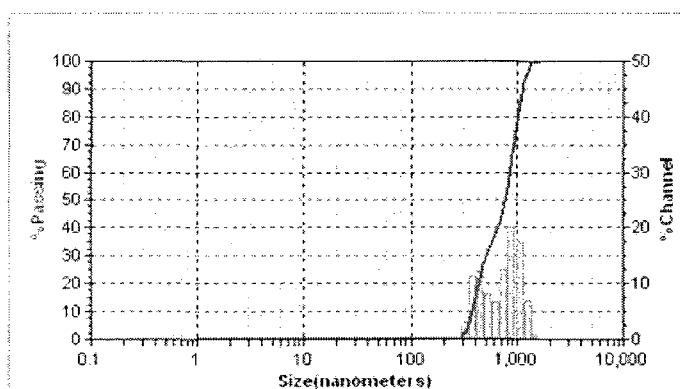


Figure 42 Bowl shape retention of calixarenes due to hydrogen bonding



Figure 43 Color generated from complexation of resorcinarens/calixarenes with $\text{Sc}_3\text{N}@\text{C}_{80}$ in DMF

a) $\text{Sc}_3\text{N}@\text{C}_{80}$ in toluene
 MV(nm) = 753 ($\pm 42\%$)



b) $\text{Sc}_3\text{N}@\text{C}_{80}$ and
 resorcinarene-2 in
 toluene
 MV(nm) = 465 ($\pm 15\%$)

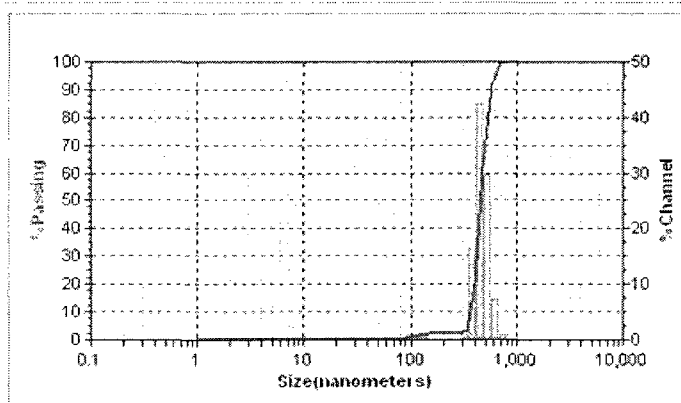


Figure 44 Particle size of $\text{Sc}_3\text{N}@\text{C}_{80}$ in the presence and absence of resorcinarene in toluene

3.7 Conclusions

In summary, DLS results of samples provided strong evidence for the formation of $\text{Sc}_3\text{N}@\text{C}_{80}$ resorcinarene/calixarene complexes. This study was limited to DLS; however additional NMR experiments are currently being explored by other group members. Dispersions of $\text{Sc}_3\text{N}@\text{C}_{80}$ were successfully prepared in DMF, which provides great hope for eventual incorporation into polymer films.

CHAPTER IV

DISPERSION OF ASPHALTENES

4.1 Introduction

Asphaltenes are the heaviest, most polar, and most aromatic fraction of crude oil [152] and exist as a core of stacked, polyaromatic rings connected at their periphery by aliphatic chains and/or naphthenic-aromatic ring systems [153]. Due to their complex nature, asphaltenes cannot be defined by a simple molecular structure or grouped into a specific family of compounds; however a representative structure is provided in Figure 48. Asphaltenes are a solubility class and defined by their solubility in toluene and insolubility in n-heptane. This fraction has been studied extensively because of its role in oil field flow assurance, and the structure and properties of asphaltenes mainly depend on the source of the crude oil [152]. Due to the presence of nitrogen, oxygen, and sulfur heteroatoms, asphaltenes are considered the basic organic components of crude oils. The molecular weight distribution (MWD) of asphaltenes is still under debate. Over the past two decades, several groups have probed the asphaltene molecular mass distribution, and the most accepted range is 500-1000 units even though some discrepancies still exist [154-160].

Naphthenic acid is used as a general term for the organic acids present in crude oil [161]. These compounds are found mainly in immature, heavy crude oils [162, 163]. Naphthenic acids consist of a mixture of alkyl-substituted acyclic and cycloaliphatic carboxylic acids with a broad range of molecular weights and structures, [164, 165] and examples used in this study are presented in Table 27. They have the empirical formula,

$C_nH_{2n+Z}O_2$, where Z is zero or a negative, even integer which indicates the hydrogen deficiency and n is the number of carbon atoms [164, 165]. Cyclic naphthenic acids not only bear a carboxylic acid group, but they are also believed to possess substituted alkyl groups [164]. The rings of naphthenic acids can be bonded in one of two ways, bridged or directly fused [164]. Similar to asphaltenes, the physical and chemical properties of naphthenic acids depend on the nature and source of the crude oil.

Asphaltene molecules/aggregates tend to associate and precipitate from suspension, forming heavy organic deposits in oil reservoirs, oil wells, and pipelines, thereby reducing crude oil flow. In fact, Kokal and Sayegh [166] referred to asphaltenes as the “cholesterol of petroleum”, because their deposition on pipeline surfaces reduces crude oil flow. Once formed, the deposit slowly thickens, further reducing oil flow, and results in a substantial loss in revenue [167]. Asphaltenes become unstable and can precipitate when the solution conditions of the crude oil change as a result of recovery and production operations [168]. These problems have affected oil companies around the world, resulting in large economic losses. Asphaltenes associate and precipitate from suspension as a result of many factors such as a change in temperature, pressure, or composition, etc.

Since heavier and heavier crude oils are being utilized for the production of light oil fractions, understanding asphaltene behavior is an extremely important issue to the oil industry. The forces responsible for asphaltene aggregates are the same as the ones present between organic and organometallic compounds [169]. The interactions between two molecules can have contributions from several forces such as, charge transfer,

electrostatic, van der Waals, induction, and repulsion forces [170, 171]. Therefore, the mechanism of asphaltene aggregation involves van der Waals dispersion forces between aromatic rings, hydrogen bonding between polar groups, and charge transfer interactions [169].

The recent work of Ostlund et al.[172] suggests that asphaltenes and naphthenic acids do associate and that this association is influenced by the concentration and asphaltene type. In a two-part study by Varadaraj and Brons [173, 174], concerning the oil-water interfacial properties of extracted crude oil asphaltenes, much of the interaction at the interface was contributed to the presence of surface-active naphthenic acids that were coincidentally extracted with the asphaltenes. A strong acid-base interaction was found to exist between the nitrogen-containing asphaltenes and the acid-containing naphthenic acids, which produced acid-base complexes. Although several studies exist on the self-association and aggregation behavior of asphaltenes, the interaction of asphaltenes and naphthenic acids largely overlooked. Molecular mechanics calculations were used to study the interactions between asphaltenes and different naphthenic acids to identify required characteristics for naphthenic acids as dispersing agents.

There are a large number of representative naphthenic acids available from commercial sources, and Mr. David Heaps experimentally demonstrated their application in the dispersion of asphaltene aggregates [175]. Molecular modeling results are correlated with Mr. Heap's experimental results. This series of calculations enabled the investigation and potential correlation of a number of structure-property relationships, including the relative effects of hydrogen bonding and vdW interactions.

Primary attractive forces for asphaltene and asphaltene-naphthenic acid aggregation are expected to consist of hydrogen bonding, other electrostatic forces and vdW interactions. The forcefield approach is well suited to this application due to the absence of chemical transformations. Molecular mechanics with CVFF forcefield was used for these calculations and interaction energies for the asphaltene dimer were determined to estimate the strength of aggregation. Interaction energies between asphaltenes and several naphthenic acids were investigated to characterize the specific interactions between the basic and acidic components of crude oil.

4.2 Method Description and Association of Asphaltene Dimers

Interfacial binding characteristics of asphaltenes and their interactions with naphthenic acids were investigated using molecular mechanics and molecular dynamics simulations using CVFF forcefield. A representative structure of Asphaltene was obtained from a literature source [176] for the calculations. Six naphthenic acids were studied in the calculations: 5 β -cholanic acid, naphthalenepentanoic acid, naphthalenoic acid, methyl abietate, hydrogenated methyl abietate, and 5 β -Cholanic acid-3-one, Table 27. An atom based summation method was used with a non-bonded interactions cutoff set to 15.5 Å accompanied by a spline width of 5.0 Å, and a buffer width of 2.0 Å. The models were first minimized using the steepest descent convergence method to 1000 kcal/mol/Å, followed by a conjugate gradient method to 10 kcal/mol/Å, and Newton methods until the convergence reaches 1.0×10^{-5} kcal/mol/Å.

The optimized structure for asphaltene was obtained using the following procedure. In the first step, energy of the structure was minimized. In the second step,

molecular dynamics was run for 100 pico seconds, and the five lowest energy conformations were selected. In the third step, energies of the five selected conformations were minimized, and the conformation with the lowest energy was selected for the rest of the calculations.

Initial modeling studies were performed on asphaltene dimers. For the construction of dimer a docking process was used. The spatial disposition of the two asphaltene molecules involved was changed, and after each change the interaction energy was calculated. The IE values were plotted against rotation angle, Figure 45. Individual calculated IE values are presented in Table 26. The maximum IE determined for asphaltene dimers is determined to be -82.14 kcal/mol. There exists a significant orientational dependence on the IE spacing nearly 20 kcal/mol. The two most thermodynamically stable conformations are illustrated in Figure 46.

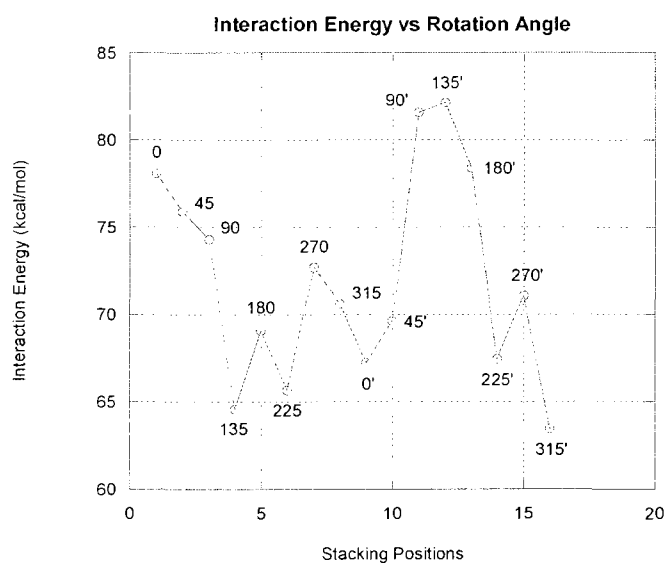


Figure 45 Interaction energy vs rotation angle plot for asphaltene dimer

Table 26 Change in total and interaction energy values with rotation angle for asphaltene dimer

| Rotation angle | Total energy (kcal/mol) | Interaction energy (kcal/mol) |
|----------------|-------------------------|-------------------------------|
| 0 | 1004.27 | -78.08 |
| 45 | 1006.46 | -75.88 |
| 90 | 1008.05 | -74.30 |
| 135 | 1017.80 | -64.55 |
| 180 | 1013.28 | -69.07 |
| 225 | 1016.69 | -65.66 |
| 270 | 1009.66 | -72.69 |
| 315 | 1011.76 | -70.59 |
| 0 | 1015.13 | -67.22 |
| 45 | 1012.74 | -69.61 |
| 90 | 1000.76 | -81.58 |
| 135 | 1000.21 | -82.14 |
| 180 | 1003.98 | -78.37 |
| 225 | 1014.92 | -67.43 |
| 270 | 1011.29 | -71.06 |
| 315 | 1018.89 | -63.45 |

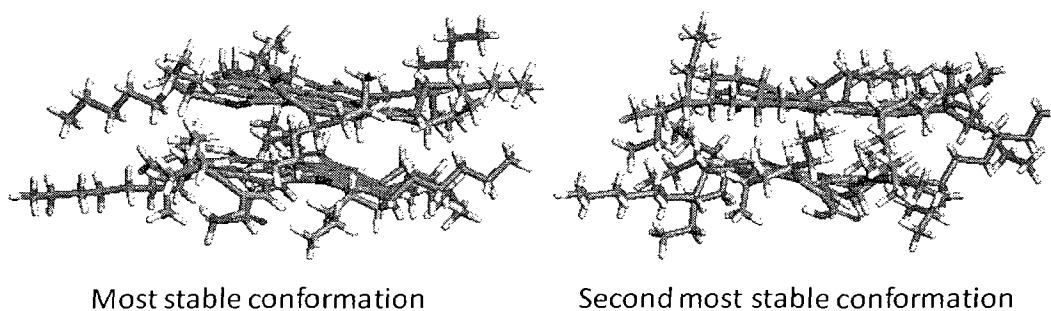


Figure 46 Most stable and second most stable conformations of asphaltene dimer

4.3 Calculations with Naphthenic Acids

Interfacial interaction energy

The attraction between asphaltene and a naphthenic acid molecule results from the electrostatic and van der Waals forces in the molecular system. Generally, the IE is estimated from the energy difference, ΔE , between the total energy of the composite and

the sum of the energies of individual molecules as shown in Equation 10, where $E_{(total)}$ is the total energy of the composite, $E_{(asphaltene)}$ is the energy of the asphaltene without the naphthenic acid, and $E_{(naphthenic\ acid)}$ is the energy of the naphthenic acid without the asphaltene. In other words the interaction energy can be calculated as the difference between the minimum energy and the energy at the infinite separation of the asphaltene and naphthenic acid.

$$E_{interaction} = \Delta E = E_{(total)} - E_{(asphaltene)} - E_{(naphthenic\ acid)} \quad \text{Equation 10}$$

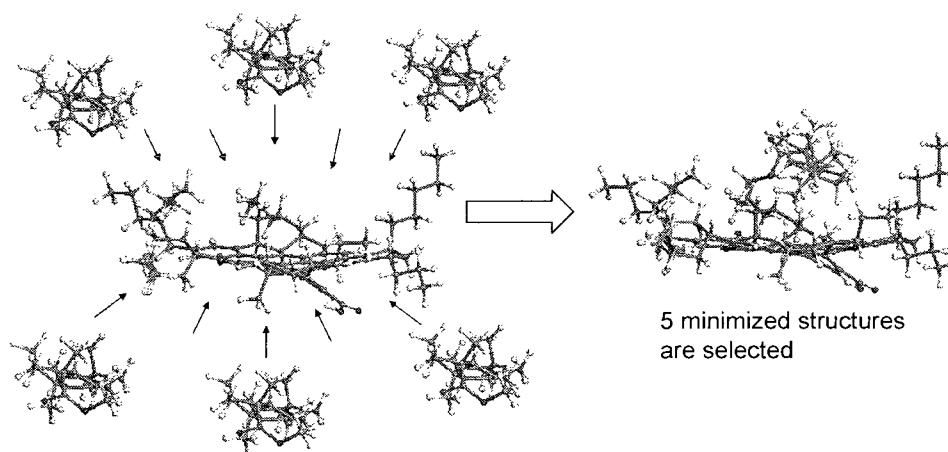


Figure 47 Schematic showing interaction energy calculations for naphthenic acids

Unlike the SWNTs or resorcinarenes, the surface of an asphaltene is discontinuous, presenting different functional groups. As a result IEs calculated at more than one location on the surface of asphaltene are necessary. In this approach, 10 to 15 initial orientations were minimized and IEs are calculated for each naphthenic acid. Five interaction energy values are selected for each, Figure 47.

Naphthenic acids form hydrogen bonds with electronegative atoms present in the asphaltene structure. Due to differences in their chemical structure, different naphthenic

acids prefer different electronegative atoms on asphaltene (from interaction energy values). For convenience, the functional groups of asphaltene are labeled as shown in Figure 48.

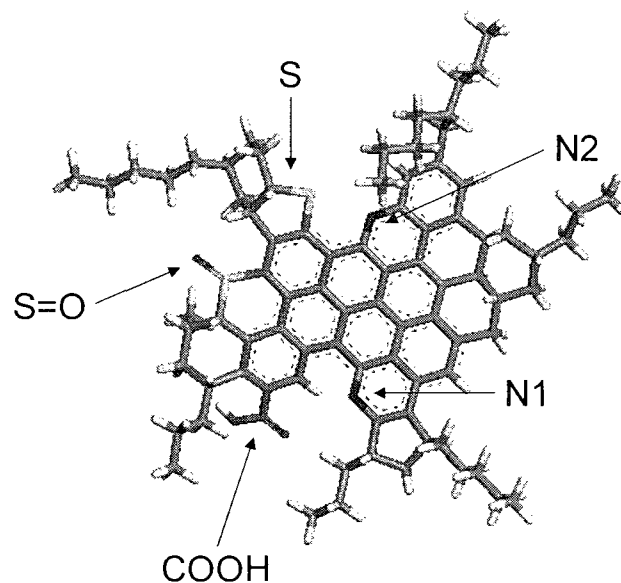
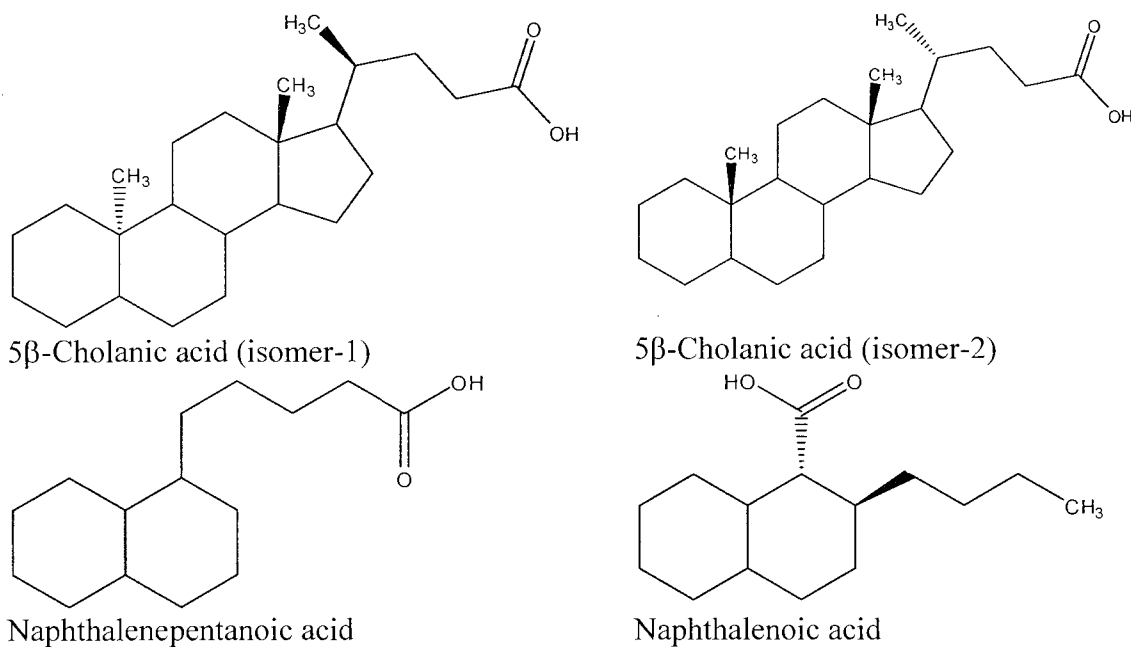
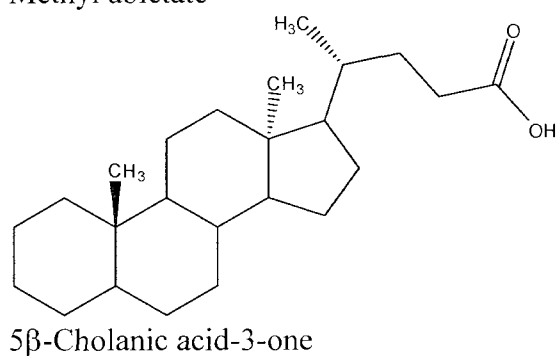
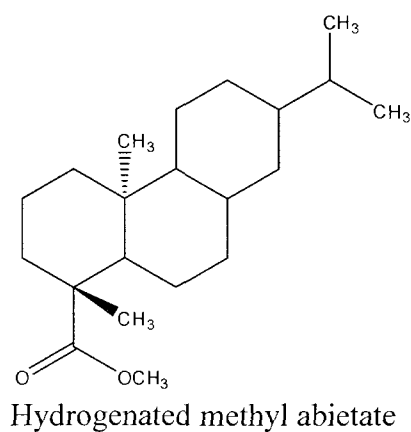
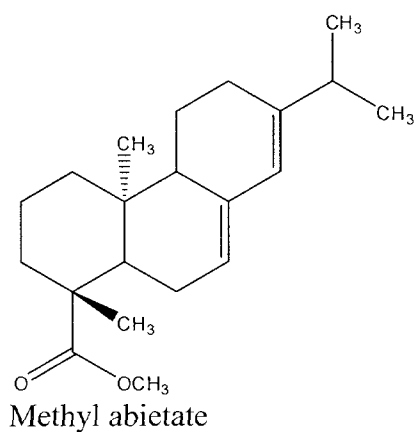


Figure 48 Sites of hydrogen bonding for naphthenic acids on asphaltene molecule

Table 27 Structures of naphthenic acids used in calculations





Five IE values for each naphthenic acid from Table 27, are tabulated as follows, Table 28 to Table 34. Contributions from electrostatic interactions (hydrogen bonding, dipole interactions) and vdW interactions to the total IE were calculated. Significant results are discussed.

Table 28 Interaction energy values for 5β-Cholanic acid (isomer-2)

| 5β-Cholanic acid (isomer-2) | | |
|-----------------------------|---------------|--------|
| S=O | IE | -42.06 |
| | vdW | -36.18 |
| | electrostatic | -7.26 |
| COOH | IE | -36.22 |
| | vdW | -30.15 |
| | electrostatic | -5.76 |
| N2 | IE | -33.34 |
| | vdW | -29.74 |

| | | |
|----|---------------|--------|
| | electrostatic | -3.86 |
| S | IE | -34.31 |
| | vdW | -31.94 |
| | electrostatic | -5.23 |
| N1 | IE | -31.36 |
| | vdW | -33.32 |
| | electrostatic | -1.73 |

IEs were calculated between asphaltene and cholanoic acid at different locations on the surface. Five interaction energy values are tabulated when the $-COOH$ of cholanoic acid formed hydrogen bonding with electronegative atoms of asphaltene. The largest IE was obtained when $-COOH$ of cholanoic acid formed a hydrogen bond with the $-S=O$ of asphaltene. The electrostatic component of the interaction energy (-7.26 kcal/mol) is mainly due to this hydrogen bonding.

Table 29 Interaction energy values for naphthalenepentanoic acid

| | Naphthalenepentanoic acid | |
|------|---------------------------|--------|
| S=O | IE | -29.82 |
| | vdW | -26.77 |
| | electrostatic | -4.33 |
| COOH | IE | -26.51 |
| | vdW | -22.32 |
| | electrostatic | -3.78 |
| N2 | IE | -30.19 |
| | vdW | -27.37 |
| | electrostatic | -2.90 |
| S | IE | -27.92 |
| | vdW | -27.05 |
| | electrostatic | -0.72 |
| N1 | IE | -27.51 |

| | | |
|--|---------------|--------|
| | vdW | -27.58 |
| | electrostatic | 0.31 |

Naphthalenepentanoic acid has its largest IE value when it forms a hydrogen bond with N2 of asphaltene. It has an electrostatic contribution of -2.90 kcal/mol, but the electrostatic interaction is stronger when -COOH formed a hydrogen bond with -S=O (-4.33 kcal/mol) or -COOH (-3.78 kcal/mol). The best IE value is obtained when sum of the vdW and electrostatic interaction energies is at the highest. In other words, the best electrostatic interaction and best vdW interaction are simultaneously possible only when the structures are optimum for these interactions.

Table 30 Interaction energy values for naphthalenoic acid

| Naphthalenoic acid | | |
|--------------------|---------------|--------|
| S=O | IE | -26.61 |
| | vdW | -25.47 |
| | electrostatic | -5.39 |
| COOH | IE | -33.07 |
| | vdW | -21.2 |
| | electrostatic | -11.63 |
| N2 | IE | -30.70 |
| | vdW | -28.31 |
| | electrostatic | -2.74 |
| S | IE | -29.02 |
| | vdW | -25.94 |
| | electrostatic | -2.95 |
| N1 | IE | -30.80 |
| | vdW | -26.82 |
| | electrostatic | -3.88 |

Naphthalenoic acid has the highest interaction energy when $-COOH$ of naphthalenoic acid forms hydrogen bond with $-COOH$ of asphaltene (-11.63 kcal/mol). This arrangement of asphaltene and naphthalenoic acid gave a lower vdW interaction (-21.24 kcal/mol).

Table 31 Interaction energy values for methyl abietate

| | Methyl abietate | |
|--------------------|-----------------|--------|
| Orient-1 | IE | -34.35 |
| | vdW | -34.17 |
| | electrostatic | -0.72 |
| COOH of asphaltene | IE | -31.62 |
| | vdW | -30.59 |
| | electrostatic | -3.85 |
| Orient-2 | IE | -30.03 |
| | vdW | -30.30 |
| | electrostatic | -2.03 |
| Orient-3 | IE | -33.17 |
| | vdW | -34.45 |
| | electrostatic | 0.01 |
| Orient-4 | IE | -33.17 |
| | vdW | -34.45 |
| | electrostatic | 0.01 |

Methyl abietate has one hydrogen bond acceptor ($-COOCH_3$) and does not have a hydrogen bond donor. Our model asphaltene has one hydrogen bond donor ($-COOH$). The electrostatic contribution for total interaction energy is very low except when the $-COOH$ of asphaltene forms a hydrogen bond with $-COOCH_3$ of methyl abietate (-3.85 kcal/mol).

Table 32 Interaction energy values for reduced methyl abietate

| | Reduced methyl abietate | |
|--------------------|-------------------------|--------|
| Orient-1 | IE | -31.90 |
| | vdW | -31.40 |
| | electrostatic | -0.43 |
| Orient-2 | IE | -29.54 |
| | vdW | -29.81 |
| | electrostatic | -0.39 |
| Orient-2 | IE | -29.22 |
| | vdW | -28.22 |
| | electrostatic | -1.06 |
| COOH of asphaltene | IE | -29.05 |
| | vdW | -29.09 |
| | electrostatic | -4.13 |
| Orient-4 | IE | -28.44 |
| | vdW | -28.51 |
| | electrostatic | 0.45 |

Reduced methyl abietate is obtained after the reduction of two double bonds in methyl abietate. IE values with asphaltene are relatively low for reduced methyl abietate due to the absence of two double bonds. Absence of two double bonds lowers the van der Waals interaction (low π - π interactions) and so decreases the overall interaction energy. Reduced methyl abietate has one hydrogen bond acceptor (-COOCH₃) and does not have a hydrogen bond donor. Asphaltene has one hydrogen bond donor (-COOH). The electrostatic contribution for total interaction energy is very low except when the -COOH of asphaltene formed a hydrogen bond with -COOCH₃ of reduced methyl abietate (-4.13 kcal/mol).

Table 33 Interaction energy values for 5 β -Cholanic acid (isomer-1)

| | 5 β -Cholanic acid (isomer-1) | |
|------|-------------------------------------|--------|
| S=O | IE | -35.51 |
| | vdW | -29.49 |
| | electrostatic | -6.11 |
| COOH | IE | -32.07 |
| | vdW | -27.99 |
| | electrostatic | -6.40 |
| N2 | IE | -36.65 |
| | vdW | -34.77 |
| | electrostatic | -3.09 |
| S | IE | -31.47 |
| | vdW | -32.44 |
| | electrostatic | -1.51 |
| N1 | IE | -33.59 |
| | vdW | -29.03 |
| | electrostatic | -6.32 |

Cholanic acid has highest interaction energy when it forms a relatively weak hydrogen bond with N2, and the vdW contribution is highest for this arrangement. It formed strong hydrogen bonds with –COOH, N1, and –S=O. As mentioned before, the magnitude of interaction energy is highest when the sum of the electrostatic interaction and vdW interaction is largest.

Table 34 Interaction energy values for 5 β -Cholanic acid-3-one

| | 5 β -Cholanic acid-3-one | |
|------|--------------------------------|--------|
| S=O | IE | -32.46 |
| | vdW | -32.10 |
| | electrostatic | -5.28 |
| COOH | IE | -38.92 |
| | vdW | -28.31 |

| | | |
|----|---------------|--------|
| | electrostatic | -10.07 |
| | | |
| N2 | IE | -34.64 |
| | vdW | -34.06 |
| | electrostatic | -0.49 |
| | | |
| S | IE | -32.33 |
| | vdW | -31.85 |
| | electrostatic | -2.01 |
| | | |
| N1 | IE | -30.95 |
| | vdW | -31.81 |
| | electrostatic | -1.95 |

Cholanoic acid-3-one has one hydrogen bond donor (-COOH) and one two hydrogen bond acceptors (-COOH, -C=O). Due to its long structure, two simultaneous hydrogen bonds are not possible in the majority of the arrangements. Cholanoic acid-3-one has the highest interaction energy when it formed hydrogen bonding with -COOH of asphaltenes (-38.92 kcal/mol). For the same arrangement, it has the highest electrostatic interaction (-10.07 kcal/mol).

4.4 Summary of Asphaltene-Naphthenic Acid IEs

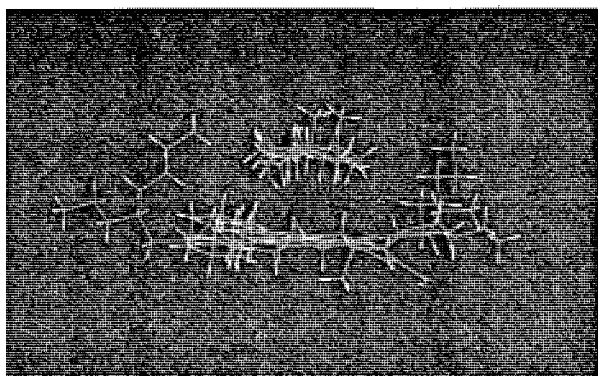
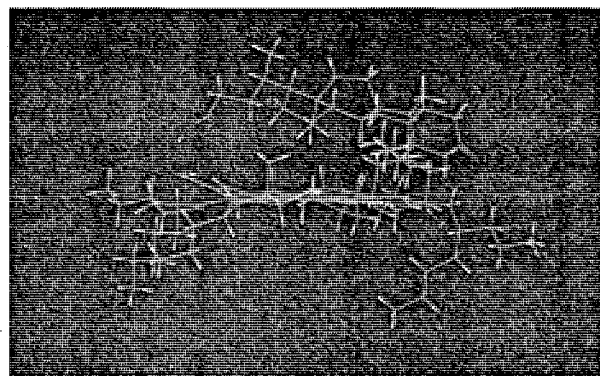
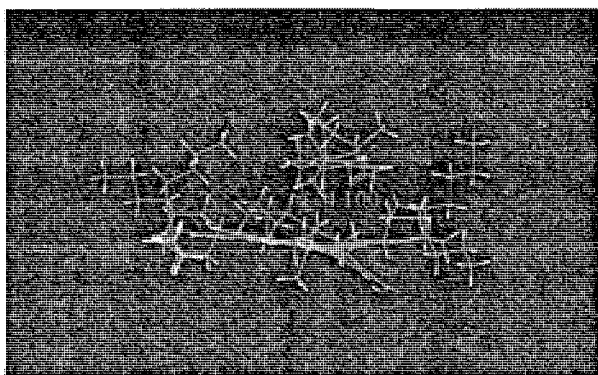
Average IEs between asphaltene and individual naphthenic acids are summarized in Table 35. The electrostatic part of the interaction energy is an indication of Hydrogen bonding [typical values: O—H...:N (6.9 kcal/mol), O—H...:O (5.0 kcal/mol), N—H...:N (3.1 kcal/mol), N—H...:O (1.9 kcal/mol)]. In some minimized structures, the -COOH of naphthenic acids is unable to form a hydrogen bond due to geometric constraints. In such cases polar components of naphthenic acids and asphaltene interact with each other. This is the justification for the higher electrostatic interaction contribution for total interaction

energy, even in the structures where no apparent hydrogen bond is present. From the interaction energy values, it is evident that several naphthenic acid molecules are required to disperse asphaltenes.

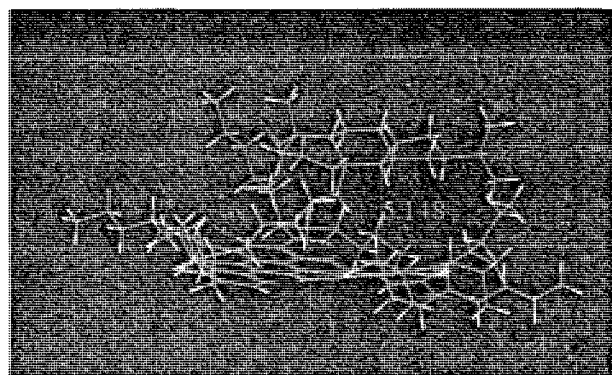
Table 35 Average interaction energies of naphthenic acids with asphaltenes

| Naphthenic acid | S=O/ Orient 1 | COOH / Orient 2 | N2/ Orient 3 | S/ Orient 4 | NI/ Orient 5 | Average IE |
|-------------------------------------|---------------------|--------------------------|--------------------|-------------------|--------------------|---------------|
| 5 β -Cholanic acid (isomer-2) | -42.06 | -36.22 | -33.34 | -34.31 | -31.36 | -35.46 |
| Naphthalenepentanoic acid | -29.82 | -26.51 | -30.19 | -27.92 | -27.51 | -28.39 |
| Naphthalenoic acid | -26.61 | -33.07 | -30.70 | -29.03 | -30.80 | -30.04 |
| Methyl abietate | -34.35 | -31.62 | -30.03 | -33.17 | -33.17 | -32.47 |
| Reduced methyl abietate | -31.90 | -29.54 | -29.22 | -29.05 | -28.44 | -29.63 |
| 5 β -Cholanic acid (isomer-1) | -35.51 | -32.07 | -36.65 | -31.47 | -33.59 | -33.86 |
| 5 β -Cholanic acid-3-one | -32.46 | -38.92 | -34.64 | -34.64 | -30.95 | -34.32 |

Minimized structures of methyl abietate, 5 β -cholanic acid, and 5 β -cholanic acid-3-one with asphaltene are shown in Figure 49. Asphaltene formed a bowl conformation in almost all minimized geometries for the accommodation of naphthenic acids. Generally all naphthenic acids preferred to be in the bowl (from interaction energy values), except for 5 β -cholanoic acid-3-one, which preferred other side of asphaltene (from interaction energy values). The measured distance between the two molecules is 3.988 Å for 5 β -cholanic acid and 4.100 Å for methyl abietate. But measured distance is high and varying for 5 β -cholanic acid-3-one. These observations are in consistent with aggregation prevention capabilities of these naphthenic acids in precipitation onset values for asphaltenes.

5 β -cholanic acid5 β -cholanic acid-3-one

Methyl abietate



Hydrogenated methyl abietate

Figure 49 Most stable conformations of methyl abietate, 5 β -cholanic acid, hydrogenated methyl abietate, and 5 β -cholanic acid-3-one with asphaltene

Further, comparison of aggregation prevention capabilities of methyl abietate and reduced methyl abietate are in consistent with observed IE values. The distances in minimized geometries of methyl abietate and hydrogenated methyl abietate are 4.100 Å and 5.148 Å, Figure 49. Reduced methyl abietate does not have double bonds. Due to reduced vdW interaction (π - π), reduced methyl abietate has lower interaction energy and it is farther from asphaltene surface in minimized structure. In summary, using a representative asphaltene structure, IEs were calculated for asphaltene dimers and found to be orientationally dependent (stacks). Interaction energies were calculated between

asphaltene and select naphthenic acids and IE values indicated specific unique interactions for each acid or acid derivative. Those naphthenic acids which delayed precipitation of asphaltenes were found to have strong affinities and minimized orientations in the “cup bowl” of asphaltene.

APPENDIX

SUPPLEMENTARY SWNT-POLYMER INTERACTION ENERGY VALUES

Table 36 Interaction energy values for a specific length of polymer with SWNT

| Polymer | Length of polymer (A°) (25 units) | IE/ 100 A° polymer (kcal/mol) |
|-----------------|-----------------------------------|-------------------------------|
| PTester | 98.14 | -313.67 |
| PANI | 125.40 | -154.65 |
| PVA | 64.00 | -142.83 |
| PAA | 63.42 | -102.02 |
| PEG | 88.57 | -120.84 |
| Dextran | 148.00 | -95.50 |
| PSS | 50.61 | -436.42 |
| PTsulfonic acid | 95.85 | -657.72 |
| PAA(HCl) | 63.42 | -103.15 |
| EMER | 132.46 | -170.52 |

Table 37 Interaction energies between polymer strands in polymer wrapped SWNT

| Polymer | Required units | TPE of polymer around NT (kcal/mol) | Calculated TPE of polymer (kcal/mol) | Poly-poly interaction in wrapped NT (kcal/mol) |
|-----------------|----------------|-------------------------------------|--------------------------------------|--|
| PT | 28 | 1980.99 | 1724.77 | 256.22 |
| PANI | 36 | -666.82 | -599.52 | -67.29 |
| PEG | 84 | -37.34 | 96.54 | -133.88 |
| PVA | 117 | -3023.40 | -2899.65 | -123.75 |
| PAA | 66 | -589.12 | -536.86 | -52.25 |
| PSS | 44 | -5555.83 | -5839.52 | 283.69 |
| Dextran | 55 | 2062.84 | 2482.28 | -419.45 |
| PTsulfonic acid | 21 | -1389.37 | -1142.72 | -246.65 |
| EMER | 36 | -1983.46 | -1523.62 | -459.84 |

Table 38 Interaction energies between free polymers strands

| Polymer | Required units | Two strands (kcal/mol) | One strand 10 units (kcal/mol) | IE dimer (kcal/mol) | IE dimer/ required units (kcal/mol) |
|-----------------|----------------|------------------------|--------------------------------|---------------------|-------------------------------------|
| PT | 28 | 1130.14 | 615.99 | -101.84 | -142.58 |
| PANI | 36 | -382.11 | -166.53 | -49.04 | -88.28 |
| PEG | 84 | 1.28 | 11.49 | -21.71 | -91.17 |
| PVA | 117 | -517.27 | -247.83 | -21.60 | -126.37 |
| PAA | 66 | -185.45 | -81.34 | -22.77 | -75.12 |
| PSS | 44 | -2747.36 | -1327.16 | -93.03 | -204.66 |
| Dextran | 55 | 840.77 | 451.32 | -61.88 | -170.16 |
| PTsulfonic acid | 21 | -1258.16 | -544.15 | -169.86 | -178.35 |
| EMER | 36 | -884.92 | -423.23 | -38.46 | -69.23 |
| PAA(HCl) | 66 | -2411.37 | -1190.24 | -30.90 | -101.96 |

Table 39 Normalized interaction energies for polymer-SWNT composites

| Polymer | IE/25 units (kcal/mol) | Number of strands | Required units | IE (per required units) (kcal/mol) |
|-----------------|------------------------|-------------------|----------------|------------------------------------|
| PT | -307.83 | 4 | 28 | -344.77 |
| PANI | -193.93 | 9 | 36 | -279.26 |
| PEG | -107.02 | 14 | 84 | -359.59 |
| PVA | -91.40 | 13 | 117 | -427.75 |
| PAA | -64.69 | 6 | 66 | -170.78 |
| PSS | -220.87 | 4 | 44 | -388.73 |
| Dextran | -141.34 | 5 | 55 | -310.95 |
| PTsulfonic acid | -630.45 | 3 | 21 | -529.58 |
| EMER | -225.85 | 9 | 36 | -325.22 |
| PAA(HCl) | -65.42 | 6 | 66 | -172.71 |

REFERENCES

1. Leach, A.R., *Molecular Modelling: Principles and Applications*. 2000. 720 pp.
2. Shao, J., *Molecular modeling applications in protein-ligand binding*. 2005. p. 104 pp.
3. Parr, R.G. and W. Yang, *Density-functional Theory of Atoms and Molecules*. 1989. 333 pp.
4. Tinoco, I., Jr., K. Sauer, and J.C. Wang, *Physical Chemistry : Principles and Applications in Biological Sciences, 3rd Edition*. 1995. 761 pp.
5. Boyd, D.B., *Aspects of molecular modeling*. Rev. Comput. Chem., 1990: p. 321-54.
6. Vreven, T., et al., *Geometry optimization with QM/MM, ONIOM, and other combined methods. I. Microiterations and constraints*. Journal of Computational Chemistry, 2003. **24**(6): p. 760-769.
7. Eurenium, K.P., et al., *Enzyme mechanisms with hybrid quantum and molecular mechanical potentials. I. Theoretical considerations*. International Journal of Quantum Chemistry, 1996. **60**(6): p. 1189-1200.
8. Warshel, A., *Computer Modeling of Chemical Reactions in Enzymes and Solutions*. 1991. 236 pp.
9. Young, D.C., *Computational Chemistry: A Practical Guide for Applying Techniques to Real World Problems*. 3rd ed. 2001, New York: John Wiley. 408.
10. Jensen, F., *Introduction to Computational Chemistry* 2nd ed. 2006: Wiley. 624.
11. Dickie, A.J., *Molecularly self-assembled thin films: theoretical evaluation and experimental fabrication*. 2003. p. 293 pp.
12. Sun, H., *COMPASS: An ab Initio Force-Field Optimized for Condensed-Phase Applications - Overview with Details on Alkane and Benzene Compounds*. Journal of Physical Chemistry B, 1998. **102**(38): p. 7338-7364.
13. Halgren, T.A., *Merck molecular force field. I. Basis, form, scope, parameterization, and performance of MMFF94*. Journal of Computational Chemistry, 1996. **17**(5 & 6): p. 490-519.

14. Allinger, N.L., *Conformational analysis. 130. MM2. A hydrocarbon force field utilizing V1 and V2 torsional terms*. Journal of the American Chemical Society, 1977. **99**(25): p. 8127-34.
15. Weiner, S.J., et al., *A new force field for molecular mechanical simulation of nucleic acids and proteins*. Journal of the American Chemical Society, 1984. **106**(3): p. 765-84.
16. Cornell, W.D., et al., *A Second Generation Force Field for the Simulation of Proteins, Nucleic Acids, and Organic Molecules*. Journal of the American Chemical Society, 1995. **117**(19): p. 5179-97.
17. Jorgensen, W.L. and J. Tirado-Rives, *The OPLS [optimized potentials for liquid simulations] potential functions for proteins, energy minimizations for crystals of cyclic peptides and crambin*. Journal of the American Chemical Society, 1988. **110**(6): p. 1657-66.
18. Gaudreault, R., *Mechanisms of flocculation with poly(ethylene oxide) and novel cofactors: Theory and experiment*. 2004. p. 262 pp.
19. Materials-Visualizer, *Materials Studio Modeling v4.0.0.0*. 2005: Accelrys Software Inc., San Diego.
20. Discover, *Materials Studio Modeling v4.0.0.0*. 2005: Accelrys Software Inc., San Diego.
21. Sun, H. and D. Rigby, *Polysiloxanes: ab initio force field and structural, conformational and thermophysical properties*. Molecular and Biomolecular Spectroscopy, 1997. **53A**(8): p. 1301-1323.
22. Rigby, D., H. Sun, and B.E. Eichinger, *Computer simulations of poly(ethylene oxide): force field, PVT diagram and cyclization behavior*. Polymer International, 1997. **44**(3): p. 311-330.
23. Spyriouni, T. and C. Vergelati, *A Molecular Modeling Study of Binary Blend Compatibility of Polyamide 6 and Poly(vinyl acetate) with Different Degrees of Hydrolysis: An Atomistic and Mesoscopic Approach*. Macromolecules, 2001. **34**(15): p. 5306-5316.
24. Kitson, D.H. and A.T. Hagler, *Theoretical studies of the structure and molecular dynamics of a peptide crystal*. Biochemistry, 1988. **27**(14): p. 5246-57.

25. Rappe, A.K. and W.A. Goddard, III, *Charge equilibration for molecular dynamics simulations*. Journal of Physical Chemistry, 1991. **95**(8): p. 3358-63.
26. Gasteiger, J. and M. Marsili, *Iterative partial equalization of orbital electronegativity: a rapid access to atomic charges*. Tetrahedron, 1980. **36**(22): p. 3219-22.
27. Iijima, S., *Helical microtubules of graphitic carbon*. Nature (London, United Kingdom), 1991. **354**(6348): p. 56-8.
28. McEuen, P.L., et al., *One-dimensional transport in carbon nanotubes*. Microelectronic Engineering, 1999. **47**(1-4): p. 417-420.
29. Hamada, N., S. Sawada, and A. Oshiyama, *New one-dimensional conductors: graphitic microtubules*. Physical Review Letters, 1992. **68**(10): p. 1579-81.
30. Thess, A., et al., *Crystalline ropes of metallic carbon nanotubes*. Science (Washington, D. C.), 1996. **273**(5274): p. 483-487.
31. Baughman, R.H., A.A. Zakhidov, and W.A. de Heer, *Carbon nanotubes-the route toward applications*. Science (Washington, DC, United States), 2002. **297**(5582): p. 787-792.
32. Mickelson, E.T., et al., *Fluorination of single-wall carbon nanotubes*. Chemical Physics Letters, 1998. **296**(1,2): p. 188-194.
33. Stevens, J.L., et al., *Sidewall aminofunctionalization of single-walled carbon nanotubes through fluorination and subsequent reactions with terminal diamines*. Nano Letters, 2003. **3**(3): p. 331-336.
34. Sung, J.H., et al., *Nanofibrous Membranes Prepared by Multiwalled Carbon Nanotube/Poly(methyl methacrylate) Composites*. Macromolecules, 2004. **37**(26): p. 9899-9902.
35. Park, S.J., et al., *Synthesis and dispersion characteristics of multi-walled carbon nanotube composites with poly(methyl methacrylate) prepared by in-situ bulk polymerization*. Macromolecular Rapid Communications, 2003. **24**(18): p. 1070-1073.
36. Shaffer, M.S.P. and K. Koziol, *Polystyrene grafted multi-walled carbon nanotubes*. Chemical Communications (Cambridge, United Kingdom), 2002(18): p. 2074-2075.

37. Bahr, J.L. and J.M. Tour, *Covalent chemistry of single-wall carbon nanotubes*. Journal of Materials Chemistry, 2002. **12**(7): p. 1952-1958.
38. Kumar, S., *Polymer /carbon nanotube composites: challenges and opportunities*. PMSE Preprints, 2004. **90**: p. 59-60.
39. Ajayan, P.M., et al., *Aligned carbon nanotube arrays formed by cutting a polymer resin-nanotube composite*. Science (Washington, DC, United States), 1994. **265**(5176): p. 1212-14.
40. Cooper, C.A., R.J. Young, and M. Halsall, *Investigation into the deformation of carbon nanotubes and their composites through the use of Raman spectroscopy*. Composites, Part A: Applied Science and Manufacturing, 2001. **32A**(3-4): p. 401-411.
41. Gao, G., T. Cagin, and W.A. Goddard, III, *Energetics, structure, mechanical and vibrational properties of single-walled carbon nanotubes*. Nanotechnology, 1998. **9**(3): p. 184-191.
42. Uchida, T. and S. Kumar, *Single wall carbon nanotube dispersion and exfoliation in polymers*. Journal of Applied Polymer Science, 2005. **98**(3): p. 985-989.
43. de Heer, W.A., *Nanotubes and the pursuit of applications*. MRS Bulletin, 2004. **29**(4): p. 281-285.
44. McEuen, P.L., et al., *Disorder, Pseudospins, and Backscattering in Carbon Nanotubes*. Physical Review Letters, 1999. **83**(24): p. 5098-5101.
45. Berber, S., Y.-K. Kwon, and D. Tomanek, *Unusually High Thermal Conductivity of Carbon Nanotubes*. Physical Review Letters, 2000. **84**(20): p. 4613-4616.
46. Coleman, J.N., et al., *Percolation-dominated conductivity in a conjugated-polymer-carbon-nanotube composite*. Physical Review B: Condensed Matter and Materials Physics, 1998. **58**(12): p. R7492-R7495.
47. Valter, B., M.K. Ram, and C. Nicolini, *Synthesis of Multiwalled Carbon Nanotubes and Poly(o-anisidine) Nanocomposite Material: Fabrication and Characterization of Its Langmuir-Schaefer Films*. Langmuir, 2002. **18**(5): p. 1535-1541.
48. Bryning, M.B., et al., *Very low conductivity threshold in bulk isotropic single-walled carbon nanotube-epoxy composites*. Advanced Materials (Weinheim, Germany), 2005. **17**(9): p. 1186-1191.

49. Jishi, R.A., M.S. Dresselhaus, and G. Dresselhaus, *Symmetry properties of chiral carbon nanotubes*. Phys. Rev. B: Condens. Matter FIELD Full Journal
Title:Physical Review B: Condensed Matter and Materials Physics, 1993. **47**(24): p. 16671-4.
50. Wildoer, J.W.G., et al., *Electronic structure of atomically resolved carbon nanotubes*. Nature (London), 1998. **391**(6662): p. 59-62.
51. Mpourmpakis, G., et al., *Theoretical study of alkaline metal cations in carbon nanotubes*. Rev. Adv. Mater. Sci., 2006. **11**(1): p. 92-97.
52. Ramasubramaniam, R., J. Chen, and H. Liu, *Homogeneous carbon nanotube/polymer composites for electrical applications*. Applied Physics Letters, 2003. **83**(14): p. 2928-2930.
53. Numata, M., et al., *Inclusion of Cut and As-Grown Single-Walled Carbon Nanotubes in the Helical Superstructure of Schizophyllan and Curdlan (b-1,3-Glucans)*. Journal of the American Chemical Society, 2005. **127**(16): p. 5875-5884.
54. O'Connell, M.J., et al., *Reversible water-solubilization of single-walled carbon nanotubes by polymer wrapping*. Chemical Physics Letters, 2001. **342**(3,4): p. 265-271.
55. Star, A. and J.F. Stoddart, *Dispersion and Solubilization of Single-Walled Carbon Nanotubes with a Hyperbranched Polymer*. Macromolecules FIELD Full Journal
Title:Macromolecules, 2002. **35**(19): p. 7516-7520.
56. Gao, H. and Y. Kong, *Simulation of DNA-nanotube interactions*. Annual Review of Materials Research, 2004. **34**: p. 123-150.
57. Star, A., et al., *Starched carbon nanotubes*. Angewandte Chemie, International Edition, 2002. **41**(14): p. 2508-2512.
58. Srebnik, S., I. Gurevitz, and S. Levchenko, *Nanoscale ordering of polymer adsorbed on nanotubes*. AIChE Annual Meeting, Conference Proceedings, Philadelphia, PA, United States, Nov. 16-21, 2008, 2008: p. 553/1-553/8.
59. Deria, P., et al., *Single-chain, helical wrapping of individualized, single-walled carbon nanotubes by semiconducting polymers in both aqueous and nonaqueous solvents*. Abstracts of Papers, 238th ACS National Meeting, Washington, DC, United States, August 16-20, 2009, 2009: p. PHYS-283.

60. Giulianini, M., et al., *Regioregular poly(3-hexyl-thiophene) helical self-organization on carbon nanotubes*. Applied Physics Letters, 2009. **95**(1): p. 013304/1-013304/3.
61. Dresselhaus, M.S., et al., *Science of Fullerenes and Carbon Nanotubes*. 1996. 965 pp.
62. von Helden, G., et al., *Carbon cluster cations with up to 84 atoms: structures, formation mechanism, and reactivity*. Journal of Physical Chemistry, 1993. **97**(31): p. 8182-92.
63. Kroto, H.W., et al., *C60: buckminsterfullerene*. Nature (London) FIELD Full Journal Title:Nature (London, United Kingdom), 1985. **318**(6042): p. 162-3.
64. Kraetschmer, W., et al., *Solid C60: a new form of carbon*. Nature (London) FIELD Full Journal Title:Nature (London, United Kingdom), 1990. **347**(6291): p. 354-8.
65. Haufler, R.E., et al., *Efficient production of C60 (buckminsterfullerene), C60H36, and the solvated buckide ion*. Journal of Physical Chemistry, 1990. **94**(24): p. 8634-6.
66. Lamb, L.D. and D.R. Huffman, *Fullerene production*. Journal of Physics and Chemistry of Solids, 1993. **54**(12): p. 1635-43.
67. Diederich, F., et al., *The higher fullerenes: isolation and characterization of C76, C84, C90, C94, and C70O, an oxide of D5h-C70*. Science (Washington, D. C., 1883-) FIELD Full Journal Title:Science (Washington, DC, United States), 1991. **252**(5005): p. 548-51.
68. Kroto, H., *Space, stars, C60, and soot*. Science (Washington, D. C., 1883-) FIELD Full Journal Title:Science (Washington, DC, United States), 1988. **242**(4882): p. 1139-45.
69. Cheung, J.T. and H. Sankur, *Growth of thin films by laser-induced evaporation*. Crit. Rev. Solid State Mater. Sci. FIELD Full Journal Title:Critical Reviews in Solid State and Materials Sciences, 1988. **15**(1): p. 63-109.
70. Howard, J.B., et al., *Fullerenes synthesis in combustion*. Carbon, 1992. **30**(8): p. 1183-201.
71. Curl, R.F., *Pre-1990 Evidence For The Fullerene Proposal*. Carbon, 1992. **30**(8): p. 1149-1155.

72. Smalley, R.E. and B.I. Yakobson, *The future of the fullerenes*. Solid State Communications, 1998. **107**(11): p. 597-606.
73. Taylor, R. and D.R.M. Walton, *The Chemistry Of Fullerenes*. Nature, 1993. **363**(6431): p. 685-693.
74. Stevenson, S., et al., *Automated Hplc Separation Of Endohedral Metallofullerene Sc-At-C-2n And Y-At-C-2n Fractions*. Analytical Chemistry, 1994. **66**(17): p. 2675-2679.
75. Stevenson, S., et al., *Isolation And Monitoring Of The Endohedral Metallofullerenes Y-At-C-82 And Sc3-At-C-82 - Online Chromatographic-Separation With Epr Detection*. Analytical Chemistry, 1994. **66**(17): p. 2680-2685.
76. Kobayashi, K., et al., *Endohedral metallofullerenes. Are the isolated pentagon rule and fullerene structures always satisfied?* Journal of the American Chemical Society, 1997. **119**(51): p. 12693-12694.
77. Nagase, S., K. Kobayashi, and T. Akasaka, *Recent progress in endohedral dimetallofullerenes*. Theochem-Journal Of Molecular Structure, 1997. **398**: p. 221-227.
78. Shinohara, H., *Endohedral metallofullerenes*. Reports on Progress in Physics, 2000. **63**(6): p. 843-892.
79. Wang, C.R., et al., *A scandium carbide endohedral metallofullerene: (Sc2C2)@C-84*. Angewandte Chemie-International Edition, 2001. **40**(2): p. 397-399.
80. Tran, N.E. and J.J. Lagowski, *A study of the synthesis of endohedral metallofullerenes and empty fullerenes by the carbon-arc and RFICP technique*. Carbon, 2002. **40**(6): p. 939-948.
81. Inoue, T., et al., *Spectroscopic and structural study of Y2C2 carbide encapsulating endohedral metallofullerene: (Y2C2)@C-82*. Chemical Physics Letters, 2003. **382**(3-4): p. 226-231.
82. Lu, X., et al., *Isolation and spectroscopic study of a series of monogadolinium endohedral metallofullerenes*. Fullerenes Nanotubes And Carbon Nanostructures, 2005. **13**(1): p. 13-20.

83. Cveticanin, J., et al., *Endohedral fullerenes of different elements*. Journal Of Optoelectronics And Advanced Materials, 2006. **8**(5): p. 1892-1894.
84. Chen, N., et al., *Size effect of encaged clusters on the exohedral chemistry of endohedral fullerenes: A case study on the pyrrolidino reaction of Sc_xGd_{3-x}N@C-80 (x=0-3)*. Organic Letters, 2007. **9**(10): p. 2011-2013.
85. Dunsch, L. and S.F. Yang, *Endohedral clusterfullerenes - playing with cluster and cage sizes*. Physical Chemistry Chemical Physics, 2007. **9**(24): p. 3067-3081.
86. Kitaura, R. and H. Shinohara, *Endohedral metallofullerenes and nano-peapods*. Japanese Journal of Applied Physics Part 1-Regular Papers Brief Communications & Review Papers, 2007. **46**(3A): p. 881-891.
87. Qian, M.C., et al., *Magnetic endohedral metallofullerenes with floppy interiors*. Physical Review B, 2007. **75**(10).
88. Liu, L., et al., *The structural determination of endohedral metallofullerene Gd@C-82 by XANES*. Chemical Communications, 2008(4): p. 474-476.
89. Stevenson, S., et al., *Small-bandgap endohedral metallofullerenes in high yield and purity*. Nature, 1999. **401**(6748): p. 55-57.
90. Olmstead, M.M., et al., *Isolation and crystallographic characterization of ErSc₂N@C-80: an endohedral fullerene which crystallizes with remarkable internal order*. Journal of the American Chemical Society, 2000. **122**(49): p. 12220-12226.
91. Kobayashi, K., Y. Sano, and S. Nagase, *Theoretical study of endohedral metallofullerenes: Sc_{3-n}LanN@C-80 (n=0-3)*. Journal of Computational Chemistry, 2001. **22**(13): p. 1353-1358.
92. Krause, M., et al., *Structure and stability of endohedral fullerene Sc₃N@C-80: A Raman, infrared, and theoretical analysis*. Journal of Chemical Physics, 2001. **115**(14): p. 6596-6605.
93. Olmstead, M.H., et al., *Isolation and structural characterization of the endohedral fullerene Sc₃N@C₇₈*. Angewandte Chemie-International Edition, 2001. **40**(7): p. 1223-1225.
94. Campanera, J.M., et al., *Bonding within the endohedral fullerenes Sc₃N@C-78 and Sc₃N@C-80 as determined by density functional calculations and reexamination of the crystal structure of {Sc₃N@C-78}center dot Co(OEP)center*

- dot 1.5(C6H6)center dot 0.3(CHCl3)*. Journal of Physical Chemistry A, 2002. **106**(51): p. 12356-12364.
95. Feng, L., et al., *Isolation and characterization of the endohedral metallofullerene Tb3N@C-80*. Chemical Journal Of Chinese Universities-Chinese, 2002. **23**(6): p. 996-998.
96. Stevenson, S., et al., *Preparation and crystallographic characterization of a new endohedral, Lu3N@C-80 center dot 5(o-xylene), and comparison with Sc3N@C(80)5 center dot(o-xylene)*. Chemistry--A European Journal, 2002. **8**(19): p. 4528-4535.
97. Dunsch, L., et al., *New clusters in endohedral fullerenes: The metalnitrides*. Synthetic Metals, 2003. **135**(1-3): p. 761-762.
98. Olmstead, M.M., et al., *Sc3N@C-68: Folded pentalene coordination in an endohedral fullerene that does not obey the isolated pentagon rule*. Angewandte Chemie-International Edition, 2003. **42**(8): p. 900-+.
99. Dunsch, L., et al., *Endohedral nitride cluster fullerenes - Formation and spectroscopic analysis of L3-xMxN@C-2n (0 <= x <= 3; N=39,40)*. Journal of Physics and Chemistry of Solids, 2004. **65**(2-3): p. 309-315.
100. Heine, T., K. Vietze, and G. Seifert, *C-13 NMR fingerprint characterizes long time-scale structure of SC3N@C-80 endohedral fullerene*. Magnetic Resonance in Chemistry, 2004. **42**: p. S199-S201.
101. Cardona, C.M., A. Kitaygorodskiy, and L. Echegoyen, *Trimetallic nitride endohedral metallofullerenes: Reactivity dictated by the encapsulated metal cluster*. Journal of the American Chemical Society, 2005. **127**(29): p. 10448-10453.
102. Krause, M., et al., *The electronic and vibrational structure of endohedral Tm3N@C-80 (I) fullerene - Proof of an encaged Tm3+*. Journal of Physical Chemistry A, 2005. **109**(32): p. 7088-7093.
103. Krause, M., J. Wong, and L. Dunsch, *Expanding the world of endohedral fullerenes - The Tm3N@C-2n (39 <= n <= 43) clusterfullerene family*. Chemistry-A European Journal, 2005. **11**(2): p. 706-711.
104. Liu, X., et al., *Electronic structures of the pristine and K-intercalated Tm3N@C-80 endohedral fullerenes*. Physical Review B, 2005. **72**(8).

105. Wolf, M., et al., *Magnetic moments of the endohedral cluster fullerenes Ho₃N@C-80 and Tb₃N@C-80: The role of ligand fields*. *Angewandte Chemie-International Edition*, 2005. **44**(21): p. 3306-3309.
106. Yang, S.F. and L. Dunsch, *A large family of dysprosium-based trimetallic nitride endohedral fullerenes: Dy₃N@C-2n (39 ≤ n ≤ 44)*. *Journal of Physical Chemistry B*, 2005. **109**(25): p. 12320-12328.
107. Beavers, C.M., et al., *Tb₃N@C-84: An improbable, egg-shaped endohedral fullerene that violates the isolated pentagon rule*. *Journal of the American Chemical Society*, 2006. **128**(35): p. 11352-11353.
108. Krause, M., A. Popov, and L. Dunsch, *Vibrational structure of endohedral fullerene Sc₃N@C-78 (D-3h⁻): Evidence for a strong coupling between the Sc₃N cluster and C-78 cage*. *Chemphyschem*, 2006. **7**(8): p. 1734-1740.
109. Yanov, I., et al., *Local minima conformations of the Sc₃N@C-80 endohedral complex: Ab initio quantum chemical study and suggestions for experimental verification*. *International Journal of Quantum Chemistry*, 2006. **106**(14): p. 2975-2980.
110. Qian, M.C. and S.N. Khanna, *An ab initio investigation on the endohedral metallofullerene Gd₃N-C-80*. *Journal of Applied Physics*, 2007. **101**(9).
111. Wang, D.L., X.P. Sun, and Y.C. Zhai, *DFT studies on non-IPR C-68 and endohedral fullerene Sc₃N@C-68*. *Chinese Journal of Structural Chemistry*, 2007. **26**(3): p. 321-327.
112. Yang, S., A.A. Popov, and L. Dunsch, *The role of an asymmetric nitride cluster on a fullerene cage: The Non-IPR endohedral DySc₂N@C-76*. *Journal of Physical Chemistry B*, 2007. **111**(49): p. 13659-13663.
113. Yang, S.F., A.A. Popov, and L. Dunsch, *Violating the Isolated Pentagon Rule (IPR): The endohedral Non-IPR cage of Sc₃N@C-70*. *Angewandte Chemie-International Edition*, 2007. **46**(8): p. 1256-1259.
114. Zhang, L., et al., *Electrochemistry of Sc₃N@C-78 and Sc₃N@C-80 (I-h): On achieving reversible redox waves of the trimetal nitride endohedral fullerenes*. *Journal of Electroanalytical Chemistry*, 2007. **608**(1): p. 15-21.
115. Stevenson, S., et al., *Internal and external factors in the structural organization in cocrystals of the mixed-metal endohedrals (GdSc₂N@I-h-C-80, Gd₂ScN@I-h-C-*

- 80*, and *TbSc2N@I-h-C-80*) and nickel(II) octaethylporphyrin. *Inorganic Chemistry*, 2008. **47**(5): p. 1420-1427.
116. Stevenson, S., et al., *Rapid Removal of D5h Isomer Using the "Stir and Filter Approach" and Isolation of Large Quantities of Isomerically Pure Sc3N@C80 Metallic Nitride Fullerenes*. *Journal of the American Chemical Society*, 2007. **129**(19): p. 6072-6073.
117. Stevenson, S., et al., *Effect of copper metal on the yield of Sc3N@C80 metallofullerenes*. *Chemical Communications (Cambridge, United Kingdom)*, 2007(41): p. 4263-4265.
118. Stevenson, S., et al., *A stable non-classical metallofullerene family*. *Nature (London)*, 2000. **408**(6811): p. 427-428.
119. Echegoyen, L., et al., *X-Ray crystallographic and EPR spectroscopic characterization of a pyrrolidine adduct of Y3N@C80*. *Chemical Communications (Cambridge, United Kingdom)*, 2006(25): p. 2653-2655.
120. Lee, H.M., et al., *Crystallographic Characterization and Structural Analysis of the First Organic Functionalization Product of the Endohedral Fullerene Sc3N@C80*. *Journal of the American Chemical Society*, 2002. **124**(14): p. 3494-3495.
121. Biryulin, Y.F., et al., *Investigation of C-60 fullerene films on polymer substrates*. *Microelectronic Engineering*, 2003. **69**(2-4): p. 505-510.
122. Bulusheva, L.G. and A.V. Okotrub, *Electronic interactions in two-dimensional polymers of the C-60 fullerene*. *Physics Of The Solid State*, 2006. **48**(1): p. 185-191.
123. Makarova, T.L., et al., *Magnetism in photopolymerized fullerenes*. *Carbon*, 2003. **41**(8): p. 1575-1584.
124. Ueda, S., et al., *Dimensional dependence of electronic structure of fullerene polymers*. *Journal Of Physical Chemistry B*, 2006. **110**(45): p. 22374-22381.
125. Wood, R.A., et al., *In situ x-ray diffraction studies of three-dimensional C-60 polymers*. *Journal Of Physics-Condensed Matter*, 2002. **14**(45): p. 11615-11621.
126. Wood, R.A., et al., *Ferromagnetic fullerene*. *Journal Of Physics-Condensed Matter*, 2002. **14**(22): p. L385-L391.

127. Hirsch, A., *The Chemistry of the Fullerenes*. Thieme Organic Chemistry Monograph Series. 1994, Stuttgart: Georg Thieme Verlag.
128. Taylor, R., *The Chemistry of Fullerenes*. Advanced Series in Fullerenes, ed. R. Taylor. Vol. 4. 1995, New Jersey: World Scientific.
129. Sinnott, S.B., et al., *Mechanical properties of nanotubule fibers and composites determined from theoretical calculations and simulations*. Carbon FIELD Full Journal Title:Carbon, 1998. **36**(1-2): p. 1-9.
130. Hu, Y., et al., *Carbon nanostructures for advanced composites*. Rep. Prog. Phys. FIELD Full Journal Title:Reports on Progress in Physics, 2006. **69**(6): p. 1847-1895.
131. Wang, Y., *Photoconductivity of fullerene-doped polymers*. Nature (London) FIELD Full Journal Title:Nature (London, United Kingdom), 1992. **356**(6370): p. 585-7.
132. Sariciftci, N.S., et al., *Photoinduced electron transfer from a conducting polymer to buckminsterfullerene*. Science (Washington, DC, United States), 1992. **258**(5087): p. 1474-6.
133. Uchida, S., et al., *Organic small molecule solar cells with a homogeneously mixed copper phthalocyanine: C60 active layer*. Applied Physics Letters, 2004. **84**(21): p. 4218-4220.
134. Veenstra, S.C., et al., *Sexithiophene-C60 blends as model systems for photovoltaic devices*. Synthetic Metals, 1997. **84**(1-3): p. 971-972.
135. Yoo, S., B. Domercq, and B. Kippelen, *Efficient thin-film organic solar cells based on pentacene/C60 heterojunctions*. Applied Physics Letters, 2004. **85**(22): p. 5427-5429.
136. Ge, Z.X., et al., *Purification of endohedral trimetallic nitride fullerenes in a single, facile step*. Journal of the American Chemical Society, 2005. **127**(46): p. 16292-16298.
137. Stevenson, S., et al., *Nonchromatographic "stir and filter approach" (SAFA) for isolating Sc3N@C-80 metallofullerenes*. Journal of the American Chemical Society, 2006. **128**(27): p. 8829-8835.
138. Stevenson, S., et al., *Rapid removal of D-5h isomer using the "stir and filter approach" and isolation of large quantities of isomerically pure Sc3N@C-80*

- metallic nitride fullerenes*. Journal of the American Chemical Society, 2007. **129**(19): p. 6072-6073.
139. Stevenson, S., et al., *Effect of copper metal on the yield of Sc₃N@C-80 metallofullerenes*. Chemical Communications, 2007(41): p. 4263-4265.
140. Stevenson, S., et al., *Chemically adjusting plasma temperature, energy, and reactivity (CAPTEAR) method using NO_x and combustion for selective synthesis of Sc₃N@C-80 metallic nitride fullerenes*. Journal of the American Chemical Society, 2007. **129**(51): p. 16257-16262.
141. Stevenson, S., et al., *Small-bandgap endohedral metallofullerenes in high yield and purity*. Nature (London), 1999. **401**(6748): p. 55-57.
142. Hamilton, K.Y., *Synthesis, characterization, and application of water-soluble chiral calix[4]arene derivatives in spectroscopy and capillary electrokinetic chromatography*. 2003. p. 162 pp.
143. Gutsche, C.D., *Calixarenes*. Accounts of Chemical Research, 1983. **16**(5): p. 161-70.
144. Andreetti, G.D., R. Ungaro, and A. Pochini, *Crystal and molecular structure of cyclo{quater[(5-tert-butyl-2-hydroxy-1,3-phenylene)methylene]} toluene (1:1) clathrate*. Journal of the Chemical Society, Chemical Communications, 1979(22): p. 1005-7.
145. Haino, T., et al., *Fullerene encapsulation with calix[5]arenes*. Tetrahedron, 2006. **62**(9): p. 2025-2035.
146. Haino, T., C. Fukunaga, and Y. Fukazawa, *Complexation of higher fullerenes by calix[5]arene-based host molecules*. Journal of Nanoscience and Nanotechnology, 2007. **7**(4/5): p. 1386-1388.
147. Giesa, S., et al., *Experiments towards an analytical application of host-guest complexes of [60] fullerene and its derivatives*. European Mass Spectrometry, 1998. **4**(3): p. 189-196.
148. Atwood, J.L., et al., *Association and orientation of C₇₀ on complexation with calix[5]arene*. Chemical Communications (Cambridge, United Kingdom), 2003(18): p. 2270-2271.
149. Castillo, R., et al., *Langmuir Films of Calix[8]arene/Fullerene Complexes*. Journal of Physical Chemistry, 1996. **100**(2): p. 709-13.

150. Ghosh, K., et al., *Spectrophotometric study of the supramolecular complexes of [60]- and [70]Fullerenes with biscalix[6]arene and crown[4]calix[6]arene*. *Molecular and Biomolecular Spectroscopy*, 2007. **66A**(4-5): p. 1122-1125.
151. Kunsagi-Mate, S., et al., *Complex formation between water-soluble sulfonated calixarenes and C60 fullerene*. *Tetrahedron Letters*, 2004. **45**(7): p. 1387-1390.
152. Corraera, S., *Living and dead theories for asphaltene stability*, in *EniTecnologie Conference - Advances in flow assurance technology*. 2006: San Donato Milanese.
153. centre, O.h.o.s. *What are asphaltenes?* 1997-2007 [cited; Available from: <http://www.lloydminsterheavyoil.com/asphaltenes.htm>].
154. Herod, A.A., K.D. Bartle, and R. Kandiyoti, *Characterization of Heavy Hydrocarbons by Chromatographic and Mass Spectrometric Methods: An Overview*. *Energy Fuels FIELD Full Journal Title:Energy & Fuels*, 2007. **21**(4): p. 2176-2203.
155. Mullins, O.C., B. Martinez-Haya, and A.G. Marshall, *Contrasting Perspective on Asphaltene Molecular Weight. This Comment vs the Overview of A. A. Herod, K. D. Bartle, and R. Kandiyoti*. *Energy Fuels FIELD Full Journal Title:Energy & Fuels*, 2008. **22**(3): p. 1765-1773.
156. Martinez-Haya, B., et al., *Laser desorption/ionization determination of molecular weight distributions of polyaromatic carbonaceous compounds and their aggregates*. *J. Mass Spectrom. FIELD Full Journal Title:Journal of Mass Spectrometry*, 2007. **42**(6): p. 701-713.
157. Hurtado, P., A.R. Hortal, and B. Martinez-Haya, *Matrix-assisted laser desorption/ionization detection of carbonaceous compounds in ionic liquid matrices*. *Rapid Commun. Mass Spectrom. FIELD Full Journal Title:Rapid Communications in Mass Spectrometry*, 2007. **21**(18): p. 3161-3164.
158. Hortal, A.R., et al., *Molecular-Weight Distributions of Coal and Petroleum Asphaltene from Laser Desorption/Ionization Experiments*. *Energy Fuels FIELD Full Journal Title:Energy & Fuels*, 2007. **21**(5): p. 2863-2868.
159. Pomerantz, A.E., et al., *Two-Step Laser Mass Spectrometry of Asphaltene*. *J. Am. Chem. Soc. FIELD Full Journal Title:Journal of the American Chemical Society*, 2008. **130**(23): p. 7216-7217.

160. Becker, C., K. Qian, and D.H. Russell, *Molecular Weight Distributions of Asphaltenes and Deasphalted Oils Studied by Laser Desorption Ionization and Ion Mobility Mass Spectrometry*. Anal. Chem. (Washington, DC, U. S.) FIELD Full Journal Title: Analytical Chemistry (Washington, DC, United States), 2008. **80**(22): p. 8592-8597.
161. Meredith, W., S.J. Kelland, and D.M. Jones, *Influence of biodegradation on crude oil acidity and carboxylic acid composition*. Organic Geochemistry, 2000. **31**(11): p. 1059-1073.
162. Brient, J.A., P.J. Wessner, and M.N. Doyle, *In Kirk-Othmer Encyclopedia of Chemical Technology*, ed. J.I. Kroshwitz and A. Seidel. 1995, New York: John Wiley & Sons. 1017-29.
163. Seifert, W.K., *Carboxylic acids in petroleum and sediments*. Fortschr. Chem. Org. Naturst., 1975. **32**: p. 1-49.
164. Clemente, J.S. and P.M. Fedorak, *A review of the occurrence, analyses, toxicity, and biodegradation of naphthenic acids*. Chemosphere, 2005. **60**(5): p. 585-600.
165. Merlin, M., S.E. Guigard, and P.M. Fedorak, *Detecting naphthenic acids in waters by gas chromatography-mass spectrometry*. Journal of Chromatography A, 2007. **1140**(1-2): p. 225-229.
166. Kokal, S.L. and S.G. Sayegh, *Asphaltenes: The cholesterol of petroleum*, in *SPE Middle East Oil Show*. 1995.
167. Creek, J.L., *Freedom of action in the state of asphaltenes: Escape from conventional wisdom*. Energy & Fuels, 2005. **19**(4): p. 1212-1224.
168. Hammami, A., et al., *Asphaltene precipitation from live oils: An experimental investigation of onset conditions and reversibility*. Energy & Fuels, 2000. **14**(1): p. 14-18.
169. Murgich, J., *Intermolecular forces in aggregates of asphaltenes and resins*. Petroleum Science and Technology, 2002. **20**(9-10): p. 983-997.
170. Israelachvili, J., *Intermolecular and Surface Forces*. 2nd ed. 1991, New York: Academic.
171. Stone, A.J., *The Theory of Intermolecular Forces*. 1996, Oxford: Clarendon Press.

172. Ostlund, J.A., et al., *Interactions between asphaltenes and naphthenic acids*. Energy & Fuels, 2003. **17**(1): p. 113-119.
173. Varadaraj, R. and C. Brons, *Molecular origins of heavy oil interfacial activity part 1: Fundamental interfacial properties of asphaltenes derived from heavy crude oils and their correlation to chemical composition*. Energy & Fuels, 2007. **21**(1): p. 195-198.
174. Varadaraj, R. and C. Brons, *Molecular origins of heavy crude oil interfacial activity part 2: Fundamental interfacial properties of model naphthenic acids and naphthenic acids separated from heavy crude oils*. Energy & Fuels, 2007. **21**(1): p. 199-204.
175. Heaps, D., *Onset of Precipitation of Asphaltenes in the Presence of Naphthenic Acids*. Unpublished Work, 2009.
176. Kilpatrick, P.K., *Colloid and Interfacial Phenomena in Petroleum: Emulsions in Heavy Petroleum Fluids and Their Mixtures*, in AIChE Spring National Meeting. 2002, AIChE.